

TOWARD COMPLETE STATISTICS OF MASSIVE BINARY STARS: PENULTIMATE RESULTS FROM THE CYGNUS OB2 RADIAL VELOCITY SURVEY

Henry A. Kobulnicky¹, Daniel C. Kiminki², Michael J. Lundquist¹, Jamison Burke^{1,3}, James Chapman^{1,4}, Erica Keller^{1,5}, Kathryn Lester^{1,6}, Emily K. Rolen^{1,7}, Eric Topel^{1,8}, Anirban Bhattacharjee¹, Rachel A. Smullen¹, Carlos A. Vargas Álvarez¹, Jessie C. Runnoe^{1,9}, Daniel A. Dale¹, Michael M. Brotherton¹

ABSTRACT

We analyze orbital solutions for 48 massive multiple-star systems in the Cygnus OB2 Association, 23 of which are newly presented here, to find that the observed distribution of orbital periods is approximately uniform in $\log P$ for $P < 45$ d, but it is not scale-free. Inflections in the cumulative distribution near 6 d, 14 d, and 45 d, suggest key physical scales of $\simeq 0.2$, $\simeq 0.4$, and $\simeq 1$

¹Dept. of Physics & Astronomy, University of Wyoming, Laramie, WY 82070, USA
chipk@uwyo.edu

²Dept. of Astronomy, University of Arizona, Tucson, AZ 85721, USA

³Department of Physics and Astronomy, Swarthmore College, Swarthmore, PA 19081, USA
jburke2@swarthmore.edu

⁴Massachusetts College of Liberal Arts, 375 Church St., North Adams, MA 01247, USA
jc6380@mcla.edu

⁵Department of Astronomy, Mt. Holyoke College, 50 College Street, South Hadley, MA 01075, USA
kelle22e@mtholyoke.edu

⁶Department of Physics, Lehigh University, 16 Memorial Drive East, Bethlehem, PA 18015, USA
kvl214@lehigh.edu

⁷Department of Physics and Astronomy, Vanderbilt University, Nashville, TN 37235, USA
emily.k.rolen@vanderbilt.edu

⁸Department of Physics, 1520 St. Olaf Avenue, Northfield, MN 55057, USA
topel@stolaf.edu

⁹Department of Physics, Department of Astronomy & Astrophysics, The Pennsylvania State University, 525 Davey Lab, University Park, PA 16802, USA

A.U. where yet-to-be-identified phenomena create distinct features. No single power law provides a statistically compelling prescription, but if features are ignored, a power law with exponent $\beta \simeq -0.22$ provides a crude approximation over $P=1.4 - 2000$ d, as does a piece-wise linear function with a break near 45 d. The cumulative period distribution flattens at $P > 45$ d, even after correction for completeness, indicating either a lower binary fraction or a shift toward low-mass companions. A high degree of similarity (91% likelihood) between the Cyg OB2 period distribution and that of other surveys suggests that the binary properties at $P \lesssim 25$ d are determined by local physics of disk/clump fragmentation and are relatively insensitive to environmental and evolutionary factors. Fully 30% of the unbiased parent sample is a binary with period $P < 45$ d. Completeness corrections imply a binary fraction near 55% for $P < 5000$ d. The observed distribution of mass ratios $0.2 < q < 1$ is consistent with uniform, while the observed distribution of eccentricities $0.1 < e < 0.6$ is consistent with uniform plus an excess of $e \simeq 0$ systems. We identify six stars, all supergiants, that exhibit aperiodic velocity variations of $\sim 30 \text{ km s}^{-1}$ attributed to atmospheric fluctuations.

Subject headings: Stars: massive — (Stars:) binaries: spectroscopic — (Stars:) binaries: general — (Stars:) binaries:(including multiple): close — (Stars:) early-type — Stars: kinematics and dynamics — Techniques: radial velocities

1. Introduction

Massive stars ($M > 8M_{\odot}$) earlier than about B2.5V dominate the cosmic production of ionizing photons and stellar wind momentum before terminating in nature’s most energetic explosive events, leaving behind neutron stars and black holes. Formation scenarios for these explosions and subsequent compact stellar remnants require the existence of a close stellar companion. In X-ray binaries the massive star becomes a neutron star accreting from an evolved star. Mergers of compact objects (neutron star-neutron star or black hole-neutron star) produce gravitational waves (GW) that should be detected by the immanent generation of GW experiments (Dominik et al. 2013). “Runaway” or “high-velocity stars also owe their extreme kinematics to hard interactions with massive binary systems (Blaauw 1961; Gies & Bolton 1986; Hoogerwerf et al. 2001). In particular, stars in the range 8–25 M_{\odot} that have close companions may become the progenitors of Type Ibc supernovae when the H envelope of the more massive star is stripped during a phase of common envelope evolution (Nomoto et al. 1995; Smartt et al. 2009; Eldridge et al. 2013; Smith 2014). Close binaries may even produce all type Ibc supernova if single H-poor Wolf-Rayet stars collapse to

become black holes without producing a supernova (Fryer et al. 2007). Furthermore, supernovae of type Ic and γ -ray bursts appear to happen simultaneously, suggesting a connection between the two types of events that may have their origins in massive binary progenitors (Woosley & Bloom 2006). Close massive binaries also produce the population of low-mass X-ray binary systems through evolution of the more massive star to a supernova, production of a neutron star or black hole, and then the subsequent evolution of the lower-mass companion that becomes the mass donor (van den Heuvel 1983).

The Cygnus OB2 Radial Velocity Survey (Kiminki et al. 2007) is an optical spectroscopic survey of 128 photometrically selected O and early-B stars comprising an unbiased (with respect to binarity) sample within the core region of the nearby Cygnus OB2 Association (~ 1.4 kpc; Hanson 2003). This sample contains 45 stars of spectral type O and 83 stars of spectral type B. Luminosity class V (i.e., unevolved) stars account for 91 of the 128. The Survey is designed to statistically measure the binary properties of massive stars within a common formation environment at a similar age. Although massive star formation in Cyg OB2 may not be coeval, studies suggest an age of 3–4 Myr, young enough that the most massive stars are still present and the majority of these stars are still on the main sequence (Hanson 2003). Papers I–VI in this series (Kiminki et al. 2007, Kiminki et al. 2008, Kiminki et al. 2009, Kiminki et al. 2012, Kiminki & Kobulnicky 2012, Kobulnicky et al. 2012) describe the Survey and document orbital parameters for 25 massive binary systems known from the inception of the Survey in 1999 through the 2011 observing season. In particular, Paper V (Kiminki & Kobulnicky 2012) provides a high-level overview of the Survey’s constraints on statistics of massive binary stars by use of a Monte Carlo analysis. Stars down to spectral type $\sim B2.5V$ are included in the Survey because they are expected to dominate the population of supernova progenitors, given typical initial mass functions. Other large studies of binarity among massive stars include the spectroscopic surveys of Garmany et al. (1980), Sana et al. (2012), and Chini et al. (2012) as well as the imaging surveys of Kouwenhoven et al. (2007) and Mason et al. (2009).

In this contribution we report the observations (Section 2) and orbital solutions for 22 new single-lined spectroscopic binaries and one new double-lined binary (Section 3). These data contribute to the growing census of massive binary statistics in a complete sample of massive stars defined in Paper I. This increasingly complete compilation of orbital periods, eccentricities, and mass ratios provides a rich dataset to constrain our understanding of massive star formation, evolution through binary channels, and massive star end states. Section 3 also contains a list of 16 stars that show minimal velocity variations after extensive observation and six stars—all supergiants—that exhibit irregular variations presumed to originate from atmospheric pulsations. An appendix provides an update on orbital solutions for six stars from Papers II and III for consistency with the most recent Cyg OB2

analyses. We conclude by tabulating orbital parameters for the 48 known binary (and several triple) systems and conducting a high-level analysis of the distribution of orbital parameters (Section 4). Nomenclature of objects discussed herein follows the MT91 ### notation of Massey & Thompson (1991), with “S #” indicating the numeration of Schulte (1958) and “CPR2002-A##” or “B##” for that of Comerón et al. (2002).

2. Spectroscopic Observations, Reductions, and Radial Velocity Measurement

Observational methodologies and data reduction procedures closely follow those described in Kobulnicky et al. (2012) and earlier papers. Paper I describes instrumental setups and dates of observation for observing runs using Keck+HIRES spectrograph (1999–2001), Lick+Hamilton echelle spectrograph (1999–2000), and WIYN+Hydra spectrograph (2001–2008). Results presented here principally use spectra obtained at the Wyoming Infrared Observatory (WIRO) 2.3 meter telescope+Longslit optical spectrograph using a 2000 l mm^{-1} grating in first order during the 2011–2013 observing seasons, with a small number of observations obtained in 2014 May. Resolutions of $R \approx 4500$ were achieved using a $1''.2$ slit. Multiple 600 s spectra of each target were obtained over the wavelength range 5400–6700 Å. Data from WIRO in 2010 and earlier used either a 600 l mm^{-1} grating in second order or an 1800 l mm^{-1} grating in first order to achieve spectral resolutions of $R \approx 2500$ and 4000, respectively. These observations are more fully described in earlier papers in this series. Routine CuAr lamp exposures provided wavelength solutions having a typical rms of 0.012–0.030 Å. Spectra were combined and transformed into the Heliocentric reference frame, yielding a final signal-to-noise ratio (SNR) of 60–200 in the vicinity of the He I 5876 Å line used to measure radial velocities. The ensemble of spectra spanning hours to years were shifted by small amounts (2–8) km s^{-1} so that the interstellar Na II $\lambda\lambda$ 5889/96 lines align at the mean velocity across all observations. This corrects for small changes in the wavelength solution zero point across epochs. Data from Keck and WIYN did not cover the Na II lines so these spectra potentially have systematic velocity zero point differences compared to the WIRO data. However, our analysis of constant-velocity stars in the Survey shows good agreement, at the level of 3–6 km s^{-1} , between the velocities obtained from Keck, WIYN, and WIRO spectra. Nevertheless, solutions are obtained solely from WIRO data, where possible. When necessary, data from Keck and/or WIYN are included in the solutions. Data from Lick were generally of lower quality and are not used.

Radial velocities were measured by fitting Gaussian profiles to the He I 5876 Å photospheric line (He I 4471 Å for the Keck and WIYN spectra) adopting a rest wavelength of 5875.69 Å (4471.55 Å for Keck and WIYN spectra). Constant-velocity stars showed good

agreement (3–6 km s⁻¹) between velocities from the various telescopes and instruments, lending confidence to the solutions that involve all three sources of data. Our fitting code¹ fixes the Gaussian width and depth to be the mean determined from all the spectra, after rejecting outliers, and it solves for the best-fitting line center and its uncertainty. Since the primary goal of the Cygnus OB2 radial velocity survey is to obtain orbital parameters for massive binaries, a goal that requires good *relative* radial velocities, we did not observe radial velocity standard stars, and consequently the absolute space velocities reported are likely to be accurate to $\sim 3\text{--}5$ km s⁻¹. Nevertheless, there is good agreement between the mean velocities of our Cyg OB2 OB star sample ($V_{ave} = -15.6$ km s⁻¹; $\sigma_V = 8.2$ km s⁻¹) and results from other workers ($V_{ave} \simeq -18$ km s⁻¹; N. Wright, private communication).

Table 1 records the heliocentric Julian Date, orbital phase, the heliocentric radial velocity, the velocity uncertainty, and the observed-minus-computed (O-C) velocity for each measurement based on the orbital solutions that follow. All systems, with the exception of MT91 646, are single-lined spectroscopic binaries so that only one velocity is reported for each epoch. MT91 268 is a probable triple system exhibiting two periodicities, so both velocity components appear in Table 1. Figure 1 shows a three-color view of the Cygnus OB2 region with 4.5, 8.0, and 24 μm mosaic images from the *Spitzer Cygnus-X Legacy Survey* (Hora et al. 2007) in blue, green, and red, respectively. White points depict massive stars in the Cygnus OB2 Radial Velocity Survey parent sample, while magenta points mark known binary or higher-order systems. The 5 pc bar at lower left marks the linear scale at the adopted distance of 1.4 kpc. Binaries are apparently distributed across the face of the Association without preference for radial distance from center.

3. Orbital Solutions

We analyzed the radial velocity power spectrum for each object to select likely periods and then examined the folded velocity curve for periods corresponding to the strongest peaks. In most cases the strongest peak yielded a clear, unambiguous period and a convincing phased velocity curve. Secondary peaks and possible aliases could be eliminated by visual inspection owing to the much larger dispersion in the data at any given phase. We used the binary orbital solution package “BINARY” by D. Gudehus² with these initial period estimates and the radial velocity data to solve for the full suite of orbital parameters and associated uncertainties. Tables 2 through 6 compile these best-fitting parameters and uncertainties for

¹We use the robust curve-fitting algorithm MPFIT as implemented in IDL (Markwardt 2009).

²<http://www.chara.gsu.edu/~gudehus/binary.html>

each object. Listed within the table are the period in days (P), eccentricity of the orbit (e), longitude of periastron in degrees (ω), systemic radial velocity (γ), epoch of periastron (T_0), primary velocity semi-amplitude (K_1) and (if applicable) secondary velocity semi-amplitude (K_2), spectral classifications from this survey (S.C.₁ & S.C.₂, if available), estimates of the inclination (i), the adopted primary stellar mass (M_1) and (if applicable) secondary mass (M_2), mass ratio (q), semi-major axis (a), and reduced chi squared values of the best fitting solution. Tables 2 through 6 list orbital parameters for 22 new systems reported in this work. Masses for OB stars are taken from Martins et al. (2005) for O stars and Hunter et al. (2008) for early B stars. Upper and lower limits on the inclinations are obtained, in most cases, by adopting 90° and the lowest inclination compatible with the absence of secondary spectral features (i.e., where the mass of the secondary approaches that of the primary).

3.1. New Binary Systems

MT91 021—Kiminki et al. (2007) classified the MT91 021 primary ($V=13.74$; Massey & Thompson 1991) as a probable single-lined binary system on the basis of four data points. Using a combination of three WIYN spectra we revise the spectral type to B1.5V by comparison in the Walborn & Fitzpatrick (1990) spectral atlas. Table 1 lists the 14 radial velocity measurements from WIRO spanning 2010 August – 2013 September. Figure 2 shows the best-fitting orbital solution (solid curve) and folded velocity data (points with error bars). Table 2 summarizes the full suite of orbital parameters. If we adopt a mass of $12 M_\odot$ for the primary (MT91 021a), an inclination of $i=85^\circ$ implies a secondary (MT91 021b) mass of $2.2 M_\odot$, while $i=15^\circ$ requires the secondary (MT91 021b) mass to approach that of the primary. This system is interesting for having such a high eccentricity despite its short period. However, the eccentricity is strongly dependent on just a few data points, and a solution with fixed eccentricity of zero still yields a similar χ^2 value.

Finally, we note that the reduced χ^2 of the fit (3.2) is large. The O-C residuals appear to show evidence for periodic variation at ~ 4.3 days with an amplitude near 15 km s^{-1} , suggesting the possibility of this being a triple system. This would make the tertiary, MT91 021c, a probable solar mass star with a minimum mass of $0.5 M_\odot$. Additional measurements will be needed to confirm the periodicity and amplitude of a second velocity component in this single-lined system. Inclusion of older (but less precise) WIYN (2 spectra) and Keck (2 spectra) measurements strengthen the evidence for more than one velocity component in MT91 021.

MT91 187—The B1 V primary of this $V=13.24$ system was not initially detected as a probable binary on the basis of five measurements (Kiminki et al. 2007). The present

dataset consisting of two Keck spectra, four WIYN spectra, and 19 WIRO spectra spanning 1999–2013 (Table 1) reveals this systems to be a $P=13.531\pm0.002$ d binary with $K_1=6.5\pm1.1$ km s⁻¹. Figure 3 shows the best-fitting orbital solution (solid line) and folded velocity curve data (points with error bars). This is one of the lowest amplitude systems yet detected in the Survey. The velocity variability is consistent with a binary (reduced $\chi^2=0.82$ for 12 degrees of freedom) but not a constant-velocity system (reduced $\chi^2=1.8$ for 19 degrees of freedom, yielding a probability of <2%). The eccentricity is not well constrained at $e=0.51\pm0.12$. An alternative period of $P \simeq 6.1$ d is also possible, but less probable based on the power spectrum and the higher eccentricity required in the best fit. There are no known eclipses from this system, so the inclination is essentially unconstrained. If we adopt a mass of 14 M_\odot for the B1V primary, an inclination of $i=85^\circ$ implies a secondary (MT91 187b) mass of 0.43 M_\odot , while $i=3^\circ$ allows a secondary mass approaching that of the primary. Given the probable low-mass secondary and extreme mass ratio, this system is a candidate for being a progenitor of a low-mass X-ray binary system if the system remains bound once the primary reaches its end-state as a neutron star.

MT91 202—This $V=14.40$ binary is listed as an SB1 by Kiminki et al. (2007) on the basis of five data points, and they type the primary as B2V. We find an orbital period of $P=43.07\pm0.05$ d with no credible aliases and an amplitude of $K_1=19.7\pm2.6$ km s⁻¹ using 17 measurements from WIRO. The eccentricity is $e=0.23\pm0.11$. Adopting 11 M_\odot for the primary yields $M_2=2.0 M_\odot$ if $i=90^\circ$. The lack of known eclipses does not provide useful constraints on the inclination given the relatively long period. The mass of the secondary (MT91 202b) approaches that of the primary if $i=15^\circ$. These rough mass constraints mean that the secondary spectral type probably lies in the range A to mid-B, assuming a main-sequence star. Although there are hints of line width variations that may suggest a double-lined system, the low SNR of our spectra on this faint star coupled with the broad linewidth and small velocity amplitude means that no attempt was made to separate components. Figure 4 shows the best-fitting orbital solution and folded velocity data.

MT91 234—This $V=13.25$ system is dominated by its B1.5V (revised from B2V in Paper I) primary star that exhibits long-term radial velocity variations. The solution required a combination of data spanning the whole range of the Cygnus OB2 Radial Velocity Survey from 1999 October using Keck+HIRES (two measurements) through 2001 August–2008 June using WIYN+Hydra (10 measurements), and 2011–2013 October using WIRO (14 measurements).

Figure 5 shows the best-fitting orbital solution and folded velocity data. Symbol types designate data from Keck (triangles), WIYN (diamonds), and WIRO (squares). The period of 13.6 ± 0.9 years makes this the longest period system yet uncovered in Cyg OB2.

The eccentricity is small (0.12 ± 0.16) and consistent with zero. A velocity amplitude of $K_1 = 17.1 \pm 2.2 \text{ km s}^{-1}$ is large for such a long-period system and implies a fairly massive companion. Adopting a primary mass of $12 M_\odot$ yields a minimum secondary (MT91 234b) mass of $11 M_\odot$ for $i = 90^\circ$. This suggests that the system is seen nearly edge-on and that the secondary is also a B star.

MT91 241—A B1.5V (revised here from B2V in Paper I) primary star, the 11 WIRO data combined with three Keck and five WIYN measurements show that MT91 241a has a period of $671 \pm 2 \text{ d}$ (1.83 yr) and semi-amplitude $18.7 \pm 1.2 \text{ km s}^{-1}$ with eccentricity of 0.45 ± 0.06 . Figure 6 shows the best-fitting orbital solution and folded velocity data. Adopting a primary mass of $12 M_\odot$, the implied secondary mass (MT91 241b) is $5.2 M_\odot$ for $i = 90^\circ$. The very narrow He I lines show no sign of a second component, so it seems likely that the secondary star mass is closer to this lower limit than to the primary mass, implying a mass ratio in the range $0.42 < q \lesssim 0.8$.

MT91 268—A B2V (revised from B2.5V in Paper I), this single-lined shows unambiguous evidence for being a triple system. The initial single-component solution at a period near 33.2 d displayed systematic residuals with a period near 5.0 days. We used these initial guesses to fit a joint orbital solution for two velocity components using two data from Keck, five data from WIYN, and 15 data from WIRO between 1999 and 2013. Our best-fitting solution consists of the first component having $P_1 = 33.327 \pm 0.002 \text{ d}$, $e_1 = 0.41 \pm 0.03$, $K_{1-comp1} = 33.0 \pm 2.7 \text{ km s}^{-1}$, and the second component having $P_2 = 5.082 \pm 0.006 \text{ d}$, $e_2 = 0.48 \pm 0.15$, and $K_{1-comp2} = 17.4 \pm 2.3 \text{ km s}^{-1}$. Figures 7 and 8 display the orbital solution and folded velocity data for each component. The existence of several outlier measurements in both plots is consistent with the hypothesis of this being a quadruple system.

Adopting $11 M_\odot$ for the mass of the primary star MT91 268a, the implied minimum masses for the unseen companions are $M_2 \geq 2.9 M_\odot$ for the 33.2-day component 1 (MT91 268b) and $M_3 \geq 0.7 M_\odot$ for the 5.08-day component 2 (MT91 268c). This allows that the companions are probable A–mid-B and G–B dwarfs, respectively. Given the moderate eccentricity, short period, and extreme mass ratio, this may be a dynamically unstable system.

MT91 292—With a period of $14.811 \pm 0.001 \text{ d}$, this B2V system lies just above the 7–14 day period gap noticed by Kiminki & Kobulnicky (2012). The velocity semi-amplitude of $K_1 = 25.3 \pm 2.6 \text{ km s}^{-1}$ is well-defined by the combination of 1 Keck data point, six WIYN measurements, and 13 WIRO measurements spanning nearly the entire length of the 2000–2013 survey period. Adopting a primary mass of $11 M_\odot$, an inclination of $i = 90^\circ$ implies a minimal secondary mass for MT292b of $M_2 = 1.6 M_\odot$. The secondary mass approaches that of the primary if $i \simeq 12^\circ$. Figure 9 shows the best-fitting orbital solution and folded velocity

data.

MT91 295—Fourteen measurements from WIRO during 2012 and 2013 indicate that this B1.5V (revised from B2V in Paper I) has $P=2.4628\pm 0.0008$ d and $e=0.30\pm 0.22$. This is an unusually large eccentricity for such a short-period system, but solutions with zero eccentricity yielded substantially poorer fits. The semi-amplitude of $K_1=9.2\pm 2.4$ km s⁻¹ is small but detectable given the typical uncertainty of 3.9 km s⁻¹. The power spectrum has multiple peaks consistent with this being a triple system having components with periods of 4.67 d and 1.68 d and velocity semi-amplitudes near 4–6 km s⁻¹. The two-component solution provides a somewhat better fit, but the number of free parameters approaches the number of data points. In either case, this is a short-period multiple system. Figure 10 shows the best-fitting *single-component* orbital solution and folded velocity data. Adopting 12 M_⊙ for the mass of the primary, the implied lower limit on the secondary (MT91 295b) mass is $M_2=0.3$ M_⊙. The inclination is unconstrained, as M_2 approaches M_1 for $i=3^\circ$.

MT91 336—This narrow-lined B2V (revised slightly from B3III in Paper I) has one observation from Keck, seven from WIYN, and four from WIRO spanning 1999 – 2014. The twelve data points yield a period of 2.04087 ± 0.00006 with amplitude $K_1=8.8\pm 1.1$ km s⁻¹ and eccentricity of $e=0.21\pm 0.18$. There is a possible alias near 4.24 days. Figure 11 shows the best-fitting orbital solution and folded velocity data. Adopting 11 M_⊙ for the mass of the primary, the implied lower limit on the secondary (MT91 336b) mass is $M_2=0.3$ M_⊙. The inclination is unconstrained, as M_2 approaches M_1 for $i=3^\circ$.

MT91 339—With a velocity amplitude of just $K_1=3.4\pm 0.3$ km s⁻¹ this O8V primary has one of the smallest amplitudes of any in our survey. The narrow, deep He lines allow for a high level of precision, leading to typical velocity uncertainties of ~ 2 km s⁻¹ on the 34 WIRO spectra spanning 2008–2013. The orbital period is $P=37.86\pm 0.04$ d with eccentricity 0.21 ± 0.11 . A Monte Carlo simulation wherein the Julian dates are shuffled randomly among the observed velocities shows that in only 9% of the iterations does the peak in the power spectrum exceed the observed one. We conclude that the probability of a real periodicity is high. Figure 12 shows the best-fitting orbital solution and folded velocity data. The orbital inclination is unconstrained, allowing for secondary (MT91 339b) masses from 0.5 M_⊙ to 21 M_⊙.

MT91 378—The V=13.49 B0V primary shows a velocity amplitude of $K_1=36.3\pm 1.9$ km s⁻¹ and a period of 29.41 ± 0.03 d. Figure 13 shows the best-fitting orbital solution and folded velocity data. Although there is some hint of variable line widths suggestive of a double-lined system, the limited SNR of the spectra preclude attempts at spectral deblending using the 19 data obtained at WIRO between 2010 and 2013. For an adopted primary mass of 18 M_⊙, an inclination of $i=90^\circ$ yields $M_2=4.1$ M_⊙. The secondary mass approaches the

primary mass if $i=17^\circ$. Hence, the secondary (MT91 378b) is limited to be a B spectral type, assuming it is on the main sequence.

MT91 390—With a velocity amplitude of $K_1=5.4\pm 0.9$ km s⁻¹, this O8V primary is among the lowest-amplitude systems observed in the survey. The period of $P=4.625\pm 0.001$ d using 17 radial velocity measurements from WIRO between 2011 June and 2013 August places MT91 390 among the conspicuous group of short-period binaries. There are no known eclipses, so the inclination is unconstrained. For $i=90^\circ$ the implied secondary mass is $M_2=0.32 M_\odot$, while for $i=2^\circ$ the secondary (MT91 390b) mass approaches that of the primary. Figure 14 shows the best-fitting orbital solution and folded velocity data.

MT91 403—This B1V primary exhibits a velocity semi-amplitude of $K_1=49.8\pm 2.1$ km s⁻¹ and a period of $P=16.638\pm 0.006$ d using 18 measurements from WIRO. With no known eclipses, there are no inclination constraints. The adopted primary mass of $14 M_\odot$ leads to a secondary mass of $M_2=4.1 M_\odot$ for $i=90^\circ$ and $M_2=14 M_\odot$ for $i=23^\circ$. These limits dictate that the secondary (MT91 403b) is a probable B star. Figure 15 shows the best-fitting orbital solution and folded velocity curve.

MT91 417B (Schulte #22B)—MT91 417 is a visual double consisting of MT91 417A (O3I; the northwest component) and MT91 417B (O6V; the southeast component) at a separation of $1''.5$ (~ 2100 AU projected separation at 1.4 kpc) at $PA\approx 50^\circ$. We obtained 14 spectra of MT91 417B at WIRO in good seeing conditions between 2013 August 6 and 2014 May 26 with the $1''.2$ slit oriented perpendicular to the two stars. One additional measurement from WIRO on 2008 June 26 was used. MT91 417B exhibits variability with a period of $P=38.0\pm 0.2$ d and $K_1=9.5\pm 1.7$ km s⁻¹. Figure 16 shows the best-fitting orbital solution and folded velocity curve. The implied secondary (MT91 417B-b) minimum mass is $1.8 M_\odot$ for $i=90^\circ$. The secondary mass approaches that of the primary for $i=5^\circ$. The velocity curve is not well-sampled at all phases so the derived parameters are particularly uncertain.

MT91 448—A period of $P=3.1704\pm 0.0004$ d for this O6V primary places it among the shortest period systems in Cyg OB2. The 18 WIRO data spanning 2011–2013 yield a secure velocity semi-amplitude of 27.7 ± 1.7 km s⁻¹ and a low eccentricity of $e=0.10\pm 0.06$. There are no known eclipses. An inclination of $i=90^\circ$ yields a minimum secondary (MT91 448b) mass $M_2=2.1 M_\odot$, while the secondary mass approaches that of the primary for $i=6^\circ$. Figure 17 shows the best-fitting orbital solution and folded velocity curve data.

MT91 473—This O8.5V has three measurements from Keck (1999–2000), nine from WIYN (2000–2008) and 24 from WIRO (2010–2013). The power spectrum is complex, showing multiple peaks on timescales of 2000 d to 1.9 d. The dominant peak at 1700 d

yields a folded velocity curve that appear consistent with the long-term trends observed in an unphased velocity curve. The WIRO data alone suggest a period in this same vicinity. A Monte Carlo simulation wherein the Julian dates are shuffled randomly among the observed velocities shows that in only 1.3% of the iterations does the peak in the power spectrum exceed the observed one. We conclude that the observed periodicity is highly likely to be real. Our best-fitting orbital solution gives a period of $P=1687\pm 51$ d and amplitude $K_1=7.5\pm 2.2$ km s⁻¹. Figure 18 shows the best-fitting orbital solution and folded velocity data.

Smaller peaks in the power spectrum suggest the possibility of short-period variations on the ~ 2 d timescale, and a couple of the KECK HIRES spectra suggest a possibility of a double-lined system. We fit single Gaussian curves to the He I $\lambda 4471$ lines in the Keck and WIYN spectra and the He I $\lambda 5876$ lines in the WIRO spectra. The FWHM of the lines varies over the range 3.7 – 4.4 Å with typical uncertainties of 0.25 Å. By applying a power spectrum analysis to the FWHM values, we find a peak at 1.846 d, constituting evidence for a probable double-lined system with twice this period, 3.692 d. The spectra have insufficient SNR and spectral resolution to attempt a deblending, but we conclude that MT91 473 likely consists of at least three stars. In this scenario, components MT91 473a and MT91 473b would constitute a tight binary with a period of about 3.6 d and similar spectral types near O8.5V. The inclination for this pair must be low, near 10°, such that the line splitting does not exceed the observed values. MT91 473c is the unseen companion responsible for the radial velocity curve shown in Figure 18. Adopting masses of 19 M_\odot for each of components a and b implies a mass of 5.0 M_\odot for $i=90^\circ$, meaning that the secondary must be at least a mid-B star. For inclinations as small as 11° the mass of component c could approach that of a+b.

MT91 485— MT91 485 is an O8V showing long-term radial velocity variations with $P=4066\pm 45$ d and semi-amplitude $K_1=15.0\pm 2.3$ km s⁻¹ based on two Keck measurements, nine WIYN measurements, and 17 WIRO measurements covering the period 2001 August through 2013 October. We found it necessary to fix the eccentricity during fitting to avoid extremely large values. We estimate $e=0.75\pm 0.20$ by manual experimentation. Figure 19 shows the best-fitting orbital solution and folded velocity curve data. The phase light curve is essentially the same as the unphased light curve, given that the period of 11.1 years is nearly as long as the duration of our survey. Adopting 21 M_\odot for the primary mass, the inclination of $i=90^\circ$ leads to a secondary mass of $M_2=11.4 M_\odot$. M_2 approaches M_1 for $i=40^\circ$. The secondary, MT91 485b, must be more massive than an early-B dwarf star. MT91 485 is an example of a highly eccentric system that could easily be missed in a radial velocity survey if it were not for fortuitous phase coverage.

MT91 555—One of the long-term radial velocity variables in the survey, MT91 555 (O8V) has a period $P=1279.5\pm 13.2$ d (3.50 years) and semi-amplitude $K_1=20.4\pm 3.4$ km s⁻¹. Figure 20 shows the best-fitting orbital solution and folded velocity data using 1 datum from Keck, 7 from WIYN, and 20 from WIRO. Adopting a primary mass of 21 M_⊙ yields a minimum secondary mass $M_2=10.3$ M_⊙, meaning that the secondary (MT91 555b) is constrained to be about B2V or earlier. For $i=34^\circ$ the secondary mass approaches that of the primary.

MT91 561—A B2V, the primary star of MT91 561 shows a period of $P=40.09\pm 0.03$ d and a velocity semi-amplitude of 35.2 ± 3.6 km s⁻¹ using 17 WIRO data points between 2007 and 2013. Figure 21 shows the best-fitting orbital solution and folded velocity curve. For an adopted primary mass of 11 M_⊙, the secondary mass is $M_2=3.3$ M_⊙ if $i=90^\circ$. M_2 approaches M_1 when $i=23^\circ$. This constrains the secondary (MT91 561b) to be at least as massive as a late B main sequence star, and the mass ratio lies in the range $q=0.30$ –1.

MT91 588—This B0V has a moderately eccentric orbit with $P=245.1\pm 0.3$ d, $e=0.51\pm 0.17$, and a velocity semi-amplitude of 14.5 ± 2.9 km s⁻¹ using one measurement from Keck, four from WIYN, and 16 from WIRO over the period 1999–2013. Figure 22 shows the best-fitting orbital solution and folded velocity data. Adopting a primary mass of 18 M_⊙ yields a minimum secondary mass $M_2=3.2$ M_⊙, meaning that the secondary (MT91 588b) is constrained to be an early A star or earlier. For $i=15^\circ$ the secondary mass approaches that of the primary. The sampling of the velocity curve is such that aliases of 34.9 d, 69.8 d, 104 d, 174 d are possible but less likely.

MT91 601—The two Keck, one WIYN and 28 WIRO data of this O9.5III reveal a period of 510.2 ± 0.9 d and $K_1=12.8\pm 2.1$ km s⁻¹. Owing to the incomplete phase coverage, we found it necessary to fix the eccentricity (at 0.67) to avoid extremely large eccentricities that tended to result during the fitting process. Manual experimentation suggests an eccentricity uncertainty of ~ 0.2 . Figure 23 shows the best-fitting orbital solution and folded velocity curve. Adopting a primary mass of 21 M_⊙ yields a minimum secondary mass $M_2=4.1$ M_⊙, meaning that the secondary (MT91 601b) is likely a B or O main sequence star. The reduced χ^2 of the fit is unusually large, at 3.4. We examined the O-C residuals for signs of periodicity, but no strong peaks were seen. We conclude that this evolved primary star exhibits irregular photospheric variations in addition to the identified periodic modulation.

MT91 646—Classified as B1.5V in both Massey & Thompson (1991) and Kiminki et al. (2007), spectra of this system reveal a variable line width indicating an SB2. In several of our 19 WIRO spectra the lines are sufficiently separated to see that the line depths and widths are similar, having a FWHM near 2.9 Å. We fit the most deblended of the 19 WIRO spectra with two-component fixed-width Gaussian profiles to measure velocities for each

component. The solution yields a period of $P=49.8\pm 0.2$ d with velocity semi-amplitudes $K_1=61.6\pm 53.7$ km s⁻¹ and $K_2=79.6\pm 4.7$ km s⁻¹. This implies a mass ratio of $q=0.77\pm 0.05$. Figure 24 shows the best-fitting double-lined orbital solution. The mass function implies a lower limit on the system mass of $12.5 M_\odot$, consistent with a B1V and B1.5V seen at a high inclination. As such, MT91 646 is one of the most “twinlike” systems among the Cyg OB2 sample.

MT91 745—This O7V has two observations from Keck, eight from WIYN, and 22 from WIRO over 1999–2013, yielding a period $P=151.2\pm 0.8$ d, semi-amplitude $K_1=17.5\pm 2.3$ km s⁻¹, and eccentricity $e=0.49\pm 0.14$. Figure 25 shows the best-fitting orbital solution and folded velocity curve. Adopting a primary mass of $25 M_\odot$, the implied lower limit to the secondary mass is $M_2=4.0 M_\odot$ for $i=90^\circ$. M_2 approaches M_1 for $i=15^\circ$. Thus, the secondary (MT91 745b) is at least the mass of a B dwarf star.

3.2. Stars Showing Irregular Variability

Garmany et al. (1980) noted that some of their O-star sample exhibited irregular rather than periodic velocity variations. This phenomenon is quite common in massive stars, especially evolved stars, and has been attributed to line profile variations caused by non-radial pulsations or clumps in the stellar winds (Vogt & Penrod 1983; Fullerton et al. 1996). We note here six objects that have more than 18 data measurements where significant velocity variations at the level of 25–30 km s⁻¹ are observed, but no strong periodicity is evident. Table 7 lists the Heliocentric Julian dates, velocities, and velocity uncertainties of each measurement.

MT91 138—The two Keck data, eight WIYN data, and 22 WIRO data between 1999 and 2008 show that this O8I displays a low level of irregular variability. A long-term, eccentric binary cannot be ruled out.

MT91 417A (Schulte #22A)—This O3If shows variations at the level of about 25 km s⁻¹ on the basis of 20 WIRO data from 2008 and 2014. Our lack of long-term data prevents us from ruling out the possibility of longer term orbital variations. We can only say that the observed variations appear random on the basis of the data presented in Table 7. Because of the very weak He I lines in this very hot star, velocities are measured from He II $\lambda 5411$ assuming a rest wavelength of 5411.45 Å. He I should not be present in such a hot star, but light from the PSF wings of MT91 417B may contaminate some of our spectra given the close 2'' separation.

MT91 457— One Keck, four WIYN, and 11 WIRO data on this O3If during 1999–2008

show that this star exhibits non-periodic variations at the level of $\sim 25 \text{ km s}^{-1}$.

MT91 483—This O5I/III shows low-amplitude (15 km s^{-1}) variations but exhibits power on many scales from days to months using three data from Keck, three from WIYN, and 25 data from WIRO over 1999 - 2013. We show, using a Monte Carlo analysis which randomly shuffles the dates of observation among the observed velocities, that the peaks near 124 days and five days have at least a 0.32 probability of occurring by chance. Because of the weak He I lines in this very hot star, velocities are measured from He II $\lambda 5411$ assuming a rest wavelength of 5411.45 \AA .

MT91 556—MT91 556 was observed 40 times between 2008 and 2013 at WIRO with an average velocity uncertainty of 4 km s^{-1} and variations of up to 20 km s^{-1} . Although velocity variations are observed in this B1I, there is no dominant periodicity and they are consistent with random atmospheric fluctuations.

MT91 632—MT691 32 was observed 30 times between 2008 and 2011 at WIRO with an average velocity uncertainty of 3 km s^{-1} . Although velocity variations are observed in this O9I at the level of 25 km s^{-1} , there is no dominant periodicity and they are consistent with random atmospheric fluctuations.

3.3. Stars Showing No or Little Variability After Extensive Observation

We report here 16 stars having at least 12 velocity measurements spanning at least five years that show no evidence for velocity variations. These stars are candidates for single stars, stars with very low-mass companions, or systems seen at very low inclination angles. Among this list there may be undetected binaries with long periods and/or highly eccentric orbits. Additionally, systems with periods near multiples of one year undergoing periastron during December–April when Cygnus is minimally observable have a low probability of being detected in this survey. For each non-variable system we report the mean velocity, the rms velocity dispersion, and the mean velocity uncertainty.

MT91 005—This O6V was observed twice at Keck, three times at WIYN, and ten times with WIRO over the period 1999–2013. The radial velocities have a mean systemic velocity of -5.5 km s^{-1} , an rms of 2.1 km s^{-1} and mean uncertainties of 2.5 km s^{-1} . The very narrow lines (1.9 \AA FWHM) suggest that the rotational axis may be nearly parallel to the line of sight.

MT91 020—Twelve measurements at WIRO, four from Keck, and two from WIYN spanning 1999–2011 show no evidence for variability, with a mean velocity of -3.2 km s^{-1} ,

an rms of 4.3 km s^{-1} , and mean uncertainties of 4.2 km s^{-1} .

MT91 083—With 22 measurements at three observatories spanning 1999–2008, this BII star shows no evidence for variability. The mean systemic velocity is -1.3 km s^{-1} , with an rms of 1.7 km s^{-1} and mean uncertainties of 2.4 km s^{-1} in the nine WIRO data, one Keck datum, and 7 WIYN data.

MT91 217—Having two measurements from Keck, seven from WIYN, and 17 from WIRO spanning 1999–2011, this O9V star shows no evidence for variability. The mean systemic velocity is -11.1 km s^{-1} , with an rms of 2.4 km s^{-1} and mean uncertainties of 3.0 km s^{-1} .

MT91 227—Two data from Keck, six from WIYN, and 26 from WIRO over the period 1999–2011, are remarkably constant for this O9V. The mean velocity is -3.8 km s^{-1} with an rms of 5.5 km s^{-1} and mean uncertainties of 5.1 km s^{-1} .

MT91 259—One Keck, six WIYN, and seven WIRO data over the period 1999–2011 show a mean velocity of -14.0 km s^{-1} with an rms of 1.3 km s^{-1} and mean uncertainties of 2.1 km s^{-1} .

MT91 299—This O7V has two data from Keck, six from WIYN, and 37 from WIRO between 1999 and 2013. The mean velocity is -14.4 km s^{-1} with an rms of 6.0 km s^{-1} and a typical velocity uncertainty of 5.5 km s^{-1} . This object shows some evidence for a periodicity near 405 days, but the amplitude is low compared to the observational uncertainties, and a convincing orbital solution was not obtained.

MT91 317—This O8V has two data from Keck and 11 from WIYN between 1999 and 2007. The mean velocity is -4.2 km s^{-1} with an rms of 4.4 km s^{-1} and a typical velocity uncertainty of 5.5 km s^{-1} . This object shows some evidence for a periodicity near 405 days, but the amplitude is low compared to the observational uncertainties, and a convincing orbital solution was not obtained.

MT91 376—On the basis of two Keck and 10 WIYN data over the period 1999–2006 this O8V shows a mean velocity of -23.7 km s^{-1} and rms of 6.2 km s^{-1} for a mean velocity uncertainty of 7.5 km s^{-1} .

MT91 455— This O8V has two data from Keck, 3 from WIYN, and 20 from WIRO between 1999 and 2013. The mean velocity is -12.2 km s^{-1} with and rms of 3.3 km s^{-1} and a mean velocity uncertainty of 3.6 km s^{-1} .

MT91 462— This O7III has 12 data from from WIRO between 2008 and 2014. The mean velocity is -11.9 km s^{-1} with and rms of 2.8 km s^{-1} and a mean velocity uncertainty

of 4.1 km s^{-1} .

MT91 470—Two measurements from Keck, five from WIYN, and nine from WIRO over the the period 1999–2013 show no evidence for velocity variations beyond the uncertainties. The mean velocity is -21.3 km s^{-1} with an rms of 6.9 km s^{-1} and a mean velocity uncertainty of 5.2 km s^{-1} .

MT91 480—We measured both He I and He II velocities for this broad-lined O7V using 4 WIYN and 14 WIRO data between 2001 and 2013, finding no compelling evidence for velocity variations. The line profiles are broad and appear to vary without evidence of periodicity. The mean velocity is -16.2 km s^{-1} with an rms of 13.3 km s^{-1} and a mean velocity uncertainty of 11.7 km s^{-1} .

MT91 507—Two Keck, two WIYN, and 14 WIRO data between 1999 and 2013 yield a mean velocity of -8.9 km s^{-1} with an rms of 5.1 km s^{-1} and a mean velocity uncertainty of 6.5 km s^{-1} for this O9V star.

MT91 534—Three Keck, two WIYN, and 14 WIRO data between 1999 and 2013 yield a mean velocity of -5.0 km s^{-1} with an rms of 3.8 km s^{-1} and a mean velocity uncertainty of 3.1 km s^{-1} for this O8.5V star.

MT91 611—Two Keck and 14 WIYN data between 1999 and 2008 yield a mean velocity of -23.1 km s^{-1} with an rms of 3.7 km s^{-1} and a mean velocity uncertainty of 3.9 km s^{-1} for this O7V.

3.4. Survey Summary To Date

The Cygnus OB2 Radial Velocity Survey was designed to produce a complete census of massive binaries drawn from a photometrically selected sample, namely that of Massey & Thompson (1991). The parent sample contained 150 stars—the 146 listed in Table 1 of Paper I plus MT91 267 (inadvertently excluded initially but reported as a binary in Paper VI), MT91 417B (not initially recognized as a close companion to MT91 417A), Schulte #3 and Schulte #73. Of these 150, six were found to be probable emission-line objects (MT91 186, 213, 488, 522, 650, 793) and excluded from further observation because radial velocities were considered unreliable. Another 16 objects were determined to have spectral types later than B3 and excluded from further observation (MT91 170, 189, 196, 222, 239, 271, 273, 427, 444, 453, 459, 493, 539, 554, 576, 641). This leaves 128 objects in the “unbiased” survey sample that we deem to be the complete photometrically selected targets.

In the above sections we identified 6 systems (4.6%), all supergiants, as exhibiting irregular velocity variation and 16 objects (12.5%) as consistent with having no intrinsic velocity variability. Forty-five objects of the 128 in the complete unbiased sample (35.1%) have orbital solutions presented either in this work or previous papers in this series. This leaves 63 systems (about half) that have insufficient data to make a reliable determination. The vast majority of these are B1–B2.5 primaries, although a few O stars remain in this category because there are fewer than 12 spectra of suitable quality. The average number of spectra among the 62 “indeterminate” systems is five. None have evidence for significant velocity variations. We expect that most of these will turn out to be constant-velocity objects, but we also anticipate discovery of a handful of new binaries in future observing seasons. We expect most of these to be long-period and/or high-eccentricity systems that have eluded detection because of limited data. Nevertheless, the completeness analysis in Section 3.5 leads us to conclude that the vast majority of the detectable binaries in Cyg OB2 now have complete orbital solutions, as published herein.

3.5. Modeling the Survey Completeness

We estimated the completeness of the Survey as a function of orbital period using a Monte Carlo analysis identical to that described in Kiminki & Kobulnicky (2012). Our code generates populations of binary systems with periods 1 – 5000 days having mass ratios and eccentricities described by power laws: $\text{Prob}(q) \propto q^\alpha$, and $\text{Prob}(e) \propto e^\gamma$. The nominal power-law exponents are $\alpha \simeq 0$ and $\gamma \simeq 0$, as inferred, in part, by Kiminki & Kobulnicky (2012) and strengthened by the additional data in this work. A random inclination is assigned to each system before being sampled at the actual dates and times of the Survey observations. A nominal detection threshold of 7 km s^{-1} is used to determine whether the system would be observed as a binary in the Survey. This is lower than the more conservative value of 15 km s^{-1} used in Kiminki & Kobulnicky (2012), but it better represents the sensitivity of the data to radial velocity variability given the typical resolutions of $R \simeq 4500$ (60 km s^{-1} FWHM) achieved in the majority of WIRO spectra. Velocity precisions of better than 0.1 of the spectral FWHM are typically attained by centroiding on the strong He I $\lambda 5876$ feature. Precisions are 8–15 km s^{-1} in some objects where rotation broadens the line profile. Upon careful examination, the detection threshold is really a complex function of the signal-to-noise ratio of the spectra, the spectral type of the star, and the breadth of the spectral features (i.e., rotational velocity); nevertheless, the adopted value of 7 km s^{-1} is generally applicable as a Survey average, while 15 km s^{-1} is a conservative value.

Figure 26 displays the completeness as a function of orbital period, where completeness

is defined as the ratio of detected binaries to all binaries of the same period in the synthesized population. Different line styles depict different values for the power law exponent γ and different choices for the detection velocity threshold. Completeness exceeds 80% for systems with $P < 100$ days in the case of a 7 km s^{-1} detection threshold and is only $\sim 10\%$ lower for the conservative threshold of 15 km s^{-1} . At $P=1000 \text{ d}$ we find that 40–60% of binaries are still detected. The smooth decline in completeness with orbital period reflects the difficulty in detecting wide, long-period systems. While the completeness estimates are only as valid as the input power-law assumptions for the mass ratio and period distributions, the conclusion that the vast majority of systems with periods less than a few hundred days have been detected is a robust one. Completeness estimates beyond about 2000 d should be regarded as highly uncertain.

4. Discussion and Analysis of the Orbital Parameters from Cyg OB2

4.1. Summary of Binaries

Table 8 summarizes the spectroscopic binary type (SB1/SB2), spectral types for the components, orbital period, primary semi-amplitude, eccentricity, and mass ratio constraints for all 48 massive multiple systems now known in Cygnus OB2. Twenty three are new results from this work, twenty are reported in previous papers in this series, and five stem from other published works. The final two columns provide references to published orbital solutions and additional notes on each system. The table contains six stars not initially included in Table 1 of Kiminki et al. (2007) among the unbiased list survey targets. MT91 267 and MT91 417B, explained in Section 3.4 constitute two of these. The double-lined system CPR2002 B17 was reported and analyzed by Stroud et al. (2010). Schulte #5 has been known as a binary since Wilson (1948). CPR2002 A36 and A45 were added later after being reported as suspected binaries. In summary, Schulte #5, CPR2002 A36, CPR2002 A45, and CPR2002 B17 should not be included in the “unbiased” sample used to estimate binary fractions because they were targeted only after evidence of their binary nature became known.

The compilation of 48 targets in Table 8 includes 16 SB2 and 32 SB1 systems. Fourteen contain at least one evolved component. Eight are probable triple systems based on either radial velocity data or high-angular-resolution imaging (see discussion in Section 3). Eight are known to show eclipses.

Figure 27 plots eccentricity (top panel) and mass ratio (lower panel) versus orbital period for all 48 massive binaries. Filled circles mark SB2 systems and open circles denote SB1 systems from Cyg OB2. Pluses show the O-star binaries from Sana et al. (2012). Error

bars in the lower panel illustrate the range of mass ratios allowed by the available constraints on orbital inclination. Statistically, systems will preferentially lie toward the lower end of this range since it is more likely to observe the orbital plane edge-on than face-on. The overall trend in the top panel has been noted elsewhere. The shortest-period systems have low eccentricities while longer-period systems have larger eccentricities. Any trend in the lower panel is less obvious. Mass ratios span the the range from near 1.0 for some of the shortest-period systems to about 0.1, the approximate lower limit detectable by the velocity precision of the Survey. Long-period systems generally have weak constraints on the eccentricity and mass ratio as a result of incomplete phase coverage. The two samples plotted here are affected by different target selection, sampling, and sensitivity biases, so appropriate caution should be exercised in attempts to statistically compare them. Nevertheless, the distribution of points among the two samples is similar.

4.2. The Eccentricity Distribution

Figure 28 shows the observed distribution of orbital eccentricities for the full sample of 48 Cyg OB2 binaries. The left-hand y-axis labels and the plotted points shows the cumulative fraction. The right-hand y-axis and plotted histogram shows the number of objects in each eccentricity bin. The distribution is approximately uniform ($\text{Prob}(e) \propto e^0$) between $e = 0$ and $e \simeq 0.6$. A two-sided Kolmogorov-Smirnov (K-S) test indicates that the eccentricities have a 75% chance of being drawn from the a uniform distribution between the limits $0.1 < e < 0.6$. We also employed the Anderson-Darling (A-D) two-sample statistic³ which is more sensitive to differences between two populations when differences in the the cumulative distributions are both positive and negative across the sample range, or when these differences occur near the ends of the distributions. The A-D statistic concurs that the probability of the eccentricities being drawn from a uniform distribution between $0.1 < e < 0.6$ is 75%. However, over the full eccentricity range there is an overabundance of $e < 0.1$ systems compared to a uniform distribution. The paucity of points at high eccentricity may partly be an observational bias against detecting highly eccentric systems, and it may partly reflect a real dearth of such loosely bound, easily disrupted systems. Our completeness analysis above assumes two different values, 0 and -0.6 (the nominal value from Kiminki & Kobulnicky 2012), for γ , the power law exponent describing the eccentricity distribution. Completeness is shown to be insensitive to γ . Nevertheless, a few long-period, high-eccentricity systems

³ The Anderson-Darling statistic and its advantages over the K-S statistic are described in more detail at Feigelson & Babu (2012). We use the code in the Python `scipy.stats` package to compute the A-D probabilities.

have likely evaded detection with the current dataset. Unless there are an disproportionate number of high- e systems in Cyg OB2, the e distribution can be described as approximately uniform out to periods of ~ 1000 days.

4.3. The Mass Ratio Distribution

The distribution of mass ratios among our sample can be recovered, statistically, using Monte Carlo methods, by assigning randomly chosen inclinations on the unit sphere. In most cases an upper limit on the inclination is estimated by either the observed eclipse profile or the lack of observed eclipses; for long-period systems the upper limit on the inclination is effectively 90° . A lower limit on the inclination is obtained by letting the mass of the secondary approach that of the primary; the lack of observed spectral features from a secondary star is a weak constraint on this lower bound. For each system we use the measured orbital period, adopted primary mass, observed velocity amplitude, and a random inclination between the observationally imposed limits to solve for the mass of the secondary star. The mean value of q is then computed after 1000 such iterations for each system. Figure 29 shows the resulting histogram of mass ratios. The overall distribution is approximately uniform. However, incompleteness appreciably affects the bins at $q \lesssim 0.2$, so the true number of binaries in these bins is highly uncertain. Given the large uncertainties on any individual mass ratio value, we elect not to pursue a statistical analysis of these data. In principle we could estimate the completeness factor at $q < 0.2$ given assumptions about the functional form of the underlying secondary mass distribution and period distribution (e.g., by adopting a power law distribution, following Kobulnicky & Fryer (2007); Kiminki & Kobulnicky (2012); Sana et al. (2012)). However, as we will show below, the true distribution of orbital parameters, in particular the periods, may not be a single power law.

4.4. The Orbital Period Distribution

4.4.1. General Characteristics

Figure 30 displays the observed cumulative distribution of orbital periods (in $\log P$) for the full sample of 48 massive (B3 and earlier) systems in Cyg OB2 (filled circles), O stars from six Galactic open clusters (Sana et al. 2012, plusses), and bright O stars drawn from the general Galactic population from Garmany et al. (1980, open squares). Fiducial marks near the top of the plot indicate the period in days. Other annotations mark the corresponding semi-major axis for the given period, assuming a total system mass of $30 M_\odot$.

The Garmany et al. (1980) sample has been normalized by a factor of 1.5 to allow better comparison with the other two surveys in the short-period limit where all three are highly complete. Both the Sana et al. (2012) sample and the Cyg OB2 sample are reasonably complete to periods of several hundred days, while the Garmany et al. (1980) sample lacks such longer-period systems—a consequence of the limited observing campaign. A constant slope in this plot corresponds to a uniform distribution in $\log P$. A steeper slope means a larger number of detected binaries per $\log P$ interval than a shallower slope.

The observed cumulative period distributions for the three samples appear remarkably similar at short periods, rising rapidly with similar slope from a short-period limit of about 1.4 days to near 7 days. An A-D test shows that the Cyg OB2 and Sana et al. (2012) observed distributions have a 91% chance of being drawn from the same parent populations in this range, increasing to 97% if the complete instead of the unbiased Cyg OB2 sample is used. All three samples show an abundance of short-period binaries, noted previously by Kiminki & Kobulnicky (2012); Sana et al. (2012); Zinnecker & Yorke (2007). All three samples also show a flattening of the slope beginning at about 6 days. The Cyg OB2 sample exhibits the most pronounced flattening between 6 and 14 days, indicating a paucity of systems in this range, as noted previously by Kiminki & Kobulnicky (2012). There is then an upturn between 14 and ~ 45 days, with a slope approximately matching that of the very short-period systems. The Sana et al. (2012) and Garmany et al. (1980) samples, by contrast, show lesser degrees of flattening longward of six days, with the former being steeper than the latter. The limited number of data points precludes any strong statement regarding the similarity of the three samples in this restricted range, or the reality of the change in slope near six days.

Both the Cyg OB2 and the Sana et al. (2012) samples flatten or exhibit a break near 45 d. The Garmany et al. (1980) sample has become considerably incomplete at these periods and is not considered further. Both samples exhibit similar slopes out to periods of several thousand days where both become significantly incomplete. Sana & Evans (2011) and Sana et al. (2012) considered the possibility that period distribution could be characterized by a double-Öpik (i.e., uniform in $\log P$; Öpik 1924) distribution with a break near 10 days, however they found that such a description did not provide a better fit to the data. Corrections for observational bias (i.e., incompleteness) become important at periods greater than several hundred days, and we address these in the context of the Cyg OB2 sample below.

4.4.2. *Statistical Analysis in the Short-Period and Long-Period Regimes*

A two-sample Anderson-Darling⁴ test shows that the Cyg OB2 and the Sana et al. (2012) observed cumulative distributions are individually consistent with uniform (in log P given by $\beta = 0$) between 1.4 and 45 days at the 42% and 45% levels, respectively; the Cyg OB2 and Sana et al. (2012) samples becomes consistent with uniform at the 86% and 62% level for periods <25 days. The Cyg OB2 and Sana et al. (2012) samples are consistent with each other at the 91% levels for $P < 25$ d but only 19% for $P < 45$ d. The Cyg OB2 and the Garmany et al. (1980) samples are consistent with each other at the 40% and 5% levels for upper period limits of 25 d and 45 d, respectively. Taken together, these statistics indicate that the period distributions in the Cyg OB2 and Sana et al. (2012) surveys are probably consistent with each other $P < 25$ d, but not at $P > 25$ d and are not consistent with a uniform distribution even at the shortest periods.

When all three surveys are combined, the probability that the combined sample is consistent with uniform drops to 14% and 21% for upper period limits of 25 d and 45 d, respectively. We interpret this to be evidence for structure in the period distribution that becomes apparent with sufficiently large numbers. Thus, the period distribution does not appear to be scale-free; it is suggestive of features imposed by physical phenomena occurring during the formation and/or evolution of massive systems.

The most obvious feature in the period distribution at $P < 45$ d is the flattening of the slope near 6 days seen in all three datasets. Kiminki & Kobulnicky (2012) characterized this structure as a possible excess of 3–6 d systems accompanied by a deficit of 7–14 d systems, observed here as a flattening of the slope of the cumulative distribution over that range in all three samples. This possible feature seen in the Cyg OB2 distribution is not as obvious in the other two data sets. Incompleteness in Garmany et al. (1980) sample, though not explicitly quantified in that work, probably begins in the 15–30 d range and could easily mask such a signal if it were present. By contrast, the completeness of the Cyg OB2 survey is $>90\%$ for $P < 10$ d. The reality of such a signal in the Sana et al. (2012) sample is uncertain owing to the small number of points between 6 d and 45 d (10 systems), even though the sample is likely to be similarly complete. We conclude that the Cyg OB2 period data is not convincingly consistent with uniform (a single power law of slope zero) at $P < 45$ d. There is

⁴We use the Anderson-Darling statistic exclusively hereafter in lieu of the more popular but more problematic Kolmogorov-Smirnov statistic. We find that the K-S statistic yields similar probabilities to the A-D statistic when the cumulative distributions are smooth; the A-D statistic yields lower probabilities of the null hypothesis that the two distributions are drawn from the same parent population when the cumulative distributions show multiple points of inflection. This is consistent with the discussion in Feigelson & Babu (2012).

evidence for structure in the form of a 3–6 d period ”excess” and the 6–14 d period “deficit” that becomes more pronounced when the three samples are combined.

In the period range 60 – 4000 d the Cyg OB2 and Sana et al. (2012) samples, as observed, are consistent with uniform at the 94% and 55% levels. The two samples are consistent with each other at the 99% level. By contrast, over the full period range 1.4 – 5000 days, both samples are inconsistent with uniform, having a $<0.01\%$ chance of being drawn from such a distribution. The single $\beta = 0$ power law is a poor description of the observed period distribution over the full range, but observational biases against detection of long-period systems must be considered before strong conclusions may be drawn.

4.4.3. *The Period Distribution Corrected for Survey Completeness*

Figure 31 (lower panel) shows the observed cumulative period distribution for the unbiased sample of 45 systems as observed (filled symbols) and after correction for completeness (open symbols) as described by completeness curve in Figure 26 using the solid line representing the 15 km s^{-1} (most conservative) detection threshold. The y-axis is now scaled to indicate the fraction of the total number of stars in the unbiased Cyg OB2 sample. The correction from observed to underlying period distribution is performed by tabulating the cumulative incompleteness (1-completeness) at the location of each observed system, N , starting from the shortest periods, and inserting an additional “system” when the cumulative incompleteness reaches an integer value; systems are added at periods halfway between the period of system N and $N-1$. This can result in the appearance of two or more systems plotted at the same orbital period when the completeness is low (i.e., for long periods).

Open symbols in Figure 31 trace a curve similar to the filled symbols until the correction for completeness becomes a large factor beyond about 2000 days. The difference between the filled and open symbols is small for periods less than a few hundred days but approaches 20% at the 5000-day limit of the Survey. The open symbols display an apparent change in slope near 45 days, indicating that the putative break in the cumulative distribution is not likely to be caused by observational biases. Under the adopted prescriptions for the mass ratio distribution (i.e., uniform) and the eccentricity distribution (i.e., uniform) adopted in the Monte Carlo modeling, this figure shows that the binary fraction reaches 30% by $P=45$ d. Fifty-five percent of the systems are binaries with periods less than 5000 days. This is nearly identical to the binary fraction of 51% computed for O stars in the Large Magellanic Cloud (Sana et al. 2013) and may indicate that the binarity characteristics of massive stars are insensitive to metallicity. An extrapolation of the quasi-linear trend defined by systems with $P > 100$ days would suggest a binary fraction near 70% for systems with periods less

than 10^5 days. On the other hand, a naive extrapolation of the much steeper slope at $P < 45$ days would reach a binary fraction of 100% near 10^5 days.

We used the A-D test to quantify the probability of a change in slope of the completeness-corrected cumulative period distribution by comparing it to a hypothetical uniform (i.e., linear) distribution in a moving window of encompassing seven observed systems. Window widths of five to nine do not appreciably change the results. Figure 31 (upper panel) plots the probability that the completeness-corrected period distribution is consistent with uniform. The probability drops below 1% (2.6σ , shown by the dotted horizontal line) in the vicinity of the hypothesized 45-day break. The low probability near six days and 14 days supports the hypothesis of a change slope near these locations as well. The similarity of the Cyg OB2 and the Sana et al. (2012) observed cumulative distribution slopes above 45 days in Figure 30 is noteworthy as is the apparent flattening near 45 days ($\simeq 0.9$ A.U.). The shallower slope above 45 d may indicate either a decreasing binary fraction for systems with semi major axes of >1 A.U. Alternatively, it may indicate a change in the distribution of secondary star masses toward a preference for lower masses.

We interpret the evidence for structure in the cumulative period distribution as an indication that the processes responsible for setting massive binary separations are not scale-free. Nevertheless, we investigated whether a single power law might at least approximate the data. The solid curve in the lower panel of Figure 31 is a best-fit single $\beta = -0.22$ power law to the completeness-corrected data over the range 1.4–2000 d. The completeness correction is highly uncertain beyond 2000 d, so we do not consider this regime in the fit. An A-D test indicates a 24% probability that the data is drawn from such a single power-law distribution. This probability does not constitute strong evidence in favor of this particular power law, especially given that the results are sensitive to the magnitude of the completeness corrections required for long-period systems. Nevertheless, the $\beta \simeq -0.22$ power law is not an unreasonable *approximation* over 3.3 orders of magnitude in period (1.4 days to 2000 days), even if it does not describe the fine details of the distribution at a statistically compelling level of significance.

We conclude by noting that the agreement between the observed orbital period distributions of the Cyg OB2 sample, where OB stars formed across an extent of nearly 50 pc, compared to the Sana et al. (2012) sample from several young Galactic clusters, suggests that the large-scale physical environment does not determine the orbital parameters of massive binaries formed therein. This stands in contrast to suggestions that the binary fraction depends on local stellar density, being lower in the densest regions (Sana et al. 2008; Zinnecker & Yorke 2007). Rather, the small-scale physics of cloud collapse and fragmentation on the sub-A.U. scale appear more important in establishing the high fraction of

binaries among massive stars and their mass ratio distribution which clearly shows that massive stars preferentially have massive companions. The results of the massive star surveys stand in stark contrast to those from radial velocity surveys of solar-type stars where the distribution of periods is log-normal with a mean of 180 years (Duquennoy & Mayor 1991). The inflections in the cumulative period distribution near 0.2 A.U. and near 0.9 A.U. are suggestive of key physical size scales beyond which the formation of close massive binaries becomes less efficient.

5. Conclusions

The addition of 23 new massive binary orbital solutions presented herein raises the total number known in the Cygnus OB2 Association to 48. This is the largest collection of complete solutions obtained within a single environment and constitutes a substantial fraction of all early type orbits published to date. At least 35% of massive systems in Cyg OB2 are binary or higher-order multiples, with several more long-period or highly eccentric systems expected to be discovered. The number of unobserved high-inclination or extreme-mass-ratio systems has been modeled statistically. These computations suggests that the true binary fractions are near 55% for periods $P \leq 5000$ d, nearly identical to the results from O stars in the LMC, suggesting a degree of metallicity independence. Extrapolation to longer periods suggests binary fractions in the range 65–80% for periods $P < 10^4$ d.

The distribution of orbital periods is described as approximately uniform in $\log P$ between the short-period limit of 1.2 d and $\simeq 45$ d, but there is evidence for structure in this distribution, with an excess of 3–6 d systems and a possible dearth of 7–14 d systems, along with a break near 45 days. Between 45 d and the long-period survey limit of ~ 5000 d the distribution is also approximately uniform, but with either a lower binary fraction or a population of secondary masses favoring lower-mass companions compared to the 1–45 d subsample. No single power-law distribution describes the period data at a statistically significant level. A single power law of slope $\beta = -0.22$ also provides a rough description of the cumulative period distribution between 1.4 and ~ 2000 d if structure in the distribution is ignored. The statistical power of even the present completeness-corrected sample has not yielded a convincing power-law or other analytic description of the present-day binary period distribution. It seems likely that evolutionary effects such as period migration and stellar mergers have altered the primordial distributions to the ones observed as the present-day distributions in the 3–4 Myr old Cygnus OB2 Association and other young O-star cluster. Such evolutionary effects may occur during the pre-main-sequences phases, rendering any simple primordial distribution unobservable even in principle.

One goal of this work is to provide a robust measure of massive binary parameters to help inform stellar population synthesis models, including those used to predict cosmic rates of high-energy phenomena such as supernova and γ -ray bursts. It is our hope that such models may now be grounded more solidly in the data. This compilation may also prove helpful in guiding models of massive star formation and evolution by providing observational constraints on the binary frequency and distribution of periods and mass ratios among early-type systems. We expect that there are several more discoverable binary (and multiple) systems among the Survey targets, but this present compilation likely contains the vast majority of systems discoverable using radial velocity techniques.

Insightful comments from an expert anonymous referee greatly improved this manuscript. We thank our long-term collaborator Chris Fryer for continued encouragement, in particular for a timely conversation after a colloquium at UC Santa Cruz in 1998 that launched the Cygnus OB2 Radial Velocity Survey. We acknowledge continued support from the National Science Foundation through Research Experience for Undergraduates (REU) program grant AST 10-63146, through grant AST 03-07778, and grant AST 09-08239. The Wyoming NASA Space Grant Consortium provided student support through grant #NNX10A095H. We thank Tyler Ellis, Sarah Eftekharzadeh, Ian Ewing, and Garrett Long for assistance with observing at WIRO. We are grateful to WIRO staff James Weger and Jerry Bucher whose diligent support work enabled this program to obtain spectra on more than 290 nights at the Wyoming Infrared Observatory 2.3 m telescope. Generous allocations of telescope time at the Lick and Keck telescopes through the University of California and at the WIYN 3.5 m telescope through NOAO and the University of Wisconsin made possible such a large observational project. Some of the data presented herein were obtained at the W.M. Keck Observatory, which is operated as a scientific partnership among the California Institute of Technology, the University of California and the National Aeronautics and Space Administration. The Observatory was made possible by the generous financial support of the W.M. Keck Foundation. The WIYN Observatory is a joint facility of the University of Wisconsin-Madison, Indiana University, Yale University, and the National Optical Astronomy Observatory.

Facilities: WIRO (), WIYN (), Keck:I ()

REFERENCES

- Blaauw, A. 1961, BAN, 15, 265
- Chini, R., Hoffmeister, V. H., Nasserri, A., Stahl, O., & Zinnecker, H. 2012, MNRAS, 424, 1925

- Comerón, F., Pasquali, A., Rodighiero, G., et al. 2002, *A&A*, 389, 874
- Contreras, M. E., Rodriguez, L. F., Tapia, M., Cardini, D., Emanuele, A., Badiali, M., & Persi, P. 1997, *ApJ*, 488, 153
- De Becker, M., Rauw, G., & Manfroid, J. 2004, *A&A*, 424, L39
- Dominik, M., Belczynski, K., Fryer, C., Holz, D. E., Berti, E., Bulik, T., Mandel, I., & O’Shaughnessy, R. 2013, arXiv:1308.1546
- Drilling, J. S., & Landolt, A. U. 2000, in *Astrophysical Quantities*, ed. A. N. Cox (4th ed.; New York; Springer), 381
- Duquennoy, A., & Mayor, M. 1991, *A&A*, 248, 485
- Eldridge, J. J., Fraser, M., Smartt, S. J., Maund, J. R., & Crockett, R. M. 2013, *MNRAS*, 436, 774
- Feigelson, E. D. & Babu, G. J., 2012, “Modern Statistical Methods for Astronomy with R Applications”, Cambridge Univ Press (Chpt 3)
- Fullerton, A. W., Gies, D. R., & Bolton, C. T. 1996, *ApJS*, 103, 475
- Fryer, C. L., Mazzali, P. A., Prochaska, J., et al. 2007, *PASP*, 119, 1211
- Garmany, C. D., Conti, P. S., & Massey, P. 1980, *ApJ*, 242, 1063
- Gies, D. R., & Bolton, C. T. 1986, *ApJS*, 61, 419
- González, J. F., & Levato, H. 2006, *A&A*, 448, 283
- Hall, D. S. 1974, *AcA*, 24, 69
- Hanson, M. M. 2003, *ApJ*, 597, 957
- Hoogerwerf, R., de Bruijne, J. H. J., & de Zeeuw, P. T. 2001, *A&A*, 365, 49
- Hora, J., Adams, J., Allen, L., et al. 2007, *Spitzer Proposal*, 40184
- Hubeny, I., & Lanz, T. 1995, *ApJ*, 439, 875
- Hunter, I., Lennon, D. J., Dufton, P. L., et al. 2008, *A&A*, 479, 541
- Kiminki, D. C. 2010, Ph.D. Thesis, University of Wyoming
- Kiminki, D. C., et al. 2007, *ApJ*, 664, 1120 (Paper I)

- Kiminki, D. C., McSwain, M. V., & Kobulnicky, H. A. 2008, *ApJ*, 679, 1478 (Paper II)
- Kiminki, D. C., Kobulnicky, H. A., Gilbert, I., Bird, S., Chunev, G. 2009, *AJ*, 137, 4608 (Paper III)
- Kiminki, D. C., Kobulnicky, H. A., Ewing, I., et al. 2012, *ApJ*, 747, 41 (Paper IV)
- Kiminki, D. C., & Kobulnicky, H. A. 2012, *ApJ*, 751, 4 (Paper V)
- Kobulnicky, H. A., & Fryer, C. L. 2007, *ApJ*, 670, 747
- Kobulnicky, H. A., Smullen, R. A., Kiminki, D. C., et al. 2012, *ApJ*, 756, 50 (Paper VI)
- Kobulnicky, H. A., Kiminki, D. C., et al. 2014, *ApJ*, in prep
- Kouwenhoven, M. B. N., Brown, A. G. A., Portegies Zwart, S. F., & Kaper, L. 2007, *A&A*, 474, 77
- Lanz, T., & Hubeny, I. 2003, *ApJS*, 146, 417
- Markwardt, C. B. 2009, *Astronomical Data Analysis Software and Systems XVIII*, 411, 251
- Martins, F., Schaerer, D., & Hillier, D. J. 2005, *A&A*, 436, 1049
- Mason, B. D., Hartkopf, W. I., Gies, D. R., Henry, T. J., & Helsel, J. W. 2009, *AJ*, 137, 3358
- Massey, P., & Thompson, A. B. 1991, *AJ*, 101, 1408
- Miczaika, G. R. 1953, *PASP*, 65, 141
- Nazé, Y., De Becker, M., Rauw, G., & Barbieri, C. 2008, *A&A*, 483, 543
- Nazé, Y., Mahy, L., Damerdji, Y., et al. 2012, *A&A*, 546, A37
- Nomoto, K. I., Iwamoto, K., & Suzuki, T. 1995, *Phys. Rep.*, 256, 173
- Öpik, E. J. 1924, *Tartu Obs. Publ.*, 25
- Otero, S. 2008a, *Open European Journal on Variable Stars*, 83, 1
- Otero, S. 2008b, *Open European Journal on Variable Stars*, 91, 1
- Pigulski, A., & Kolaczowski, Z. 1998, *MNRAS*, 298, 753
- Rauw, G., Vreux, J. M., & Bohannan, B. 1999, *ApJ* 517, 416

- Rios, L. Y., & DeGioia-Eastwood, K. 2004, BAAS, 205, No. 09.05
- Romano, G. 1969, MmSAI, 40, 375
- Sana, H., & Evans, C. J. 2011, IAU Symposium, 272, 474
- Sana, H., Gosset, E., Nazé Y., Rauw, G., & Linder, N. 2008, MNRAS, 386, 447
- Sana, H., de Mink, S. E., de Koter, A., et al. 2012, Science, 337, 444
- Scappini, F., Cecchi-Pestellini, C., Casu, S., & Olberg, M. 2007, A&A, 466, 243
- Sana, H., de Koter, A., de Mink, S. E., et al. 2013, A&A, 550, A107
- Schulte, D. H. 1958, AJ, 128, 41
- Smartt, S. J., Eldridge, J. J., Crockett, R. M., & Maund, J. R. 2009, MNRAS, 395, 1409
- Smith, R. J., Longmore, S., & Bonnell, I. 2009, MNRAS, 400, 1775
- Smith, N. 2014, arxiv.org/abs/1402.1237
- Stroud, V. E., Clark, J.S., Negueruela, I. , Roche, P., & Norton, A.J. 2009, A&A, 511, 84
- van den Heuvel, E. P. J. 1983, Accretion-Driven Stellar X-ray Sources, 303
- Vogt, S. S., & Penrod, G. D. 1983, ApJ, 275, 661
- Walborn, N. R. 1973, ApJ, 180, L35
- Walborn, N. R. & Fitzpatrick, E. L. 1990, PASP 102, 379
- Wilson, O. C. 1948, PASP, 60, 385
- Wilson, O. C., & Abt, A. 1951, ApJ, 144, 477
- Woosley, S. E., & Bloom, J. S. 2006, ARA&A, 44, 507
- Wozniak, P. R., et al. 2004, AJ, 127, 2436, Northern Sky Variability Survey: Public Data Release
- Zinnecker, H., Yorke, H. W. 2007, ARA&A, 45, 481

A. Re-analysis of Orbital Solutions for Systems from Papers II and III

In this Appendix we briefly re-analyze systems originally presented in Papers II and III for purposes of self-consistency, using the methods employed in this work and incorporating any new spectra, when available. Most of the solutions are essentially unchanged, but results are presented in a manner consistent with the solutions reported in Papers IV, VI, and in this contribution. In three cases (MT91 252, S 73, CPR2002 A45), additional data allowed us to discover that the original solutions were aliases and to present a better solution.

In this work, we disentangled the component spectra of double-lined binaries using the method of González & Levato (2006). One of the strengths of this method is that the radial velocities can be refined via cross correlation after each iteration (i.e, cross-correlating the the residual spectra with the resultant component spectrum as the template). The cross-correlated velocities generally have smaller uncertainties and utilize more lines, leading to a better measurement of the true stellar velocity and the binary systemic velocity.

MT91 059—Table 9 lists the updated ephemeris and Table 10 provides refined orbital elements for the single-lined binary MT91 059 originally presented in Paper II. Figure 32 displays the best-fitting solution and folded velocity data. The original period of 4.85 d is changed only slightly, but we note here the large reduced χ^2 of 4.3 that indicates either an additional velocity component or photospheric variability. Attempts to identify periodicities in the observed-minus-computed velocities in Table 9 did not yield convincing evidence for an additional velocity component. Hints of emission in the cores of the He I $\lambda 4471$ lines seen in our two high-resolution spectra from Keck support the possibility of extra-photospheric variability, perhaps as part of an accretion stream in this close (~ 0.18 A.U.) binary.

MT91 145—Table 9 lists the updated ephemeris and Table 10 provides refined orbital elements for this single-lined O9II star originally presented in Paper III. The orbital elements are only slightly revised from the original published estimate. Figure 33 displays the best-fitting solution and folded velocity data.

MT91 252—We identified this system as an SB2 in Paper II but could only perform a limited analysis owing to the small number of spectra and low SNR of the data. Using the technique described in this paper, we included 17 epochs of WIRO spectra and a KECK+HIRES spectrum to compute the solution listed in Table 11. The previously estimated period of 18–19 days has been revised to 9.558 ± 0.001 days. The power spectra for both components showed an alias at ~ 11.4 days. However, the folded velocity curve showed significantly higher scatter and was ruled out. Figure 34 shows the computed solution. No revisions to the estimated spectral classifications are provided. By adopting a mass of 11–14 M_{\odot} for the B1–2V components, the period and velocity amplitudes imply an inclination

between 30 and 40 degrees.

MT91 258—Originally presented as an SB1 in Paper II, the updated ephemeris for this 14.658 d O8V appears in Table 9 and the orbital parameters appear in Table 10. Figure 35 displays the best-fitting solution and folded velocity curve. We attribute the unusually high reduced χ^2 value to velocity zero point differences between data from different observatories used in the solution.

MT91 372—Identified as a 2.2 d binary in Paper III, this eclipsing double-lined system is analyzed in greater detail in conjunction with the eclipsing binary distance to Cygnus OB2 in a forthcoming work (Kobulnicky et al. 2014).

MT91 696—An updated ephemeris for this eclipsing O9.5+B0V+B? triple system from Paper IV will be presented in (Kobulnicky et al. 2014).

Schulte #3—An updated ephemeris for this eclipsing O6IV: + O9III system from Paper II will be presented in (Kobulnicky et al. 2014).

Schulte #73—This system was identified as a 17.28 day SB2 in Paper III. Velocities remeasured with the technique described in Papers IV, VI, and this work were used as the initial guesses for the González & Levato (2006) method of spectral deconvolution and cross correlation for all WIRO data. Owing to the limited phase coverage of the WIYN+Hydra spectra, we did not apply the González & Levato (2006) method to these data. However, since the He I 5876Å velocities show a strong linear correlation with the final cross-correlation velocities, we used this correlation to correct the WIYN He I 4471Å velocities. The final WIRO+WIYN data yielded a period 34.88 days. The power spectra showed additional strong signals at ~ 10 days, ~ 17 days, ~ 57 days, and ~ 67 days. However, these were ruled out based on the large scatter in the corresponding folded velocity curves. The updated solution is provided in Table 11 and shown in Figure 36. We slightly revise the spectral classifications, based on equivalent width ratios of He II 5411Å to He I 5876Å, as O8.5III: and O9.0III:. Using the theoretical masses from Martins et al. (2005), these classifications indicate that the system has an inclination near $\sim 40^\circ$.

CPR2002 A36—An updated ephemeris for this eclipsing B0Ib + B0III system from Paper III will be presented in (Kobulnicky et al. 2014).

CPR2002 A45—Also identified as an SB2 in Paper III, this system was previously listed with a period of 2.884 days and an uncharacteristically high eccentricity of 0.273. Using the González & Levato (2006) spectral deconvolution method and some additional observations from WIRO, the revised radial velocities indicate a period near half the original solution. Both components’ power spectra show a singular strong signal at 1.5020 days. The

final combined solution yields a period of 1.50181 ± 0.00004 d and a considerably smaller eccentricity of 0.05 ± 0.02 . The revised solution is listed in Table 11 and shown in Figure 37. We retain the primary spectral classification of B0.5V, but owing to the new, higher mass ratio of $0.72 \sim 0.02$, we revise the secondary spectral classification to B1V–B2V. Based on the theoretical masses for stars of this type, we estimate an inclination between 40 and 45° .

Table 1. Ephemerides for New Binary Systems

Date (HJD-2,400,000)	ϕ	V_{r1} (km s ⁻¹)	σ_V (km s ⁻¹)	$O_1 - C_1$ (km s ⁻¹)
MT91 021				
55418.648	0.367	-37.9	18.0	-0.20
55489.731	0.695	1.9	17.9	-4.77
55780.694	0.691	11.6	6.4	5.47
55791.720	0.828	20.8	4.2	-1.34
55805.681	0.267	-41.1	6.1	7.09
56209.582	0.906	18.7	5.3	-1.94
56215.552	0.522	-27.4	5.4	-9.83
56446.902	0.372	-38.0	8.7	-1.02
56461.683	0.896	48.6	10.6	26.77
56463.804	0.115	-51.8	6.9	-4.22
56466.758	0.419	-29.4	10.1	1.77
56470.764	0.832	8.8	6.2	-13.63
56472.721	0.034	-21.3	8.7	2.25
56566.728	0.726	32.1	7.3	21.15
MT91 187				
51467.858	0.166	-11.7	2.1	-0.85
51805.908	0.149	-8.8	4.1	1.55
52146.686	0.333	-17.3	4.1	-4.50
52162.651	0.513	-14.6	2.9	-1.96
53338.617	0.419	-15.7	5.0	-2.83
53989.652	0.532	-13.4	4.2	-0.84
54696.894	0.799	-8.3	2.3	0.89
55791.858	0.720	-14.7	2.3	-3.85
55805.801	0.750	-11.8	3.3	-1.54
55836.692	0.033	-1.7	3.6	0.87
56211.700	0.747	-8.6	3.2	1.73
56215.635	0.038	-4.0	3.3	-0.97
56494.713	0.662	-9.6	3.0	1.96
56446.784	0.120	-8.0	4.3	1.28
56459.737	0.077	-7.6	1.9	-0.91
56462.891	0.311	-12.9	2.2	-0.17
56463.903	0.385	-14.2	5.4	-1.32
56470.884	0.901	-6.5	2.4	-1.43
56472.752	0.039	-2.1	2.8	1.14
56490.729	0.368	-5.9	3.2	7.00
56493.744	0.591	-11.9	3.3	0.26
56494.745	0.665	-9.6	3.0	1.94
56495.752	0.739	-5.1	6.2	5.44
56496.901	0.824	-8.7	4.2	-0.20
56497.906	0.898	-2.9	2.8	2.32

Table 1—Continued

Date (HJD-2,400,000)	ϕ	V_{r1} (km s ⁻¹)	σ_V (km s ⁻¹)	$O_1 - C_1$ (km s ⁻¹)
MT91 202				
54696.928	0.880	-15.9	16.5	-0.13
54697.883	0.902	-18.9	15.4	0.51
55781.847	0.065	-33.9	8.8	-0.90
55836.786	0.340	12.1	21.8	16.12
56247.641	0.878	-7.7	11.0	7.73
56251.586	0.969	-32.8	8.9	-3.17
56446.855	0.502	-6.2	15.2	-10.45
56461.717	0.847	-21.2	11.2	-10.42
56464.770	0.918	-23.3	15.6	-1.28
56469.713	0.033	-25.5	16.2	8.37
56489.726	0.497	7.2	12.4	3.12
56491.691	0.543	7.1	19.8	2.02
56504.789	0.847	-7.4	11.8	3.39
56533.762	0.520	4.4	13.4	-0.24
56566.612	0.282	-6.8	14.2	2.35
56588.593	0.792	0.3	16.9	4.35
56607.643	0.235	-18.7	11.9	-4.63
MT91 234				
51467.855	0.288	-16.8	6.4	-2.74
51805.911	0.356	-33.8	7.4	-13.41
52146.686	0.424	-20.5	5.5	5.30
52161.793	0.427	-22.3	4.8	3.71
52162.851	0.427	-24.3	5.3	1.73
53338.617	0.663	-40.0	5.3	-7.75
53340.576	0.663	-33.9	4.1	-1.66
53989.652	0.793	-13.4	4.7	11.04
53990.848	0.793	-18.3	8.4	6.12
54286.904	0.852	-28.5	5.3	-10.53
54628.880	0.921	-15.5	7.1	-6.06
54630.852	0.921	-5.4	4.9	3.99
55713.928	0.138	-12.0	10.6	-11.18
55717.858	0.139	-0.8	3.9	0.02
55737.828	0.143	-3.6	5.7	-2.50
55741.587	0.144	-1.3	5.5	-0.12
55766.847	0.149	1.8	3.6	3.27
55781.912	0.152	-3.3	8.3	-1.62
55782.854	0.152	-0.2	4.7	1.48
55795.453	0.154	-4.1	4.0	-2.23
56118.661	0.219	-8.5	4.5	-1.24
56166.369	0.229	-6.5	5.2	1.70

Table 1—Continued

Date (HJD-2,400,000)	ϕ	V_{r1} (km s ⁻¹)	σ_V (km s ⁻¹)	$O_1 - C_1$ (km s ⁻¹)
56178.604	0.231	-8.2	5.8	0.21
56460.868	0.287	-13.7	5.7	0.33
56464.894	0.288	-19.4	4.8	-5.29
56468.901	0.289	-12.8	5.8	1.34
MT91 241				
51364.067	0.035	10.0	2.1	0.72
51466.739	0.188	-12.0	1.4	-0.71
51806.950	0.695	-26.7	4.1	0.66
52161.793	0.224	-7.3	4.9	7.16
53340.576	0.980	3.0	3.3	-1.70
53989.774	0.948	-4.4	5.6	-0.73
54286.901	0.390	-19.9	9.1	3.42
54628.748	0.900	4.0	7.8	18.22
56107.562	0.103	-0.4	2.6	0.01
56240.279	0.301	-22.4	2.2	-2.93
56258.544	0.328	-18.9	2.0	1.95
56445.897	0.607	-27.1	2.2	0.47
56463.763	0.634	-28.7	2.6	-1.04
56471.705	0.646	-27.7	2.5	-0.07
56472.675	0.647	-25.5	4.2	2.16
56475.891	0.652	-26.8	2.6	0.79
56555.611	0.771	-29.1	2.8	-3.41
56590.618	0.823	-22.8	1.8	0.19
56608.615	0.850	-21.4	2.2	-0.65
MT91 268-component1				
51364.087	0.872	-68.0	3.1	-4.41
51466.729	0.952	-73.0	4.1	-11.75
52146.829	0.359	-10.8	8.1	-9.03
52161.650	0.803	-63.7	6.1	-9.59
52162.828	0.839	-46.9	8.1	12.39
54628.880	0.835	-38.8	10.1	20.03
54630.852	0.895	-67.3	14.1	-1.65
56107.937	0.216	25.0	5.1	13.99
56178.806	0.343	10.7	3.8	10.82
56445.758	0.353	-9.3	6.5	-8.14
56469.761	0.073	-2.3	5.5	-7.41
56470.718	0.102	-0.3	4.4	-11.65
56490.802	0.704	-46.9	4.6	-6.79
56491.810	0.735	-43.8	5.1	0.42
56493.854	0.796	-26.7	5.0	26.32
56494.745	0.823	-43.1	5.6	13.94

Table 1—Continued

Date (HJD-2,400,000)	ϕ	V_{r1} (km s ⁻¹)	σ_V (km s ⁻¹)	$O_1 - C_1$ (km s ⁻¹)
56505.868	0.156	2.0	5.5	-11.93
56533.824	0.995	-36.5	5.4	2.89
56552.632	0.560	-32.3	4.2	-9.76
56574.679	0.221	23.9	4.0	13.26
56589.679	0.671	-30.8	4.3	4.97
56608.547	0.237	-25.3	7.2	-34.73
MT91 268-component2				
51364.087	0.658	-13.5	3.1	-2.54
51466.729	0.857	-14.8	4.1	0.48
52146.829	0.690	-7.9	8.1	4.09
52161.650	0.606	-16.6	6.1	-7.48
52162.828	0.838	4.4	8.1	19.84
54628.880	0.119	13.8	10.1	-2.93
54630.852	0.507	-9.2	14.1	-3.87
56107.937	0.175	19.3	5.1	6.88
56178.806	0.121	14.1	3.8	-2.51
56445.758	0.653	-4.8	6.5	5.92
56469.761	0.376	0.0	5.5	-0.29
56470.718	0.564	-4.0	4.4	3.54
56490.802	0.517	-8.4	4.6	-2.65
56491.810	0.715	-1.8	5.1	11.02
56493.854	0.117	22.6	5.0	5.69
56494.745	0.293	9.4	5.6	4.74
56505.868	0.481	-5.3	5.5	-0.94
56533.824	0.983	0.7	5.4	-2.55
56552.632	0.684	-9.0	4.2	2.76
56574.679	0.022	18.7	4.0	3.45
56589.679	0.974	4.1	4.3	3.71
56608.547	0.687	-29.6	7.2	-17.70
MT91 292				
51805.904	0.838	-35.0	4.1	-7.11
52146.686	0.847	-23.0	8.1	6.38
52161.793	0.867	-25.2	10.1	7.73
52162.651	0.925	-35.9	9.9	10.24
53340.576	0.458	-10.5	12.8	-3.24
53989.774	0.291	-11.0	12.1	-1.59
54403.777	0.244	-24.8	10.6	-13.19
54409.683	0.643	-12.2	5.3	-0.82
56118.870	0.046	-48.0	5.4	-1.62
56219.688	0.853	-27.6	3.7	2.78
56443.749	0.982	-55.0	6.3	2.47

Table 1—Continued

Date (HJD-2,400,000)	ϕ	V_{r1} (km s ⁻¹)	σ_V (km s ⁻¹)	$O_1 - C_1$ (km s ⁻¹)
56464.729	0.398	21.7	18.6	28.99
56496.764	0.561	-11.0	6.6	-2.27
56497.801	0.631	-14.1	5.7	-3.19
56500.729	0.829	-25.0	3.9	1.56
56502.770	0.967	-62.6	8.5	-6.82
56504.743	0.100	-26.3	5.3	4.15
56505.810	0.172	-19.6	6.4	-1.78
56555.657	0.538	-6.4	3.3	1.84
56560.782	0.884	-40.9	4.7	-4.68
MT91 295				
56118.832	0.998	-28.9	3.3	-0.17
56240.645	0.458	-17.9	3.3	-1.38
56447.807	0.574	-6.5	4.7	7.55
56465.847	0.899	-18.9	4.5	0.52
56471.784	0.309	-18.3	3.6	3.03
56489.874	0.655	-10.3	4.4	2.83
56496.690	0.422	-20.4	3.9	-2.91
56502.730	0.875	-18.4	4.8	-0.72
56504.830	0.727	-14.7	4.7	-1.55
56555.786	0.417	-13.2	4.3	4.39
56589.731	0.200	-28.0	4.0	-1.68
56590.565	0.539	-19.5	3.2	-4.79
56599.638	0.223	-24.9	3.8	0.31
56623.557	0.935	-23.4	4.4	-0.67
MT91 336				
51364.116	0.849	-20.6 (2.2)	0.95	
52146.820	0.362	-1.6 (4.8)	4.62	
52161.650	0.629	-13.3 (4.6)	-1.67	
52162.820	0.202	-8.2 (4.7)	0.98	
54629.860	0.017	-18.0 (4.6)	3.10	
54630.740	0.448	-9.6 (2.5)	-2.71	
54632.740	0.428	-1.2 (4.5)	5.43	
54633.850	0.972	-23.2 (4.6)	-0.11	
56623.601	0.922	-25.6 (2.3)	-2.04	
56798.913	0.822	-16.2 (6.2)	4.17	
56799.837	0.275	-7.4 (2.7)	-0.41	
56804.884	0.748	-15.1 (4.7)	1.68	
MT91 339				
54641.903	0.475	-10.7	1.2	1.10

Table 1—Continued

Date (HJD-2,400,000)	ϕ	V_{r1} (km s ⁻¹)	σ_V (km s ⁻¹)	$O_1 - C_1$ (km s ⁻¹)
54642.890	0.501	-14.0	4.1	-1.90
54643.757	0.524	-14.7	4.0	-2.22
54644.826	0.552	-14.0	3.7	-1.10
54647.860	0.632	-16.3	3.0	-2.28
54669.803	0.212	-10.0	2.0	-0.17
54671.884	0.267	-9.6	1.9	0.30
54672.834	0.292	-10.9	1.3	-0.93
54673.889	0.320	-10.1	1.5	0.01
54674.914	0.347	-10.4	1.9	-0.01
56118.932	0.483	-12.5	1.9	-0.61
56179.923	0.093	-10.9	2.5	0.53
56209.798	0.882	-15.6	1.2	0.99
56211.649	0.931	-18.0	1.7	-1.96
56438.789	0.930	-16.8	5.6	-0.66
56443.890	0.065	-13.6	2.8	-1.37
56444.745	0.087	-9.3	2.9	2.31
56445.742	0.114	-10.0	2.7	0.96
56446.934	0.145	-9.6	2.3	0.83
56447.930	0.171	-11.2	2.5	-1.11
56457.798	0.432	-11.2	2.1	0.04
56458.700	0.456	-10.4	2.5	1.18
56475.835	0.908	-15.2	2.0	1.22
56486.814	0.198	-11.8	2.9	-1.90
56491.785	0.330	-9.5	2.8	0.76
56493.726	0.381	-11.5	2.6	-0.86
56494.672	0.406	-10.5	2.4	0.46
56559.699	0.123	-11.0	2.2	-0.24
56566.758	0.310	-10.0	2.4	0.11
56567.769	0.336	-6.8	3.6	3.49
56574.633	0.518	-13.3	2.0	-0.94
56585.607	0.807	-16.9	3.2	-0.51
56588.682	0.889	-18.3	2.2	-1.72
56590.548	0.938	-15.8	2.0	0.17
MT91 378				
55424.755	0.861	-38.2	31.8	-16.80
55491.691	0.138	22.4	27.3	-17.51
55779.871	0.938	-12.5	10.2	-12.36
55790.594	0.303	14.1	5.6	-2.92
55866.476	0.883	-9.9	6.8	6.64
56076.633	0.030	33.2	7.0	2.70
56080.493	0.162	36.2	7.3	-1.82
56092.490	0.570	-23.3	7.2	-2.07
56093.492	0.604	-24.1	9.2	0.51

Table 1—Continued

Date (HJD-2,400,000)	ϕ	V_{r1} (km s ⁻¹)	σ_V (km s ⁻¹)	$O_1 - C_1$ (km s ⁻¹)
56097.520	0.741	-32.1	5.8	-0.12
56463.835	0.198	36.2	7.5	2.49
56465.733	0.263	25.3	7.1	1.61
56469.682	0.397	10.0	8.0	8.30
56470.827	0.436	-4.8	6.2	-0.63
56472.788	0.503	-16.5	6.1	-3.20
56489.839	0.082	37.2	8.4	-2.22
56491.859	0.151	34.1	7.3	-4.89
56518.751	0.066	40.4	7.1	2.87
56519.753	0.100	46.1	8.7	5.62
MT91 390				
55715.888	0.670	-18.7	5.2	0.73
55718.899	0.321	-13.5	2.7	-0.97
55768.806	0.111	-16.2	3.7	-0.50
55782.732	0.122	-17.8	4.8	-2.48
55796.785	0.160	-14.6	5.9	-0.53
55805.923	0.136	-13.3	6.3	1.58
56211.817	0.893	-23.0	4.5	0.08
56212.744	0.093	-14.5	3.4	1.96
56240.753	0.149	-14.2	4.4	0.20
56251.637	0.502	-16.5	2.8	-1.37
56494.867	0.090	-17.9	3.7	-1.31
56496.807	0.510	-14.0	6.7	1.32
56497.841	0.733	-21.1	3.9	-0.08
56502.855	0.817	-29.3	9.0	-6.48
56504.902	0.260	-10.9	4.1	1.60
56505.702	0.433	-11.2	4.4	2.64
56533.900	0.530	-15.0	4.8	0.75
MT91 403				
55714.893	0.479	-8.1	4.7	-2.87
55717.890	0.659	-33.6	4.0	4.45
55727.901	0.261	30.0	5.0	0.59
55738.896	0.922	-62.0	4.2	-5.76
55740.551	0.021	-2.9	3.5	4.59
55756.824	0.999	-19.6	5.4	0.94
55796.877	0.407	2.1	10.4	-5.26
55832.549	0.551	-18.7	4.2	-0.63
55855.693	0.942	-46.5	4.2	3.27
55857.646	0.059	7.7	3.8	-4.60
55906.555	0.999	-22.6	3.4	-1.73
55911.533	0.298	28.4	3.8	3.85

Table 1—Continued

Date (HJD-2,400,000)	ϕ	V_{r1} (km s ⁻¹)	σ_V (km s ⁻¹)	$O_1 - C_1$ (km s ⁻¹)
56076.514	0.214	33.7	6.5	-0.25
56080.524	0.455	-6.4	5.4	-5.43
56092.534	0.177	35.4	6.0	0.05
56093.552	0.238	33.3	6.1	1.43
56179.471	0.402	5.0	5.8	-3.23
56205.353	0.958	-41.8	5.2	1.25
MT91 417B				
54672.823	0.194	-10.1 (7.8)	2.41	
56511.750	0.528	-19.9 (6.8)	-1.87	
56512.762	0.554	-18.9 (3.6)	0.23	
56519.663	0.736	-31.2 (4.9)	-4.39	
56533.734	0.106	-17.8 (5.1)	-1.29	
56534.756	0.132	-13.4 (5.3)	1.47	
56556.732	0.710	-25.0 (3.8)	0.73	
56574.608	0.180	-10.8 (4.0)	2.07	
56582.586	0.390	-15.3 (4.4)	-1.65	
56589.552	0.573	-19.1 (4.0)	0.69	
56590.676	0.602	-22.8 (4.0)	-1.72	
56606.553	0.020	-20.9 (3.8)	2.97	
56626.550	0.545	-22.7 (3.9)	-3.94	
56795.922	0.997	-23.4 (10.0)	2.37	
56804.923	0.233	-12.6 (6.1)	-0.71	
MT91 448				
55766.875	0.552	-33.9	6.1	0.08
55781.721	0.235	-8.0	5.6	4.25
55832.632	0.293	-11.6	10.8	9.80
55834.666	0.935	16.8	6.6	-0.49
55847.701	0.046	17.2	5.8	-0.44
55876.617	0.167	-6.9	6.2	-6.88
56077.852	0.640	-29.6	4.1	-2.51
56080.797	0.569	-28.5	5.4	4.56
56092.806	0.356	-30.3	6.2	-1.32
56093.840	0.683	-12.3	6.8	9.59
56097.807	0.934	18.3	4.7	1.07
56179.749	0.780	-9.5	5.4	-3.06
56446.824	0.020	17.2	6.2	-2.13
56447.900	0.359	-26.2	5.7	3.07
56458.767	0.787	-10.2	6.6	-5.00
56463.867	0.396	-43.0	8.8	-10.72
56469.840	0.280	-20.1	4.6	-0.64
56470.796	0.581	-29.9	5.3	2.40

Table 1—Continued

Date (HJD-2,400,000)	ϕ	V_{r1} (km s ⁻¹)	σ_V (km s ⁻¹)	$O_1 - C_1$ (km s ⁻¹)
MT91 473				
51365.110	0.925	-10.1	5.1	3.51
51467.882	0.986	-12.1	5.1	0.69
51805.789	0.186	-4.1	5.1	-4.29
52161.793	0.397	-3.0	5.1	-0.71
53340.576	0.095	3.0	7.1	2.68
53989.770	0.480	-8.0	7.1	-4.64
54286.904	0.656	-12.0	7.1	-6.02
54628.748	0.859	-4.0	8.1	6.95
54629.860	0.860	-14.0	9.1	-3.03
54630.739	0.860	-14.0	5.1	-3.01
54631.850	0.861	-10.0	6.1	1.01
54633.850	0.862	-7.0	8.1	4.06
55420.926	0.328	1.8	10.4	3.30
55461.790	0.353	7.4	10.3	9.11
55490.761	0.370	-2.5	10.6	-0.56
55717.919	0.504	-0.9	5.9	2.74
55740.894	0.518	-0.3	5.8	3.54
55790.919	0.548	-4.8	7.0	-0.48
55794.758	0.550	-11.4	9.4	-7.09
55834.790	0.574	-3.7	3.8	0.99
55847.762	0.581	-2.6	4.2	2.22
55855.760	0.586	-5.3	4.1	-0.42
55856.545	0.587	-10.8	5.3	-5.92
55866.778	0.593	6.2	6.3	11.15
56128.911	0.748	-9.8	6.1	-2.05
56190.867	0.785	-9.0	5.4	-0.33
56205.661	0.794	-14.7	5.7	-5.81
56457.907	0.943	-16.0	4.7	-1.77
56472.825	0.952	-7.6	5.7	6.87
56486.779	0.960	-28.3	7.4	-13.87
56489.822	0.962	-13.3	6.7	1.15
56490.852	0.963	-18.2	5.2	-3.81
56491.892	0.963	-13.2	6.0	1.26
56493.777	0.964	-8.7	5.8	5.67
56494.689	0.965	-14.7	5.3	-0.29
56495.909	0.966	-15.2	7.5	-0.89
MT91 485				
51467.878	0.813	-23.1	4.0	-8.26
51805.804	0.896	-17.2	4.2	-4.82
52146.829	0.980	2.5	5.2	-1.17

Table 1—Continued

Date (HJD-2,400,000)	ϕ	V_{r1} (km s ⁻¹)	σ_V (km s ⁻¹)	$O_1 - C_1$ (km s ⁻¹)
52161.650	0.983	5.5	5.5	-0.26
52162.820	0.984	8.5	5.1	2.57
53339.570	0.273	-12.3	4.7	1.93
53989.870	0.433	-12.2	5.0	3.35
54285.920	0.506	-23.3	4.8	-7.47
54628.700	0.590	-16.2	7.4	-0.24
54630.739	0.590	-17.8	5.4	-1.84
54631.850	0.591	-12.2	5.6	3.76
55714.847	0.857	-9.5	3.8	4.38
55715.919	0.857	-16.7	3.5	-2.81
55718.762	0.858	-12.8	2.7	1.12
55738.873	0.863	-11.6	3.8	2.16
55740.574	0.863	-13.4	2.8	0.32
55757.764	0.868	-13.0	2.9	0.56
55768.894	0.870	-11.5	4.2	2.02
55781.819	0.874	-11.6	2.9	1.72
55834.836	0.887	-12.2	2.4	0.66
55866.756	0.894	-10.5	3.6	1.96
56076.828	0.946	-7.9	4.5	-0.49
56080.853	0.947	-8.1	4.1	-0.91
56092.861	0.950	-7.9	3.9	-1.20
56097.882	0.951	-7.1	4.1	-0.64
56460.731	0.040	-0.2	4.0	-0.03
56471.928	0.043	-1.5	3.7	-0.61
56590.763	0.072	-5.9	4.3	0.29
MT91 555				
51805.820	0.775	-21.0	4.1	-2.37
52146.686	0.042	6.3	10.1	-2.92
52161.793	0.053	4.4	13.1	-1.58
52162.651	0.054	16.2	16.1	10.41
53338.617	0.973	21.9	9.1	8.95
53340.576	0.975	16.7	9.1	3.41
53989.652	0.482	-25.2	12.1	-0.72
54628.880	0.981	-4.5	14.1	-19.13
55718.875	0.833	-11.1	5.1	3.13
55740.870	0.851	-10.5	4.6	1.98
55768.789	0.872	-9.7	4.4	-0.06
55782.825	0.883	-2.9	5.0	5.09
55791.940	0.890	-7.2	4.3	-0.43
55794.842	0.893	-12.1	6.3	-5.69
55847.678	0.934	3.4	5.1	0.74
56118.744	0.146	-12.4	6.2	-0.30
56179.888	0.194	-22.6	6.5	-6.02

Table 1—Continued

Date (HJD-2,400,000)	ϕ	V_{r1} (km s ⁻¹)	σ_V (km s ⁻¹)	$O_1 - C_1$ (km s ⁻¹)
56191.831	0.203	-12.3	6.4	5.02
56460.777	0.413	-23.4	6.7	0.64
56465.764	0.417	-22.7	6.2	1.41
56468.815	0.419	-30.8	7.0	-6.64
56518.789	0.459	-7.9	9.1	16.49
56552.756	0.485	-31.0	5.4	-6.47
56566.807	0.496	-7.5	8.3	16.98
56567.714	0.497	-20.1	12.1	4.38
56574.804	0.502	-21.2	5.6	3.28
56588.656	0.513	-22.5	5.4	1.96
56608.668	0.529	-23.9	4.4	0.56
MT91 561				
54403.790	0.752	-31.7	9.2	-1.61
54406.679	0.824	-15.5	8.5	0.27
55377.898	0.050	41.5	21.3	15.08
55426.768	0.269	12.5	21.6	6.35
55457.652	0.039	72.0	25.9	46.35
55470.731	0.365	-4.2	25.5	9.70
55758.813	0.551	-37.6	7.4	3.19
55790.941	0.353	-15.3	6.8	-4.09
56166.884	0.730	-29.2	9.7	4.33
56179.680	0.049	6.5	10.7	-19.82
56445.866	0.689	-48.3	11.2	-9.75
56461.898	0.089	32.6	9.3	4.92
56465.792	0.186	20.9	9.2	0.36
56469.808	0.286	4.9	10.8	2.21
56475.715	0.433	-27.3	9.7	-0.68
56490.877	0.811	-16.1	10.3	2.47
56494.909	0.912	7.1	11.8	2.61
MT91 588				
51805.819	0.648	-11.3	5.0	8.16
52146.686	0.038	-18.9	5.7	-2.00
52162.651	0.103	4.3	5.5	12.31
53989.652	0.558	-19.1	5.1	-2.85
53990.848	0.562	-16.3	10.1	0.12
56165.921	0.437	-13.3	6.1	-0.66
56218.697	0.652	-24.2	6.0	-4.55
56258.636	0.815	-31.2	6.8	-3.46
56460.754	0.640	-18.1	5.2	1.09
56464.704	0.656	-21.3	5.4	-1.52
56534.801	0.942	-35.8	5.8	-0.03

Table 1—Continued

Date (HJD-2,400,000)	ϕ	V_{r1} (km s ⁻¹)	σ_V (km s ⁻¹)	$O_1 - C_1$ (km s ⁻¹)
56556.854	0.032	-12.9	5.2	5.71
56559.742	0.043	-15.8	4.1	-0.14
56560.699	0.047	-17.5	4.3	-2.73
56566.830	0.072	-17.1	4.4	-6.43
56574.574	0.104	-4.6	3.9	3.39
56582.616	0.137	-6.5	4.2	0.46
56587.554	0.157	-2.2	5.8	4.58
56588.566	0.161	-10.0	3.5	-3.25
56590.729	0.170	-9.7	3.9	-2.91
56607.576	0.239	-7.5	4.8	0.25
MT91 601				
51467.916	0.681	-10.8	3.1	1.81
51805.746	0.343	-11.0	3.1	6.70
52146.686	0.012	-1.0	3.8	0.48
54643.857	0.906	0.2	4.7	2.84
54644.926	0.908	-0.4	5.1	1.95
54647.882	0.914	1.6	4.6	3.38
54669.940	0.957	4.7	2.4	0.74
54672.765	0.963	-0.3	2.1	-5.16
54673.770	0.965	4.4	2.2	-0.75
54674.896	0.967	11.1	2.1	5.69
56076.678	0.715	-5.6	2.7	6.24
56080.915	0.723	-11.8	2.5	-0.24
56092.907	0.746	-8.5	2.5	2.44
56098.779	0.758	-17.4	2.2	-6.82
56110.915	0.782	-11.8	2.5	-2.04
56118.713	0.797	-9.0	3.1	0.19
56128.951	0.817	-3.0	3.0	5.40
56166.976	0.892	-2.7	4.0	1.20
56179.913	0.917	-5.6	2.4	-4.11
56212.580	0.981	6.7	2.2	0.01
56222.715	0.001	2.6	1.8	-0.68
56440.951	0.429	-18.8	2.9	-2.04
56460.688	0.467	-26.9	2.8	-10.70
56462.832	0.471	-25.2	2.5	-9.02
56491.924	0.528	-13.9	3.4	1.47
56497.897	0.540	-15.2	2.8	-0.03
56552.875	0.648	-12.0	2.3	1.28
56559.771	0.661	-8.3	2.5	4.77
56590.754	0.722	-9.8	2.5	1.81
56622.557	0.784	-5.6	2.2	4.09
56795.895	0.124	2.8	2.2	21.40

Table 1—Continued

Date (HJD-2,400,000)	$\phi_{\text{MT91 646a}}$	V_{r1} (km s^{-1})	σ_V (km s^{-1})	$O_1 - C_1$ (km s^{-1})
56191.706	0.278	-72.7 (4.8)	0.8	
56461.866	0.701	6.4 (3.7)	-6.7	
56464.862	0.761	31.1 (4.3)	5.0	
56467.795	0.820	42.4 (10.2)	5.9	
56469.872	0.862	56.6 (6.1)	16.4	
56495.871	0.383	-65.1 (8.9)	-10.3	
56496.732	0.401	-64.6 (5.2)	-13.2	
56500.887	0.485	-44.4 (14.1)	-9.9	
56504.870	0.564	2.7 (7.1)	20.0	
56505.735	0.582	0.6 (4.4)	14.1	
56552.682	0.524	-56.9 (10.5)	-30.9	
56556.801	0.607	12.4 (5.2)	20.5	
56560.740	0.686	12.1 (8.3)	2.4	
56566.777	0.807	33.9 (3.0)	-0.7	
56574.649	0.965	11.9 (2.1)	-1.2	
56582.648	0.126	-62.3 (5.2)	16.5	
56589.771	0.269	-71.5 (2.9)	3.4	
56590.695	0.287	-70.7 (4.0)	1.4	
56599.736	0.469	-57.7 (7.6)	-19.9	
MT91 646b				
56191.706	0.278	39.3 (5.9)	0.4	
56461.866	0.701	-65.8 (4.6)	7.2	
56464.862	0.761	-81.5 (5.4)	8.3	
56467.795	0.820	-96.2 (12.7)	7.0	
56469.872	0.862	-98.8 (7.6)	9.2	
56495.871	0.383	14.7 (11.1)	-0.1	
56496.732	0.401	22.7 (6.5)	12.2	
56500.887	0.485	13.9 (17.7)	25.4	
56504.870	0.564	-55.0 (8.9)	-21.4	
56505.735	0.582	-61.6 (5.4)	-23.1	
56552.682	0.524	1.7 (13.1)	24.0	
56556.801	0.607	-60.2 (6.5)	-14.5	
56560.740	0.686	-74.9 (10.4)	-6.3	
56566.777	0.807	-105.4 (3.7)	-4.6	
56574.649	0.965	-77.6 (2.6)	-4.6	
56582.648	0.126	50.1 (6.5)	4.2	
56589.771	0.269	30.9 (3.6)	-9.8	
56590.695	0.287	36.1 (5.0)	-1.0	
56599.736	0.469	5.5 (9.5)	12.7	
MT91 745				

Table 1—Continued

Date (HJD-2,400,000)	ϕ	V_{r1} (km s ⁻¹)	σ_V (km s ⁻¹)	$O_1 - C_1$ (km s ⁻¹)
56166.691	0.507	-16.7	7.2	0.67
56211.440	0.803	-12.5	3.7	-2.52
56218.487	0.849	-14.1	5.8	-7.27
56457.883	0.432	-16.1	12.3	1.80
56460.712	0.451	-21.6	5.2	-3.82
56462.843	0.465	-20.3	3.8	-2.56
56475.700	0.550	-20.5	5.3	-3.60
56500.921	0.717	-8.3	5.0	5.29
56504.690	0.742	-10.8	5.6	1.98
56505.680	0.749	-13.7	4.9	-1.18
56511.662	0.788	-13.0	5.1	-2.21
56518.815	0.835	-10.1	4.9	-2.27
56552.859	0.061	-6.0	4.6	-3.31
56556.872	0.087	-3.3	4.1	4.61
56559.781	0.106	-11.0	3.8	-0.50
56560.621	0.112	-12.0	3.9	-0.95
56571.604	0.185	-17.2	5.2	-1.52
56585.544	0.277	-15.7	4.5	1.87
56588.724	0.298	-15.6	3.8	2.23
56599.768	0.371	-20.8	3.9	-2.73
56606.580	0.416	-14.0	3.7	4.00
56608.599	0.429	-15.2	4.3	2.69
51467.889	0.430	-21.4	4.5	-3.47
51805.782	0.665	-14.6	4.7	0.38
52146.829	0.920	4.5	5.4	2.25
52161.650	0.018	11.3	3.7	-0.20
52162.828	0.026	1.3	6.0	-7.32
53339.572	0.809	-7.1	4.6	2.55
53340.576	0.815	-1.8	4.6	7.45
53989.774	0.109	-9.3	4.7	1.48
54285.779	0.067	-12.9	6.0	-8.82
54286.904	0.074	-9.5	9.1	-3.85

Table 2. Orbital Elements of New Binaries

Element	MT91 021	MT91 187	MT91 202	MT91 234	MT91 241
P (days)	9.70±0.01	13.531±0.002	43.05±0.05	4996±330	671±2
e	0.29±0.13	0.51±0.12	0.24±0.11	0.12±0.16	0.45±0.05
ω (deg)	81±31	15±19	160±40	328±54	338±6
γ (km s ⁻¹)	-16.2±4.5	-9.6±0.6	-10.0±2.0	-17.6±1.5	-16.7±1.5
T_0 (HJD-2,400,000)	56336.58±0.79	56282.7±0.5	56468.29±4.3	55024±722	125161±189
K_1 (km s ⁻¹)	37.8±5.5	6.5±1.1	19.7±2.6	17.1±2.2	18.7±1.2
K_2 (km s ⁻¹)
S. C. ₁	B1.5V	B1V	B2V	B1.5V	B1.5V
S. C. ₂	mid-late B?	...	B,A	B?	early B
i (degrees)	16–85	3–85	15–90	~90	~90
M_1 (adopted; M _⊙)	12	14	11	12	12
M_2 (M _⊙)	11–2	14 – 0.43	11 – 2	17:	11–4.6
q	1–0.18	1 – 0.03	1–0.18	1–2?	0.8–0.42
a (AU)	~0.25	~ 0.3	~0.60	~16	~4
χ_{red}^2	3.22	0.69	0.33	1.1	1.0

Table 3. Orbital Elements of New Binaries

Element	MT91 268-c1	MT91 268-c2	MT91 292	MT91 295	MT91 236
P (days)	33.327 ± 0.002	5.082 ± 0.006	14.8106 ± 0.0011	2.4628 ± 0.0008	2.04087 ± 0.00006
e	0.41 ± 0.03	0.48 ± 0.15	0.45 ± 0.06	0.30 ± 0.22	0.21 ± 0.18
ω (deg)	256 ± 13	294 ± 28	191 ± 13	137 ± 46	216 ± 51
γ (km s ⁻¹)	-22.5 ± 1.7	-1.5 ± 2.5	-21.4 ± 1.6	-20.2 ± 1.4	-13.4 ± 1.1
T_0 (HJD-2,400,000)	56667.7 ± 1.1	56528.8 ± 0.7	56058.94 ± 0.38	56567.1 ± 0.3	2456793.1 ± 0.3
K_1 (km s ⁻¹)	33.0 ± 2.7	17.4 ± 2.3	25.3 ± 2.6	9.2 ± 2.4	8.8 ± 1.1
K_2 (km s ⁻¹)
S. C. ₁	B2V	B2V	B2V	B2V	B2V
S. C. ₂	B-A	B-G	B-F	B-K	B-M
i (degrees)	33-90	33-90	12-90	3-90	3-90
M_1 (adopted; M _⊙)	9	9	11	11	11
M_2 (M _⊙)	9-3.9	9-3.9	11-1.6	11-0.3	11-6
q	1-0.43	1-0.43	1-0.14	1-0.026	0.55-0.85
a (AU)	~0.49	~0.49	~0.32	~0.08	~0.07
χ_{red}^2	1.9	1.9	0.95	0.92	0.74

Table 4. Orbital Elements of New Binaries

Element	MT91 339	MT91 378	MT91 390	MT91 403	MT91 417B
P (days)	44.63±0.03	29.41±0.03	4.6252±0.0012	16.6379±0.0062	38.0±0.2
e	0.21±0.11	0.23±0.05	0.15±0.15	0.29±0.03	0.21±0.20
ω (deg)	251±32	299±14	240±52	260±9	244±31
γ (km s ⁻¹)	-13.0±0.3	0.4±1.4	-17.4±0.6	-12.9±1.5	-20.4±1.2
T_0 (HJD-2,400,000)	55229.7±3.9	56310.98±1.16	55971.80±0.67	55973.13±0.33	56719.9±1.6
K_1 (km s ⁻¹)	3.4±0.3	36.3±1.9	5.4±0.9	49.8±2.1	9.5±1.7
K_2 (km s ⁻¹)
S. C. ₁	B0V	O8V	B1V	O6V	
S. C. ₂	O–K	B:	O–K	B:	O6V-A
i (degrees)	2–90	19–90	2–90	23–90	5–90
M_1 (adopted; M _⊙)	21	18	21	14	31
M_2 (M _⊙)	21–0.5	17–4.1	21–0.32	14 –4.0	31–1.8
q	1–0.02	1–0.23	1–0.015	1–0.29	1–0.06
a (AU)	~0.7	~0.55	~0.15	~0.35	~0.7
χ_{red}^2	0.32	0.48	0.17	0.85	0.25

Table 5. Orbital Elements of New Binaries

Element	MT91 448	MT91 473	MT91 485	MT91 555	MT91 561
P (days)	3.1704 ± 0.0004	1687 ± 51^a	4066 ± 45	1278.7 ± 13.2	40.09 ± 0.04
e	0.10 ± 0.06	0.59 ± 0.26	0.75 (Fixed)	0.55 ± 0.09	0.05 ± 0.09
ω (deg)	3 ± 34	255 ± 28	352 ± 9	2 ± 13	325 ± 118
γ (km s $^{-1}$)	-10.6 ± 1.2	-5.0 ± 1.6	-12.1 ± 1.1	-14.4 ± 1.3	-8.9 ± 2.5
T_0 (HJD-2,400,000)	55971.2 ± 0.3	64990 ± 438	52229 ± 29	57208 ± 49	55977 ± 13.3
K_1 (km s $^{-1}$)	27.7 ± 1.7	7.5 ± 2.3	15.0 ± 2.3	20.8 ± 4.0	35.2 ± 3.6
K_2 (km s $^{-1}$)
S. C. ₁	O6V	O8.5V+O9V:	O8V	O8V	B2V
S. C. ₂	O6V-A	O-B	O-B	O-B2	O-A1
i (degrees)	6–90	12–90	40–90	34–90	24–90
M_1 (adopted; M_\odot)	31	19+19	21	21	11
M_2 (M_\odot)	31–2.0	39–5	21–11	21–10	11–3.3
q	1–0.06	1–0.12	1–0.54	1–0.49	1–0.30
a (AU)	~ 0.14	~ 10	~ 16	~ 7.5	~ 0.6
χ_{red}^2	0.87	0.61	0.58	0.94	0.84

^aProbable triple system; described here are the parameters for the combined ~ 3.6 d binary a+b components (O8.5V+O9V?) treated as a single-lined system under the influence of the unseen c component, a probable early A – O dwarf star.

Table 6. Orbital Elements of New Binaries

Element	MT91 588	MT91 601	MT91 646	MT91 745
P (days)	245.1 ± 0.3	510.2 ± 0.9	49.8 ± 0.2	151.2 ± 0.8
e	0.51 ± 0.17	0.67 (fixed)	0.31 ± 0.05	0.60 ± 0.2
ω (deg)	242 ± 16	41 ± 20	260 ± 8	15 ± 10
γ (km s $^{-1}$)	-17.8 ± 1.4	-12.6 ± 1.6	-24.4 ± 1.9	-10.7 ± 0.8
T_0 (HJD-2,400,000)	56549.1 ± 8.4	56222.3 ± 7.4	56476.7 ± 1.1	56543.7 ± 3.8
K_1 (km s $^{-1}$)	14.5 ± 2.9	12.8 ± 2.1	61.6 ± 3.7	17.5 ± 2.3
K_2 (km s $^{-1}$)	79.6 ± 4.7	...
S. C. ₁	B0V	O9.5III	B1V	O7V
S. C. ₂	B-A	O-B	B1.5V	A-B
i (degrees)	15–90	18–90	75–90	15–90
M_1 (adopted; M_\odot)	18	21	14	25
M_2 (M_\odot)	18–3.2	21–4.1	~ 12	25–4.0
q	1–0.18	1–0.20	0.77 ± 0.05	1–0.16
a (AU)	~ 2.2	~ 3.7	~ 0.6	~ 1.8
χ_{red}^2	1.0	3.4	4.5	0.60

Table 7. Velocities of Stars Showing Aperiodic Variations

Date (HJD-2,400,000)	V_{Helio} (km s ⁻¹)	σ_V (km s ⁻¹)
MT91 138		
52146.686	-14.1	5.2
52161.793	-8.8	3.5
52162.651	-5.2	6.6
53338.617	-31.6	9.1
53989.652	-6.6	5.3
53990.848	-1.6	4.1
54285.925	-23.4	4.8
54286.904	-19.6	3.9
54341.887	-17.1	3.5
54342.777	-16.5	3.7
54343.746	-15.6	3.6
54344.775	-22.4	4.2
54345.790	-17.1	3.5
54347.789	-21.9	4.4
54348.812	-20.6	3.7
54399.696	-24.8	8.1
54401.649	-22.4	7.9
54402.719	-21.0	3.4
54641.844	-22.2	1.8
54643.718	-22.5	5.4
54644.789	-16.4	3.9
54647.828	-19.5	4.3
54669.831	-19.6	2.7
54747.682	-23.4	3.6
54748.641	-22.8	2.3
54753.648	-37.1	3.1
54754.717	-22.4	1.7
54755.763	-23.1	2.1
54756.690	-22.4	4.0
54757.747	-29.3	3.9
MT91 417A ^a		
54643.768	-12.4	6.0
54644.844	-3.8	6.1
54669.787	-2.9	6.7
54672.812	-4.3	5.9
56511.725	-22.8	3.9
56512.739	-17.7	2.1
56519.639	-21.1	9.6
56533.721	-16.9	8.3
56534.739	-8.7	5.0

Table 7—Continued

Date (HJD-2,400,000)	V_{Helio} (km s ⁻¹)	σ_V (km s ⁻¹)
56556.722	-28.8	3.1
56574.599	-12.3	5.4
56582.571	-12.5	5.5
56588.703	-21.2	11.0
56589.54	-18.0	6.5
56590.665	-24.2	3.3
56599.693	-21.9	7.4
56607.561	-22.4	6.6
56626.536	-3.8	8.1
56798.871	14.6	11.5
56804.946	-7	8.9
MT91 457		
51381.776	-9.2	2.5
51382.947	-11.4	2.4
51411.719	-12.9	2.4
51412.762	-19.1	2.0
51736.792	-18.2	2.6
51737.871	-7.9	1.3
52146.829	-12.0	2.0
52161.650	-12.5	3.0
52162.828	-9.6	2.9
53339.572	-14.7	3.0
54642.776	-23.0	4.3
54643.792	-12.5	3.0
54644.736	-10.0	3.2
54645.779	-1.2	3.6
54646.755	-15.7	3.0
54647.726	-12.9	1.6
54648.830	-10.7	3.1
54669.770	-26.4	5.2
54672.734	-23.6	2.8
54673.738	-11.8	2.3
54674.770	-16.3	5.8
MT91 483 ^a		
51365.094	-8.1	1.5
51467.700	-24.0	2.2
51805.727	7.3	1.7
52146.829	-1.8	5.0
52162.828	4.5	4.4
53339.572	-15.0	5.7
54285.779	6.7	8.1

Table 7—Continued

Date (HJD-2,400,000)	V_{Helio} (km s ⁻¹)	σ_V (km s ⁻¹)
54642.793	-7.3	3.1
54644.721	6.2	3.7
54647.873	-3.9	2.7
54669.894	-7.3	2.8
54672.673	-5.5	4.2
54673.819	-6.5	3.6
54674.704	0.4	3.5
56438.944	-11.0	2.0
56457.720	-21.4	2.4
56460.945	-5.3	3.8
56462.751	-6.0	2.1
56466.921	-15.5	2.5
56486.860	-4.1	3.8
56493.800	0.8	2.4
56494.899	-1.8	3.2
56495.706	-9.0	4.0
56496.680	-4.3	2.8
56520.906	-2.3	4.5
56533.953	-3.9	3.1
56556.883	-18.0	4.1
56561.636	-15.8	3.3
56571.636	-4.1	7.3
56574.827	-4.7	2.8
MT91 556		
54643.850	2.5	5.2
54644.908	-12.5	5.7
54645.874	-12.3	5.4
54647.792	-12.0	5.0
54671.914	-3.7	4.5
54672.755	-3.8	4.8
54673.759	-5.1	4.4
54674.829	9.9	4.8
54747.789	-17.4	3.3
54748.685	-9.6	3.5
54749.582	-7.8	3.5
54753.624	-11.2	3.0
54754.754	4.1	4.3
54755.655	1.7	5.8
54756.677	-8.2	3.5
55726.901	-7.8	2.7
55738.919	17.8	5.1
55741.732	-4.9	6.1
55779.962	-13.2	3.0

Table 7—Continued

Date (HJD-2,400,000)	V_{Helio} (km s ⁻¹)	σ_V (km s ⁻¹)
55791.962	-6.3	3.6
55794.878	-4.2	7.5
55834.592	-17.6	4.1
55847.807	-27.4	2.7
55855.665	-7.8	10.8
55866.534	-0.3	2.5
55901.662	-1.2	3.2
56118.721	-2.9	3.2
56205.506	-10.8	4.2
56209.837	-16.3	3.8
56212.651	-3.6	3.4
56219.824	-17.9	3.1
56444.745	-11.9	4.2
56445.936	3.0	3.8
56457.688	1.8	3.3
56460.696	-8.9	3.4
56462.768	-12.5	4.2
56464.925	-10.9	4.5
56465.927	-11.1	6.2
56468.880	-6.0	3.6
56470.917	-10.6	3.0
56472.889	-10.8	3.3
56475.750	2.6	2.9
MT91 632		
54642.809	-8.4	4.8
54643.873	-8.1	3.9
54644.713	-6.4	4.7
54645.759	2.0	4.0
54646.738	-17.3	3.7
54647.709	-10.6	3.2
54648.810	-14.1	3.5
54669.956	-11.2	3.4
54671.710	-14.6	3.2
54672.654	-8.1	1.7
54673.787	-3.6	2.6
54674.666	-10.0	2.6
54675.777	-0.6	2.8
54746.768	17.9	2.7
54747.630	4.7	2.6
54748.617	-19.5	2.0
54748.805	-15.5	1.9
54749.573	-8.0	2.9
54753.599	1.8	2.1

Table 7—Continued

Date (HJD-2,400,000)	V_{Helio} (km s^{-1})	σ_V (km s^{-1})
54754.602	-8.5	2.3
54755.642	-0.0	2.6
54756.662	3.8	2.1
54757.639	-9.4	2.3
54758.702	-9.2	2.4
55010.732	-12.2	1.6
55011.632	8.7	1.6
55012.637	-2.5	2.4
55013.635	-10.1	2.2
56212.561	-0.0	3.5
56258.623	-10.8	3.9

^aVelocities measured from He II $\lambda 5411$ assuming a rest wavelength of 5411.45 Å.

Table 8. OB Binaries in Cyg OB2

Star	Type	S.C.	P (days)	K_1 (km s ⁻¹)	e	q	Ref.	Notes
MT91 021	SB1	B1.5V + B + ?	9.70±0.01	37.8±5.5	0.29±0.13	0.18–1	0	a
MT91 059	SB1	O8V + B	4.8523±0.0003	71.0±4.1	0.14±0.07	0.23–0.67	2,0	b
MT91 070	SB1	O9III + B	6.19 yr	9±1	0.34±0.11	0.25–1	1	
MT91 103	SB2	B1V + B2V:	22.104±0.002	72±4.0	0.32±0.05	0.71±0.10	1	
MT91 145	SB1	O9III + mid B	25.1261±0.0012	42.8±0.8	0.37±0.02	0.23–0.63	3,0	c
MT91 174	SB1	B2III + G–B	4.536±0.020	9±1	0.53±0.13	0.03–0.9	1	
MT91 187	SB1	B1V + G–B	13.472±0.013	6.5±1.1	0.21±0.24	0.018–1	0	d
MT91 202	SB1	B2V + A–B	43.07±0.05	19.7±2.6	0.24±0.11	0.18–1	0	
MT91 234	SB1	B1.5V + early B	4996±330	17.1±2.2	0.12±0.16	0.9–1	0	
MT91 241	SB1	B1.5V + early B	671±2	18.7±1.2	0.45±0.05	0.42–0.8	0	
MT91 252	SB2	B2III + B1V	9.558 μ m0.001	70±2	0.25±0.03	0.86±0.04	2,0	b
MT91 258	SB1	O8V + B	14.660±0.002	40.0±3.2	0.03±0.05	0.18–0.89	2,0	b
MT91 267	SB1	O7.5III–I + O/B	15.511±0.056	24±2	0.21±0.07	0.09–1	1	
MT91 268c1	SB1	B2V + B	33.257±0.019	33.0±2.7	0.54±0.19	0.43–1	0	a
MT91 268c2	SB1	B2V + B–G	5.082±0.006	17.4±2.3	0.48±0.15	0.06–1	0	a
MT91 292	SB1	B2V + B–F	14.8106±0.0011	25.3±2.6	0.45±0.06	0.14–1	0	
MT91 295	SB1	B1.5V + G–B	2.4628±0.000	9.2±2.4	0.30±0.22	0.03–1	0	a?
MT91 311	SB2	B2V + B3V	5.752±0.005	88±5	0.02±0.01	0.8±0.1	4	
MT91 336	SB1	B2V + B–M	2.04087±0.00006	8.8±1.1	0.22±0.18	0.55–0.85	0	
MT91 339	SB1	O8V + O–G	37.86±0.04	3.4±0.3	0.21±0.11	0.02–1	0	
MT91 372	SB2/EA	B0V + B2:V	2.227±0.001	136.5±6.0	0.04±0.02	0.43±0.1	3,5,0	e
MT91 378	SB1	B0V + B:	29.41±0.03	36.3±1.9	0.23±0.05	0.23–1	0	
MT91 390	SB1	O8V + G–O	4.6252±0.0012	5.4±0.9	0.15±0.15	0.015–1	0	
MT91 403	SB1	B1V + B	16.6379±0.0062	49.8±2.1	0.29±0.03	0.29–1	0	
MT91 417B	SB1	O6V + A–O + MT91 417A	38.0±0.2	9.5±1.7	0.21±0.20	0.06–1	0	
MT91 421	SB1/EA	O9V + B9V–A0V	4.161	~0.16–0.19	6	
MT91 429	SB1/EA	B0V + (B3V+B6V)	2.9786±0.0001	140±15	0.38±0.08	0.057:	4,6	a
MT91 431 (S9)	SB2	O5I + O4III	858.4±1.5	60.3±3.0	0.713±0.016	0.88±0.04	18,19	
MT91 448	SB1	O6V + early A–O	3.1704±0.0003	27.7±1.7	0.10±0.06	0.06–1	0	
MT91 465 (S8a)	SB2	O5.5I + O6:	21.908 (fixed)	82.8±2.5	0.24±0.04	0.86±0.04	16,17	
MT91 473 (S8d)	SB1	O8.5V + O9V + A2V–O	1687±51	7.5±2.3	0.59±0.26	0.12–1	0	a
MT91 485	SB1	O8V + early B–O	4066±45	15.0±2.3	0.75±0.2	0.54–1	0	
MT91 555	SB1	O8V + B2–O	1278.7±13.2	20.8±4.0	0.55±0.09	0.49–1	0	
MT91 561	SB1	B2V + B–O	40.09±0.04	35.2±3.6	0.05±0.09	0.30–1	0	
MT91 588	SB1	B0V + early A–B	245.1±0.3	14.5±2.9	0.51±0.17	0.18–1	0	
MT91 601	SB1	B0Iab + B–O	510.2±0.9	12.8±2.1	0.67±0.2	0.20–1	0	f
MT91 605	SB2	B1V + B1:	12.27±0.01	44±3	0.24±0.07	0.9±0.1	4	
MT91 646	SB2	B1V + B1.5V	49.8±0.2	61.6±3.7	0.31±0.04	0.77±0.05	0	
MT91 696	SB2/EW	O9.5V + B0V	1.46918±0.00002	250±10	0 (fixed)	0.802±0.003	4,7	a,e
MT91 720	SB2	B0–B1 + B1–B2	4.0677±0.0003	173±5	0.35±0.02	0.80±0.08	2,4	
MT91 734 (S11)	SB1	O5I + O/early B	72.43±0.07	26±1	0.50±0.06	0.15 –1	1	
MT91 745	SB1	O7V + B–O	151.2±0.8	17.5±2.3	0.60±0.2	0.16–1	0	
MT91 771	SB2	O7V + O9V	2.82105±0.00003	139±5	0.05±0.03	0.95±0.09	2,4	
Schulte #3	SB2/EA:	O6IV: + O9III	4.7459±0.0003	96±5	0.05±0.02	0.41±0.02	2,8	a,e
Schulte #5	SB2/EB	O7Ianf + Ofpe/WN9	6.6 (fixed)	82.8±3.5	0.0 (fixed)	0.28±0.02	9,10,11,12	a

Table 8—Continued

Star	Type	S.C.	P (days)	K_1 (km s ⁻¹)	e	q	Ref.	Notes
		(+ B0V:)	138.8±8.0	...	0.49±0.14	0.06–1	13,14,15	
Schulte #73	SB2	O8III + O8III	34.88±0.04	84±1	0.43±0.01	0.99±0.02	3	
CPR2002 A36	SB2/EA	B0Ib + B0III	4.6752±0.0007	150±6	0 (fixed)	0.61±0.02	3,20,21	e
CPR2002 A45	SB2	B0.5V + B1V:–B2V:	1.50181±0.00004	138±3	0.05±0.02	0.72±0.02	3,21	
CPR2002 B17	SB2/EB:	O7: + O9:	4.0217±0.0004	257±7	0 (fixed)	0.75 (fixed)	22,23	

Note. — Photometric types EW/KE, EA, and EB stand for eclipsing system of the W UMa type (ellipsoidal; $P < 1$ day), Algol type (near spherical), and β Lyr type (ellipsoidal; $P > 1$ day) respectively. The mass ratio for MT91 421 is calculated using the O star masses of Martins et al. (2005) and interpolated AB masses of Drilling & Landolt (2000).

a – Probable triple system.

b – Re-analyzed and updated from Paper II.

c – Re-analyzed and updated from Paper III.

d – An alternative period of 5.998 d is also possible, but less likely.

e – Preliminary updates on published orbital parameters presented here. A more complete analysis will be presented in Paper 8.

f – Exhibits irregular velocity variations in addition to the listed orbital motion.

References. — (0)This work; (1) Paper VI; (2) Paper II; (3) Paper III;(4) Paper IV;(5) Wozniak et al. (2004); (6) Pigulski & Kolaczowski (1998); (7) Rios & DeGioia-Eastwood (2004); (8) Kiminki & Kobulnicky (2012); (9) Wilson (1948); (10) Wilson & Abt (1951); (11) Miczaika (1953); (12) Walborn (1973); (13) Contreras et al. (1997); (14) Rauw et al. (1999); (15) Hall (1974); (16) Romano (1969); (17) De Becker et al. (2004); (18) Nazé et al. (2008); (19) Nazé et al. (2012); (20) Otero (2008a); (21) Hanson (2003); (22) Stroud et al. (2010); (23) Otero (2008b)

Table 9. Reanalyzed Ephemerides for Systems from Paper II and Paper III

Date (HJD-2,400,000)	ϕ	V_{r1} (km s ⁻¹)	σ_V (km s ⁻¹)	$O_1 - C_1$ (km s ⁻¹)
MT91 059				
51467.913	0.294	37.0	5.2	5.52
51805.750	0.918	-124.7	5.4	-16.85
52146.697	0.182	7.5	5.1	3.36
52162.650	0.470	27.7	5.3	7.63
53338.617	0.819	-87.0	4.2	7.59
53570.693	0.646	-16.0	9.7	16.08
53573.675	0.261	27.7	11.8	0.98
53633.634	0.618	-34.6	4.3	-12.84
53634.676	0.832	-82.8	9.4	15.38
53636.753	0.260	31.7	6.8	5.08
53657.660	0.569	10.8	4.1	16.50
53903.839	0.303	9.8	14.5	-22.42
53904.708	0.482	-28.7	9.3	-46.15
53905.821	0.711	-65.2	6.5	-8.51
53906.717	0.896	-118.0	11.7	-9.98
53907.769	0.113	-34.3	16.6	-5.98
53907.864	0.132	-33.3	8.9	-15.20
53932.831	0.278	39.7	9.2	10.28
53932.839	0.279	46.5	20.2	16.85
53935.775	0.885	-97.4	16.5	9.90
53987.695	0.584	-25.2	14.1	-14.63
53988.695	0.791	-97.2	9.1	-11.43
53989.652	0.988	-87.2	4.3	5.40
53990.848	0.234	15.2	5.0	-5.73
54285.925	0.045	-55.4	7.0	10.35
MT91 145				
51381.906	0.869	10.7	2.1	1.16
51383.775	0.943	-16.6	2.5	0.48
51467.903	0.291	-29.0	1.1	0.20
51736.897	0.997	-47.9	2.9	-0.14
51737.961	0.039	-64.9	3.9	-0.61
52146.686	0.306	-27.1	1.8	-0.49
52161.793	0.908	-2.8	1.6	-1.49
52162.650	0.942	-17.1	3.2	-0.72
53338.617	0.744	16.1	2.0	-1.62
53340.576	0.822	10.1	1.6	-5.79
53570.879	0.988	-46.4	4.2	-3.53
53632.836	0.454	-8.4	3.5	-2.74
53633.714	0.489	-14.1	4.2	-12.50
53636.865	0.614	13.6	5.3	3.07

Table 9—Continued

Date (HJD-2,400,000)	ϕ	V_{r1} (km s ⁻¹)	σ_V (km s ⁻¹)	$O_1 - C_1$ (km s ⁻¹)
53657.691	0.443	-4.7	8.0	2.27
53987.694	0.577	6.8	2.1	-0.53
53988.740	0.619	11.9	1.9	1.02
53989.651	0.655	15.5	1.8	1.94
53990.848	0.703	20.5	2.7	4.19
54285.925	0.446	-2.6	3.2	3.97
54286.655	0.475	-3.3	2.5	-0.17
54287.721	0.518	6.0	2.9	4.46
54397.705	0.895	6.6	1.5	3.78
54399.685	0.974	-36.7	1.6	-2.05
54401.662	0.053	-66.2	1.2	0.38
54402.711	0.094	-66.7	1.2	-0.36
MT91 252a				
51365.058	0.607	-63.3	1.4	-0.6
54341.855	0.038	74.4	3.7	-0.4
54342.841	0.141	60.7	4.4	4.4
54343.789	0.240	17.4	3.3	0.4
54345.845	0.455	-43.1	4.4	1.2
54346.880	0.563	-56.1	4.7	3.6
54348.783	0.762	-49.6	3.8	3.2
54410.722	0.242	18.8	4.1	2.8
54696.705	0.162	44.5	4.0	-3.7
54697.690	0.265	14.9	3.1	7.2
54698.826	0.384	-30.7	5.1	-2.0
54700.838	0.594	-55.8	4.1	6.2
54701.798	0.695	-55.0	4.1	7.0
54747.741	0.501	-62.1	5.5	-10.0
54748.781	0.610	-62.0	4.3	0.8
54755.716	0.335	-27.3	3.5	-11.7
54757.701	0.543	-57.7	5.0	-0.1
55866.304	0.524	-61.2	5.8	-5.9
MT91 252b				
51365.058	0.607	55.0	2.3	0.9
54341.855	0.038	-120.7	6.2	-15.6
54342.841	0.141	-61.5	7.4	22.4
54343.789	0.240	-42.1	5.6	-3.9
54345.845	0.455	27.8	7.3	-5.1
54346.880	0.563	52.2	7.9	1.6
54348.783	0.762	48.6	6.4	6.0
54410.722	0.242	-40.7	7.0	-3.6
54696.705	0.162	-60.2	6.5	14.1

Table 9—Continued

Date (HJD-2,400,000)	ϕ	V_{r1} (km s ⁻¹)	σ_V (km s ⁻¹)	$O_1 - C_1$ (km s ⁻¹)
54697.690	0.265	-41.0	5.1	-13.5
54700.838	0.594	49.8	6.9	-3.5
54701.798	0.695	50.6	6.8	-2.8
54747.741	0.501	34.2	9.4	-7.7
54748.781	0.610	50.1	7.1	-4.2
54757.701	0.543	47.4	8.2	-0.8
MT91 258				
51467.915	0.647	2.1	2.8	16.48
51805.748	0.694	-10.0	1.7	-5.46
52146.686	0.953	21.4	6.6	-6.22
52161.793	0.983	24.5	3.8	1.63
52162.651	0.042	8.3	4.1	0.38
53338.617	0.266	-47.1	3.5	-0.89
53340.576	0.400	-49.6	2.8	-1.28
53987.695	0.547	-37.2	4.6	-4.74
53988.741	0.618	-15.8	4.7	4.21
53989.652	0.680	-10.3	4.7	-2.89
53989.774	0.689	-2.5	4.1	3.14
53990.848	0.762	10.1	5.1	-0.00
54342.873	0.777	6.4	3.5	-6.85
54343.759	0.838	31.9	2.6	7.81
54345.811	0.978	17.9	3.8	-6.04
54347.802	0.113	-14.6	2.6	0.01
54285.925	0.892	28.3	3.7	-1.25
54286.656	0.942	32.8	9.1	4.12
54287.721	0.015	14.6	8.9	-1.03
Schulte #73a				
54628.748	0.991	-76.3	9.2	-3.9
54629.866	0.023	-108.9	10.5	-6.3
54630.739	0.048	-106.4	4.7	3.7
54631.855	0.080	-95.6	8.2	8.5
54633.859	0.137	-77.2	5.1	0.6
54628.880	0.994	-76.7	3.9	0.3
54629.759	0.020	-107.0	25.8	-6.4
54630.852	0.051	-112.9	3.0	-2.7
54633.741	0.134	-75.4	9.9	4.0
54674.865	0.313	-14.0	3.2	-3.4
54675.729	0.338	3.3	7.4	7.2
54696.744	0.940	-9.1	3.0	-0.9
54696.955	0.946	-19.6	5.0	-4.5
54697.763	0.969	-39.0	4.1	5.3

Table 9—Continued

Date (HJD-2,400,000)	ϕ	V_{r1} (km s ⁻¹)	σ_V (km s ⁻¹)	$O_1 - C_1$ (km s ⁻¹)
54697.841	0.972	-55.6	9.1	-8.3
54697.913	0.974	-40.9	4.4	9.2
54698.705	0.996	-75.0	4.3	4.0
54698.905	0.002	-86.7	4.6	-1.5
54699.713	0.025	-102.0	5.5	1.9
54699.923	0.031	-108.2	5.5	-1.6
54700.713	0.054	-108.6	4.1	1.5
54701.718	0.083	-104.6	5.1	-1.5
54701.934	0.089	-100.6	7.1	0.1
54724.680	0.741	61.6	4.9	4.3
54724.800	0.744	63.9	6.3	6.5
54725.685	0.770	60.0	4.5	2.6
54725.794	0.773	58.3	4.4	0.9
54726.694	0.799	56.1	4.3	0.0
54726.817	0.802	56.6	4.5	0.8
54729.653	0.884	34.9	5.3	-0.6
54729.834	0.889	36.4	4.7	3.6
Schulte #73b				
54628.748	0.991	68.8	5.8	0.3
54630.739	0.048	99.5	3.0	-6.4
54631.855	0.080	96.5	5.3	-3.5
54633.859	0.137	78.0	3.3	4.2
54628.880	0.995	72.6	2.5	-0.4
54630.852	0.051	100.7	1.9	-5.3
54633.741	0.134	75.0	6.4	-0.5
54674.865	0.313	-5.9	3.3	-13.0
54675.729	0.338	-6.6	6.4	-7.0
54696.744	0.940	1.3	2.8	-3.4
54696.955	0.946	12.3	3.9	0.8
54697.763	0.969	38.4	3.4	-2.2
54697.841	0.972	49.6	7.7	6.0
54697.913	0.974	46.6	4.1	0.2
54698.705	0.996	79.9	3.3	4.9
54698.905	0.002	86.8	3.5	5.6
54699.713	0.025	104.0	4.2	4.3
54699.923	0.031	112.7	4.4	10.2
54700.713	0.054	108.8	4.1	2.9
54701.718	0.083	106.6	4.1	7.6
54701.934	0.089	104.5	5.8	7.9
54724.680	0.741	-61.1	4.9	-0.7
54724.800	0.744	-62.7	5.1	-2.3
54725.685	0.770	-60.4	4.2	0.1
54725.794	0.773	-58.5	4.6	1.9

Table 9—Continued

Date (HJD-2,400,000)	ϕ	V_{r1} (km s ⁻¹)	σ_V (km s ⁻¹)	$O_1 - C_1$ (km s ⁻¹)
54726.694	0.799	-61.3	3.6	-2.1
54726.817	0.802	-56.7	4.5	2.1
54729.653	0.884	-36.3	5.3	2.3
54729.834	0.889	-33.2	3.7	2.8
CPR2002 A45a				
54403.658	0.437	127.7	5.6	-4.6
54403.738	0.491	139.8	7.8	-4.1
54405.714	0.806	-60.0	9.1	-5.0
54405.737	0.822	-67.5	8.0	-1.3
54406.642	0.424	112.5	10.3	-14.3
54406.652	0.431	106.3	10.2	-23.5
54406.770	0.509	156.0	10.7	12.4
54409.739	0.486	130.1	10.1	-13.5
54410.675	0.110	-104.7	5.4	-0.8
54641.836	0.031	-133.5	6.6	-4.0
54642.901	0.740	-2.2	7.3	-1.3
54643.707	0.277	6.9	8.1	-11.9
54647.805	0.005	-150.0	5.5	-18.1
54672.895	0.712	9.5	4.7	-14.2
54724.704	0.210	-16.2	5.9	21.9
54724.776	0.258	1.2	4.7	-0.8
54725.713	0.881	-89.0	4.7	13.5
54729.700	0.536	149.5	5.6	10.5
54746.635	0.813	-46.5	8.1	13.2
54747.583	0.444	132.0	6.4	-2.7
54748.591	0.115	-108.8	7.9	-7.6
54754.767	0.227	-25.0	6.2	-1.4
CPR2002 A45b				
54403.658	0.437	-194.2	9.8	-7.9
54403.738	0.491	-185.2	10.9	17.3
54406.642	0.424	-195.4	17.3	-16.7
54406.652	0.431	-202.9	16.9	-20.2
54406.770	0.509	-179.1	16.1	22.9
54409.739	0.486	-220.0	15.8	-17.9
54410.675	0.110	143.1	9.7	-1.1
54641.836	0.031	196.2	12.8	16.3
54642.901	0.740	-5.9	12.3	-5.9
54643.707	0.277	4.4	16.4	31.9
54647.805	0.005	178.3	15.9	-5.0
54672.895	0.712	1.8	10.4	36.1
54724.704	0.210	29.1	11.3	-23.1

Table 9—Continued

Date (HJD-2,400,000)	ϕ	V_{r1} (km s ⁻¹)	σ_V (km s ⁻¹)	$O_1 - C_1$ (km s ⁻¹)
54724.776	0.258	15.2	10.0	19.2
54725.713	0.881	145.1	9.6	2.8
54726.719	0.551	-188.6	10.4	0.9
54726.791	0.599	-162.1	13.9	-4.7
54729.700	0.536	-192.7	12.0	3.1
54746.635	0.813	68.3	14.5	-14.1
54747.583	0.444	-191.9	11.3	-2.2
54748.591	0.115	161.1	17.6	20.7
54754.767	0.227	11.1	13.8	-20.8

Table 10. Updated Orbital Elements for SB1 Systems from Prior Papers

Element	MT91 059	MT91 145	MT91 258
P (Days)	4.8523±0.0003	25.126±0.001	14.6584±0.0019
e	0.14±0.07	0.37±0.02	0.15±0.07
ω (deg)	225±22	125±3	43±28
γ (km s ⁻¹)	-30.1±2.9	-15.8±0.6	-14.4±2.1
T_0 (HJD-2,400,000)	56338.2±0.3	53922.94±0.17	2454287.5±1.0
K_1 (km s ⁻¹)	71.0±4.1	42.8±0.8	40.0±3.2
K_2 (km s ⁻¹)
S. C. ₁	O8V	O9III	O8V
S. C. ₂	O–midB	O–midB	O–B
i (degrees)	19–90	19–90	15–90
M_1 (adopted; M_\odot)	21	23	21
M_2 (M_\odot)	21–5	23–5.3	21–3.9
q	1–0.23	1–0.23	1–0.19
a (AU)	~0.18	~0.59	~0.3
χ_{red}^2	4.3	2.1	4.9

Note. — Solutions for MT91 059, MT91 145, and MT91 258 make use of the He I $\lambda 4471$ line velocities instead of He I $\lambda 5876$, so the systemic velocity should be regarded as particularly uncertain relative to the rest of the Cyg OB2 sample.

Table 11. Updated Orbital Elements for SB2 Systems from Prior Papers

Element	MT91 252	Schulte #73	CPR2002 A45
P (Days)	9.558±0.001	34.88±0.04	1.50181±0.00004
e	0.25±0.03	0.43±0.01	0.05±0.02
ω (deg)	326±8	133±2	181±25
γ (km s ⁻¹)	-9±1	-1.7±0.7	-1±2
T_0 (HJD-2,400,000)	54704.7±0.2	54698.83±0.09	72825±6
K_1 (km s ⁻¹)	70±2	84±1	138±3
K_2 (km s ⁻¹)	81±4	83±1	193±6
S. C. ₁	B1–2V	O8.5III:	B0.5V
S. C. ₂	B1–2V	O9.0III:	B1–2V
i (degrees)	30–40	~40	40–45
M_1/msin^3i (M_\odot)	1.6±0.2	6.2±0.2	3.3±0.2
M_2/msin^3i (M_\odot)	1.4±0.2	6.1±0.3	2.3±0.2
q	0.86±0.04	0.99±0.02	0.72±0.02
a (r_{sun})	0.127~0.005	0.242~0.004	0.046±0.001
χ_{red}^2	2.3	1.3	2.7

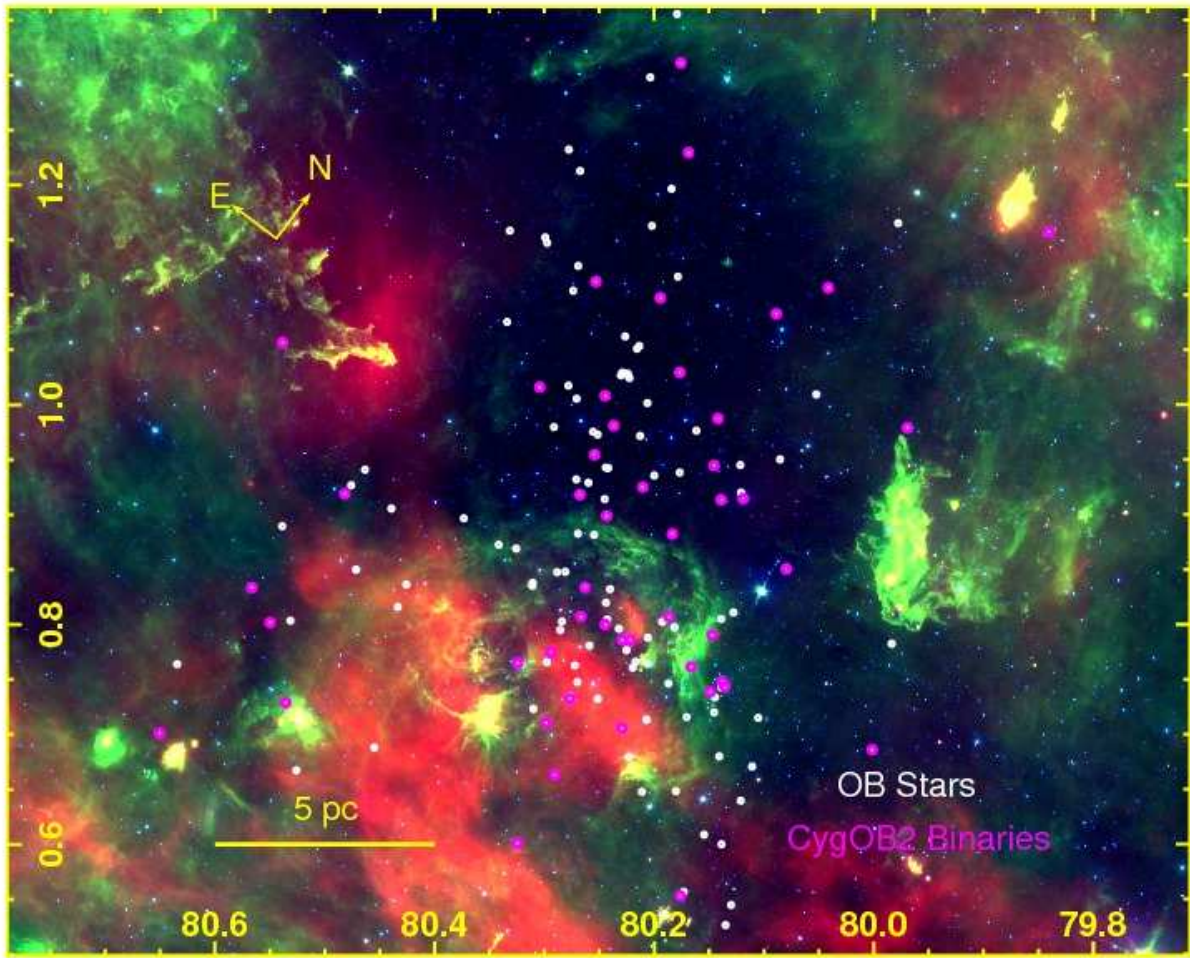


Fig. 1.— Three-color image of the Cygnus OB2 region with the *Spitzer* 4.5 μm , 8.0 μm , and 24 μm images in blue/green/red. White symbols denote O- and early B massive stars while larger magenta symbols mark the 48 known binary/multiple systems. The early-B SB2 system CPR2002 A45 lies just off the field of view to the upper right. The bar at lower left shows a linear scale of 5 pc at a distance of 1.4 kpc.

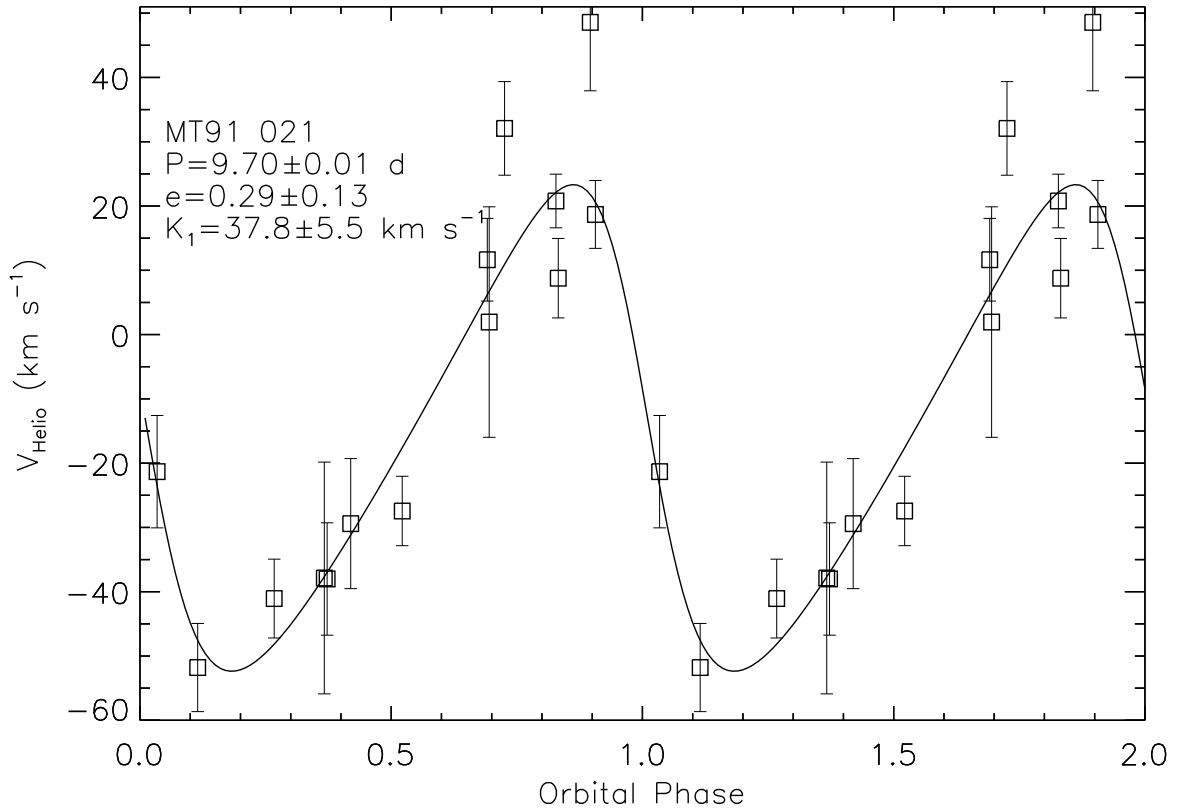


Fig. 2.— Folded radial velocity curve and best-fitting solution for MT91 021. The large reduced χ^2 of 3.2 suggests the presence of an additional velocity component in this single-lined, potentially triple system.

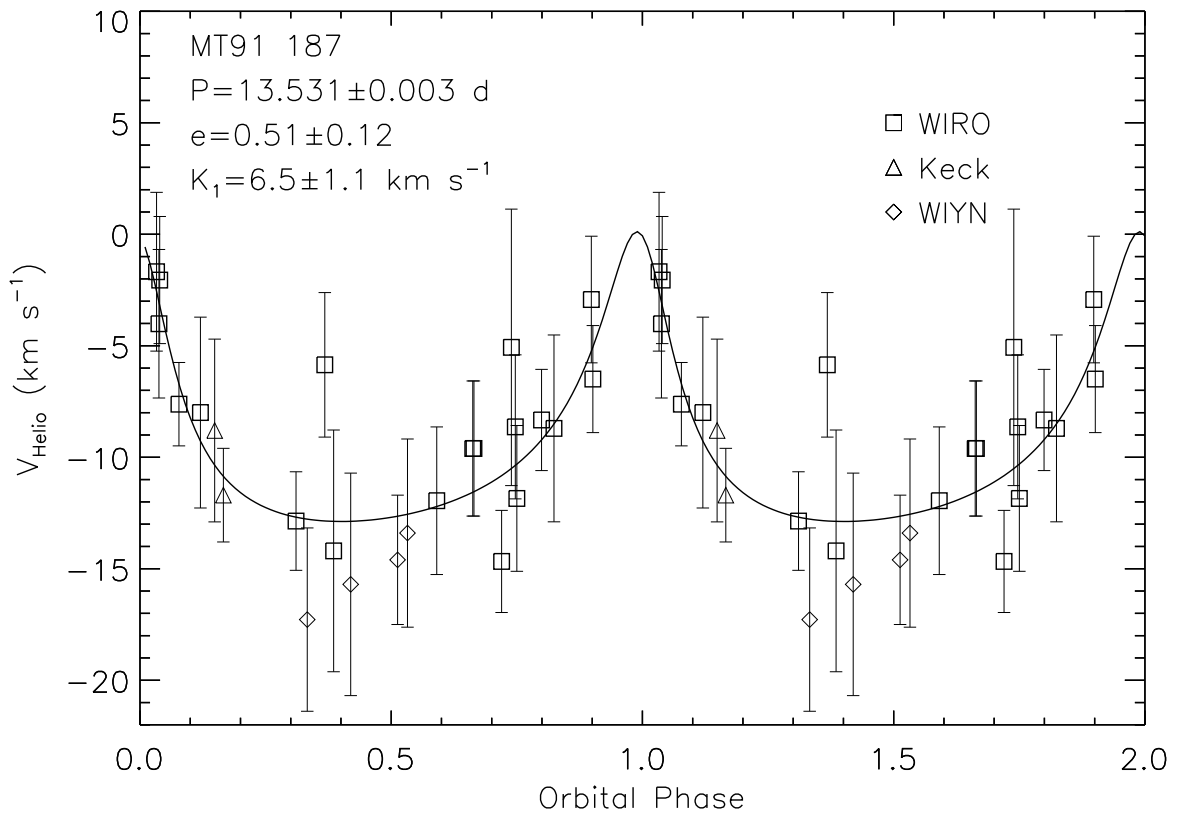


Fig. 3.— Folded radial velocity data and best-fitting solution for MT91 187.

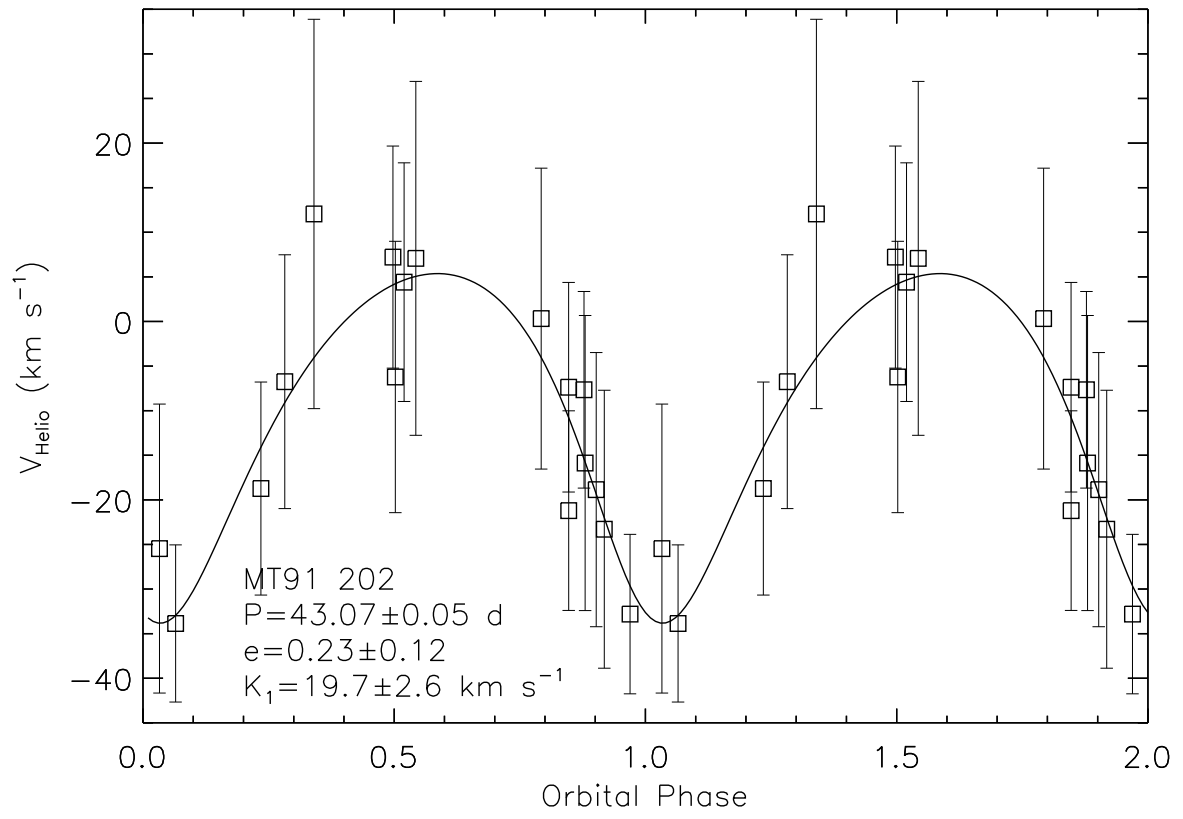


Fig. 4.— Folded radial velocity data and best-fitting solution for MT91 202.

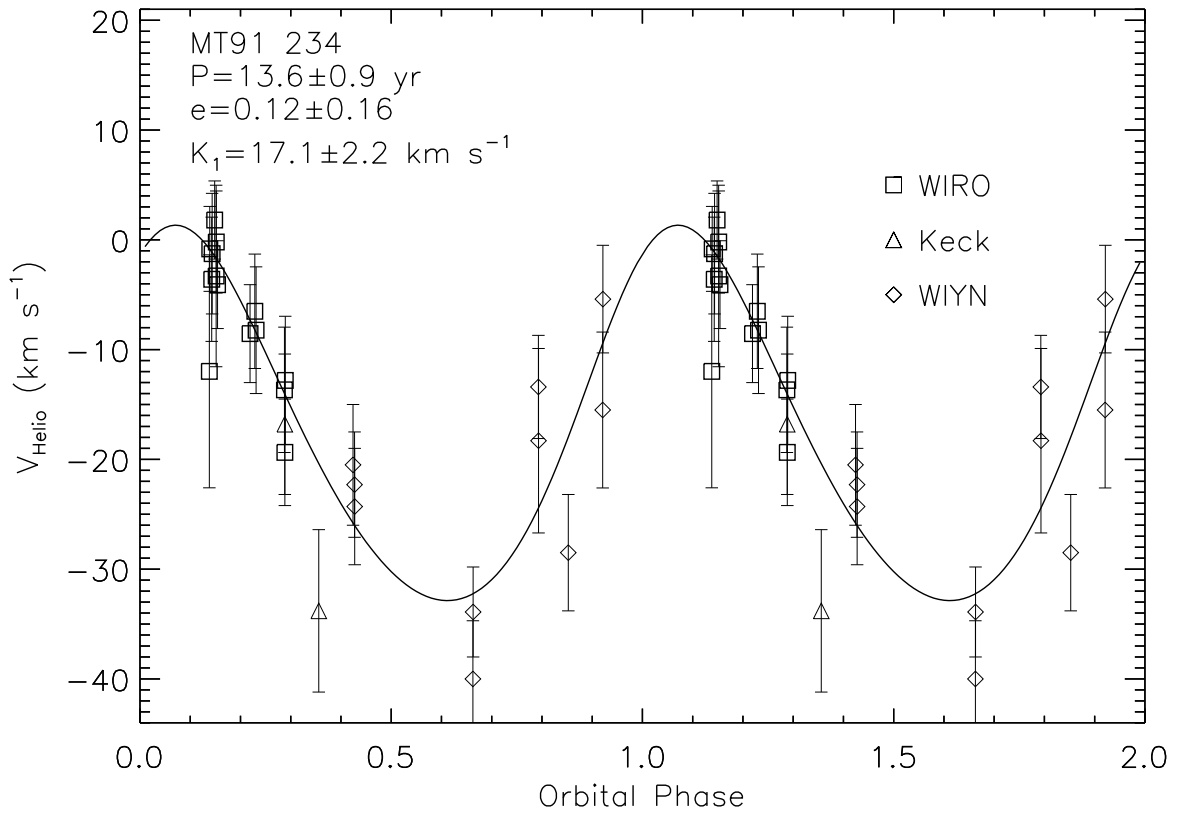


Fig. 5.— Folded radial velocity data and best-fitting solution for MT91 234.

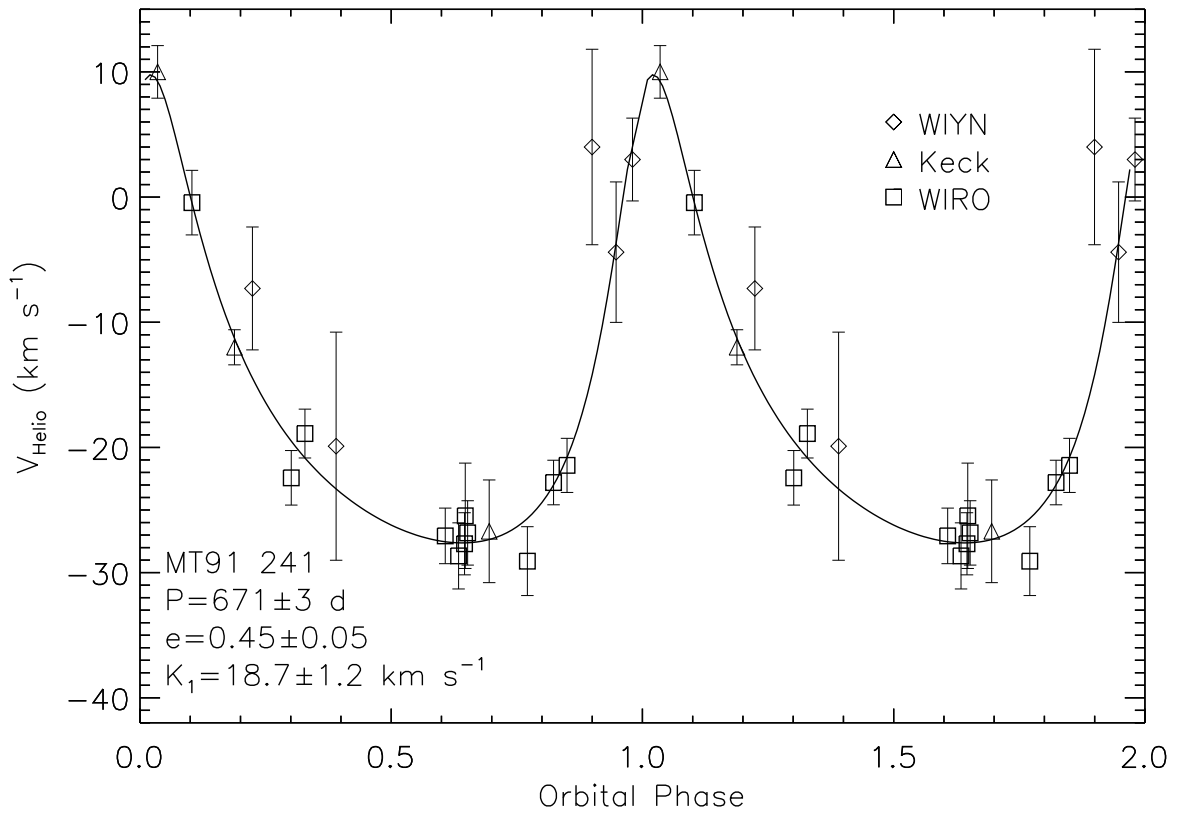


Fig. 6.— Folded radial velocity data and best-fitting solution for MT91 241.

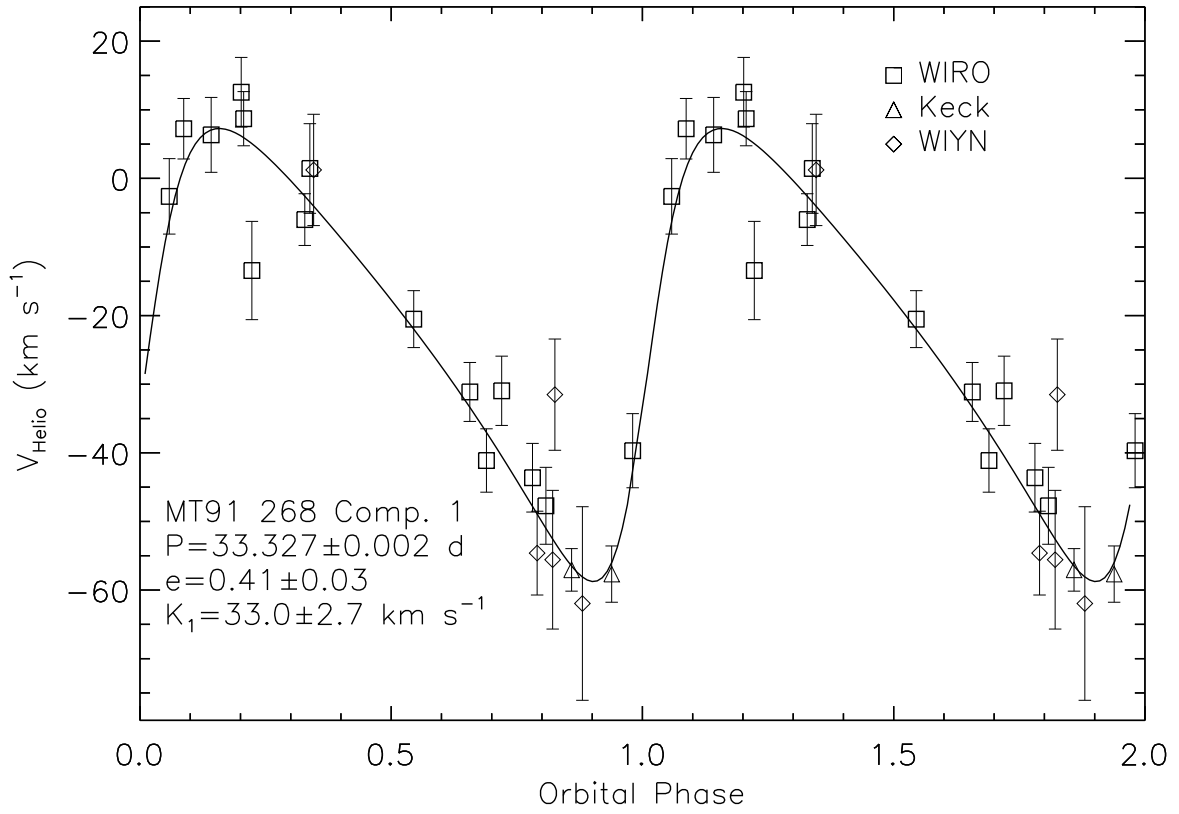


Fig. 7.— Folded radial velocity data and best-fitting solution for the single-lined triple system MT91 268, Component 1.

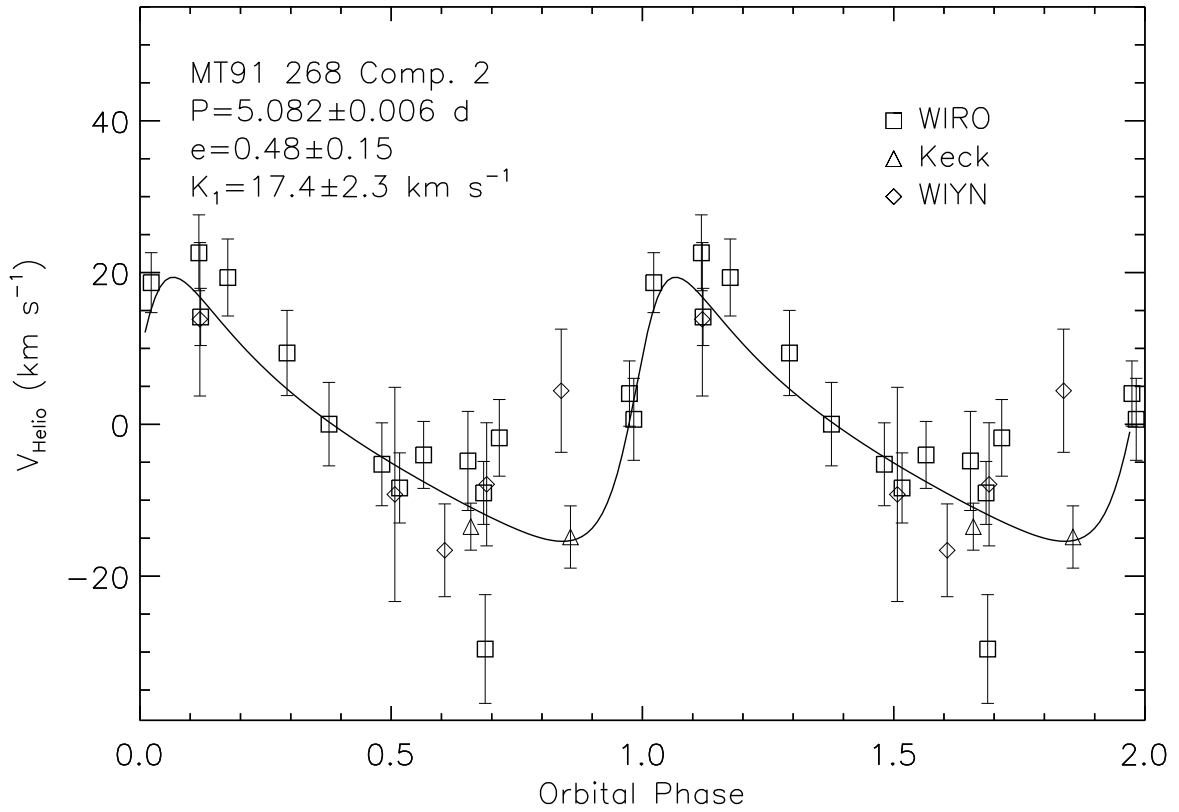


Fig. 8.— Folded radial velocity data and best-fitting solution for the single-lined triple system MT91 268, Component 2.

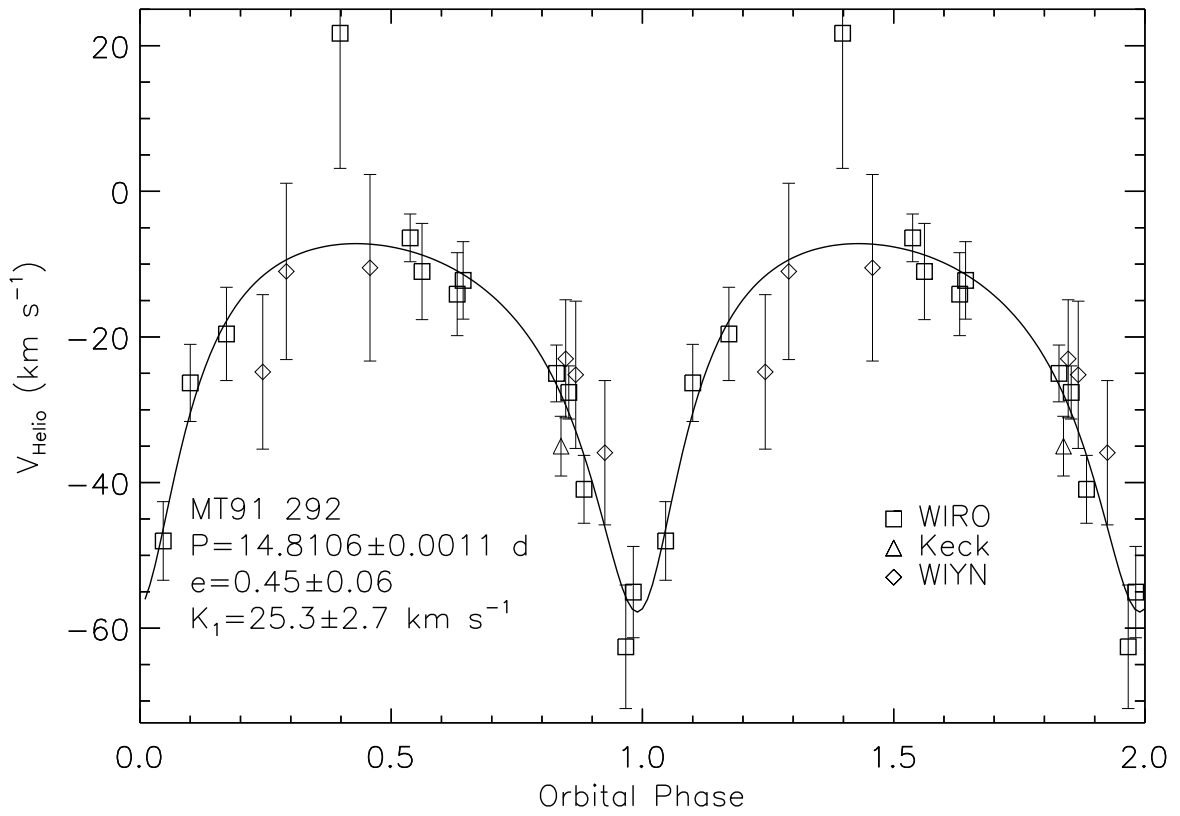


Fig. 9.— Folded radial velocity data and best-fitting solution for MT91 292.

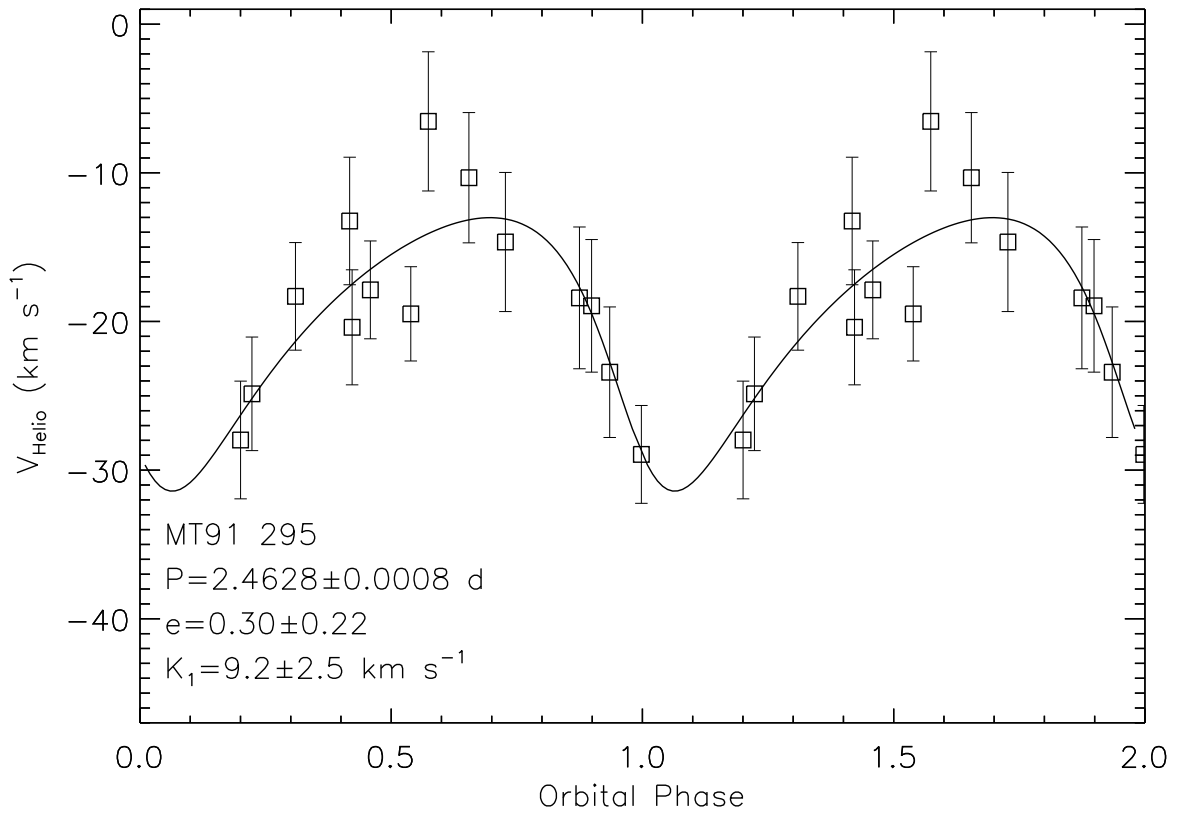


Fig. 10.— Folded radial velocity data and best-fitting solution for MT91 295.

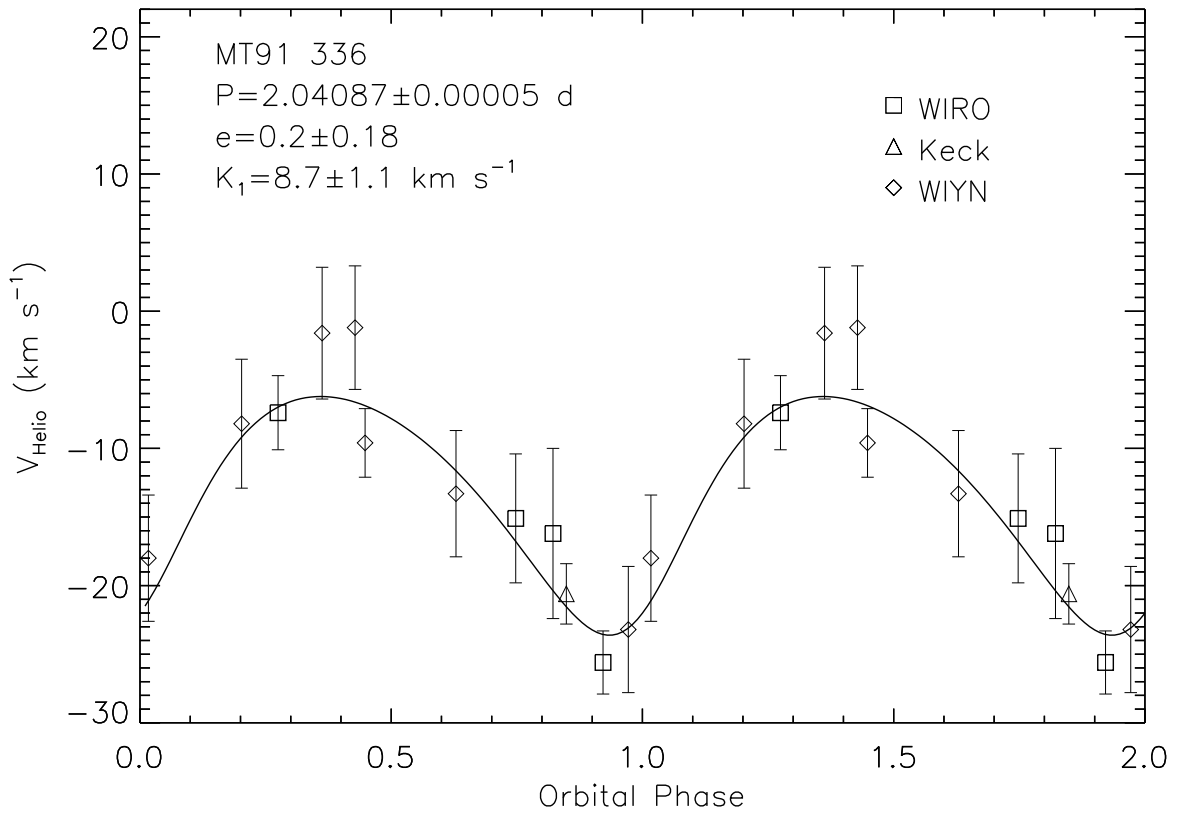


Fig. 11.— Folded radial velocity data and best-fitting solution for MT91 336.

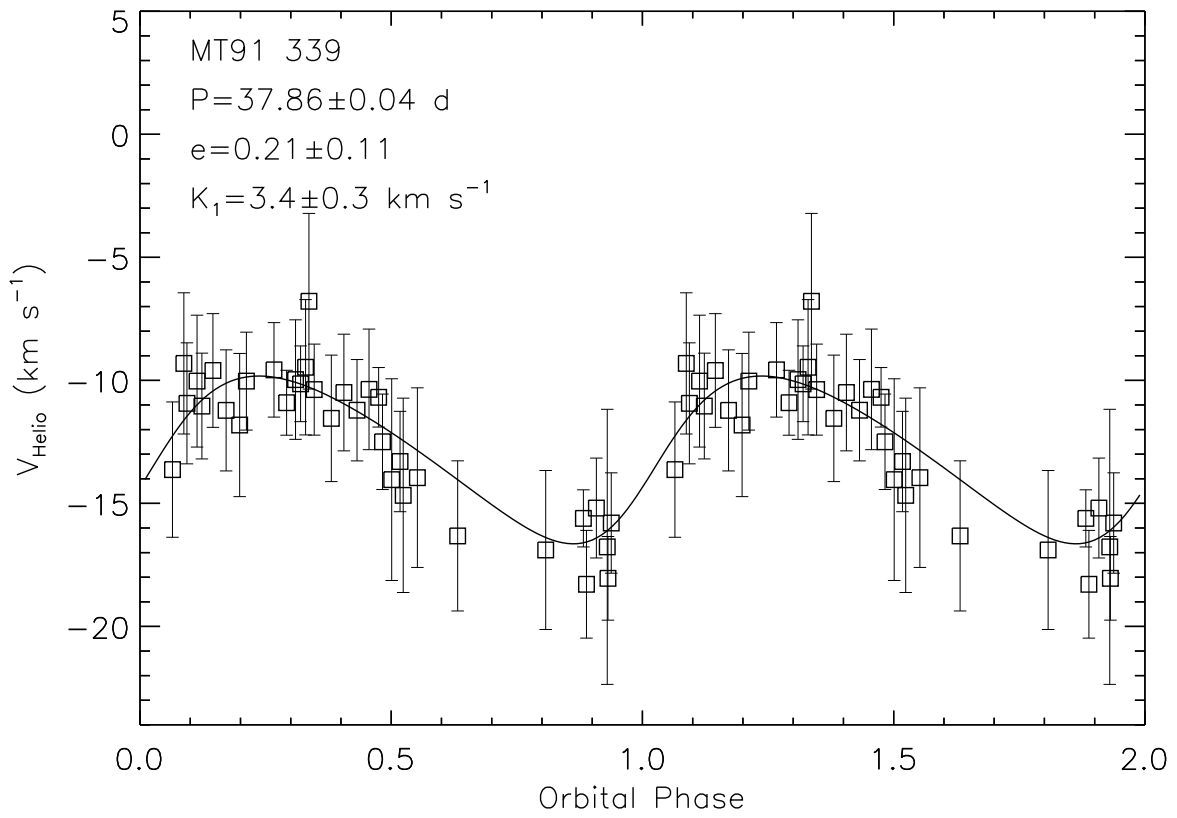


Fig. 12.— Folded radial velocity data and best-fitting solution for MT91 339.

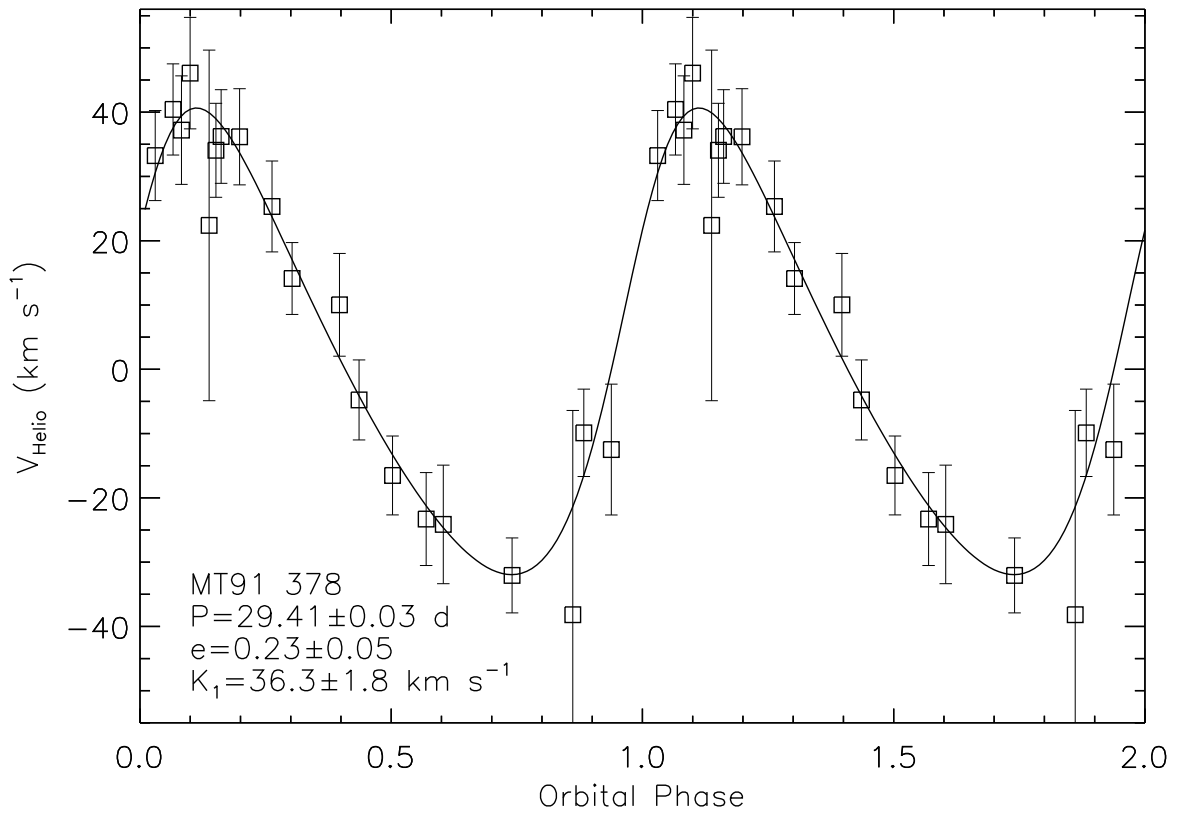


Fig. 13.— Folded radial velocity data and best-fitting solution for MT91 378.

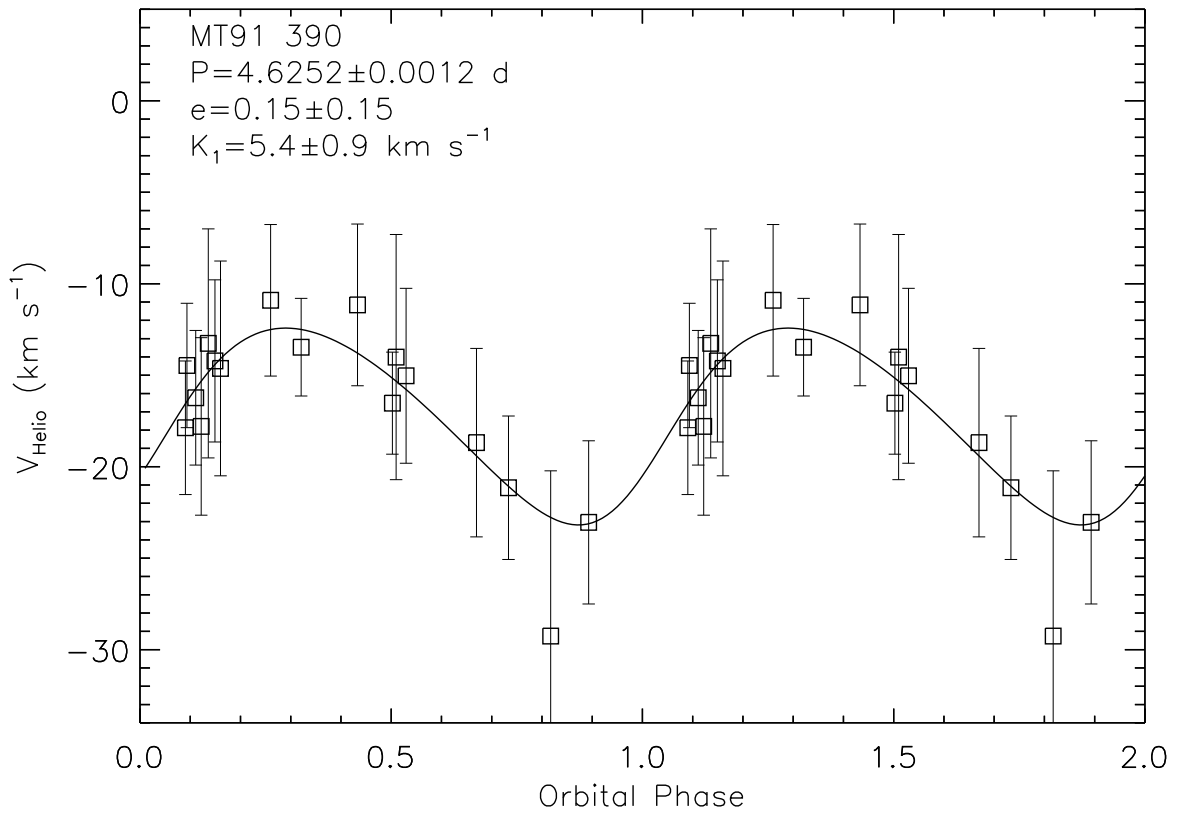


Fig. 14.— Folded radial velocity data and best-fitting solution for MT91 390.

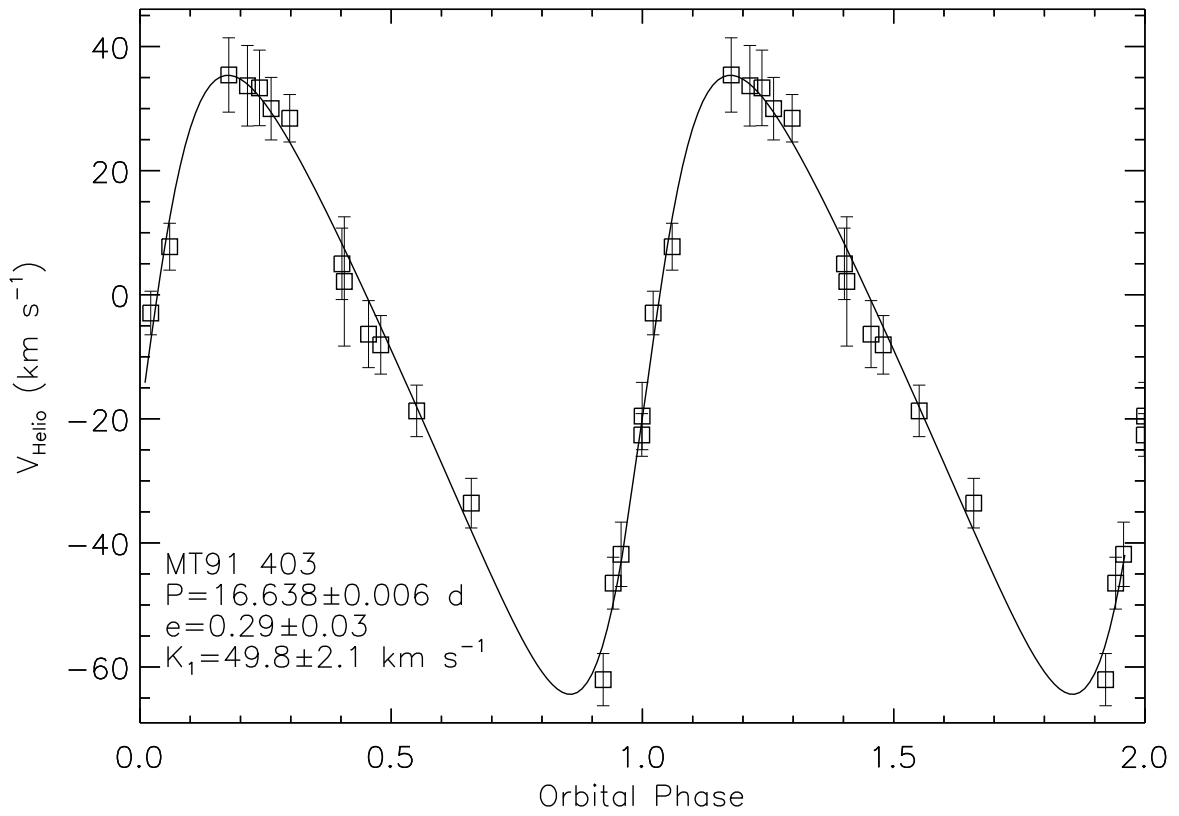


Fig. 15.— Folded radial velocity data and best-fitting solution for MT91 403.

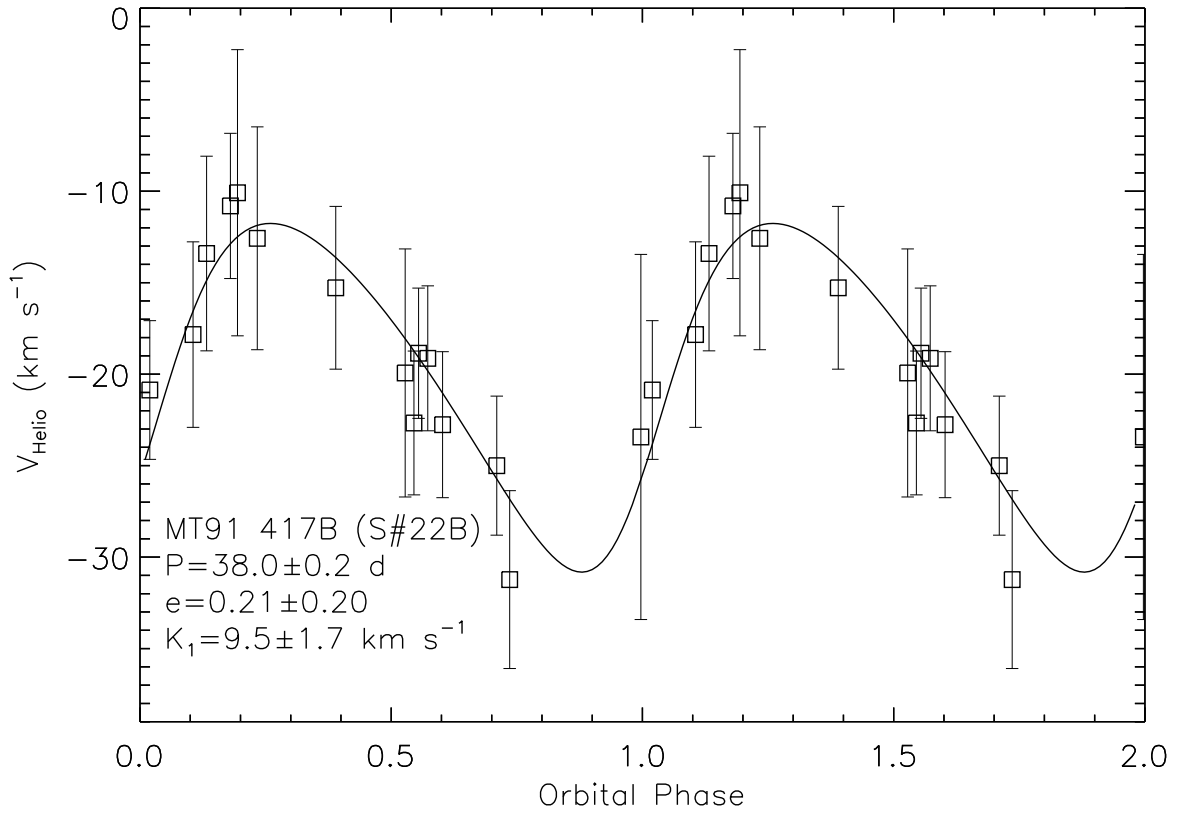


Fig. 16.— Folded radial velocity data and best-fitting solution for MT91 417B (Schulte #22B).

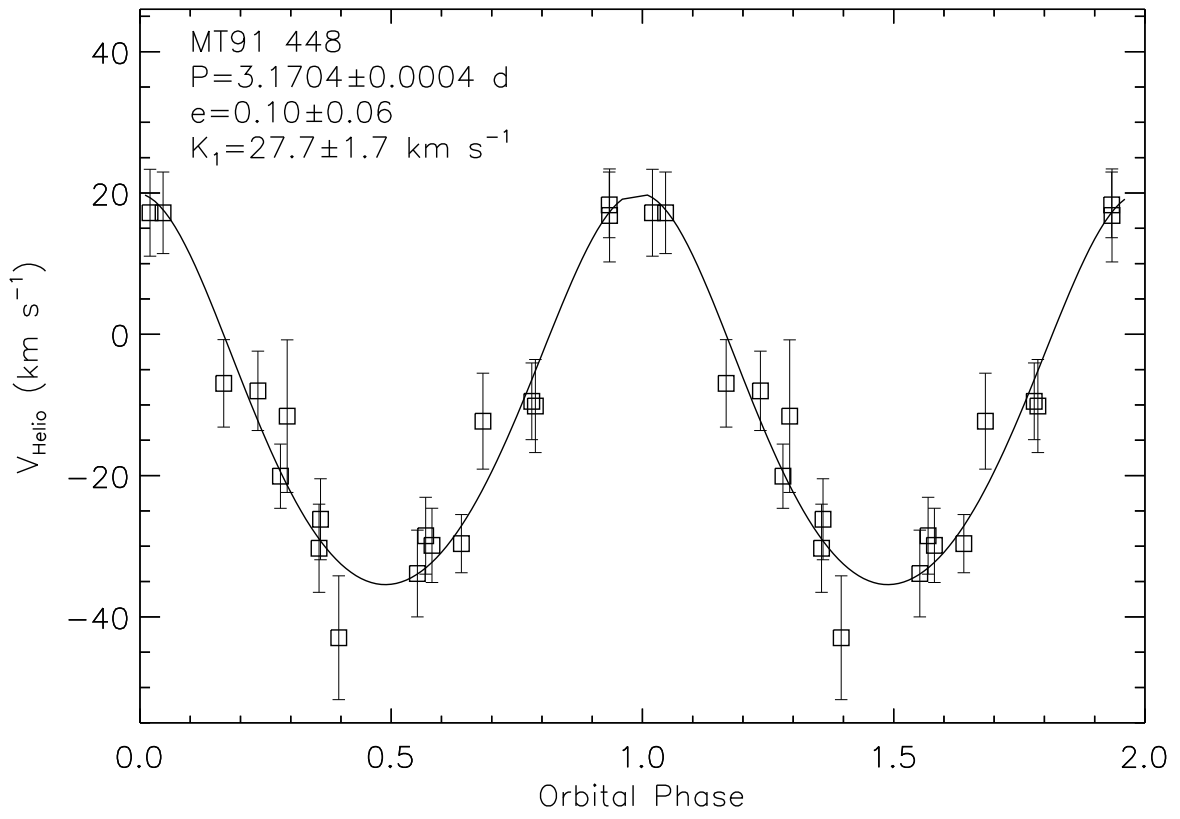


Fig. 17.— Folded radial velocity data and best-fitting solution for MT91 448.

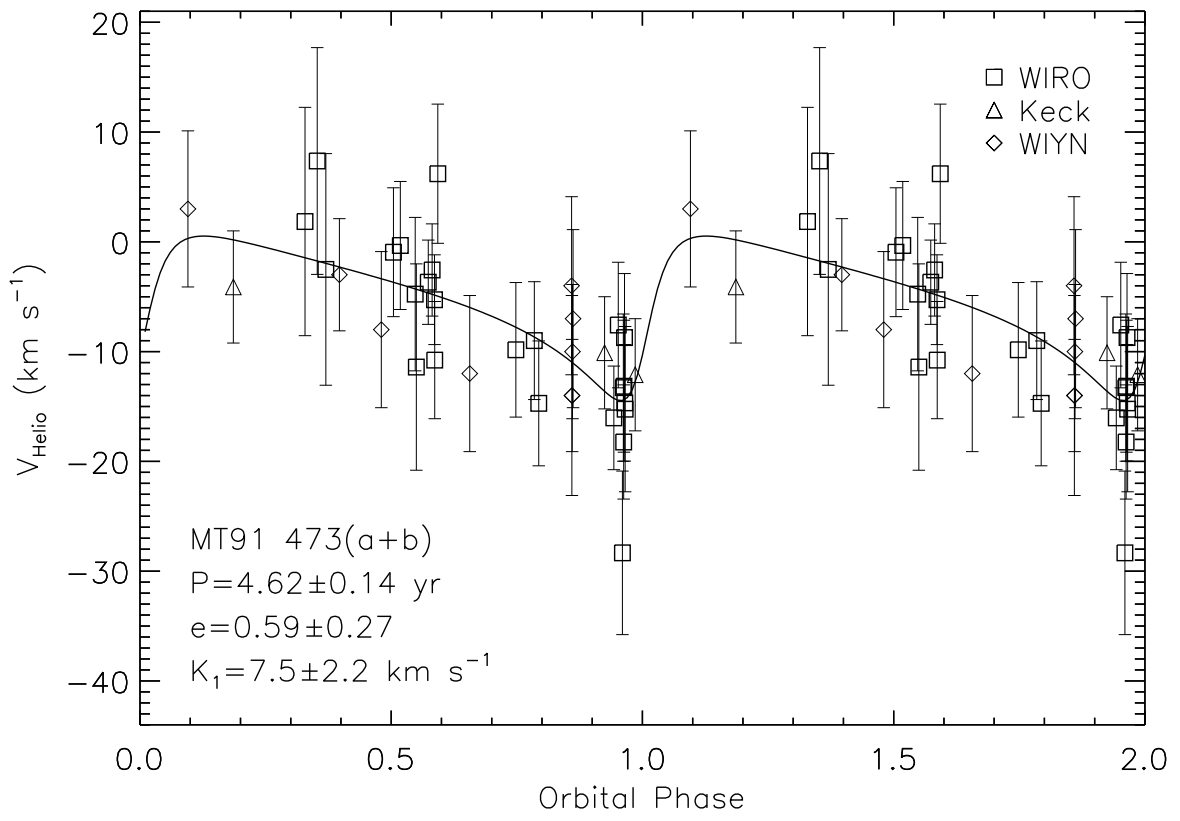


Fig. 18.— Folded radial velocity data and best-fitting solution for MT91 473.

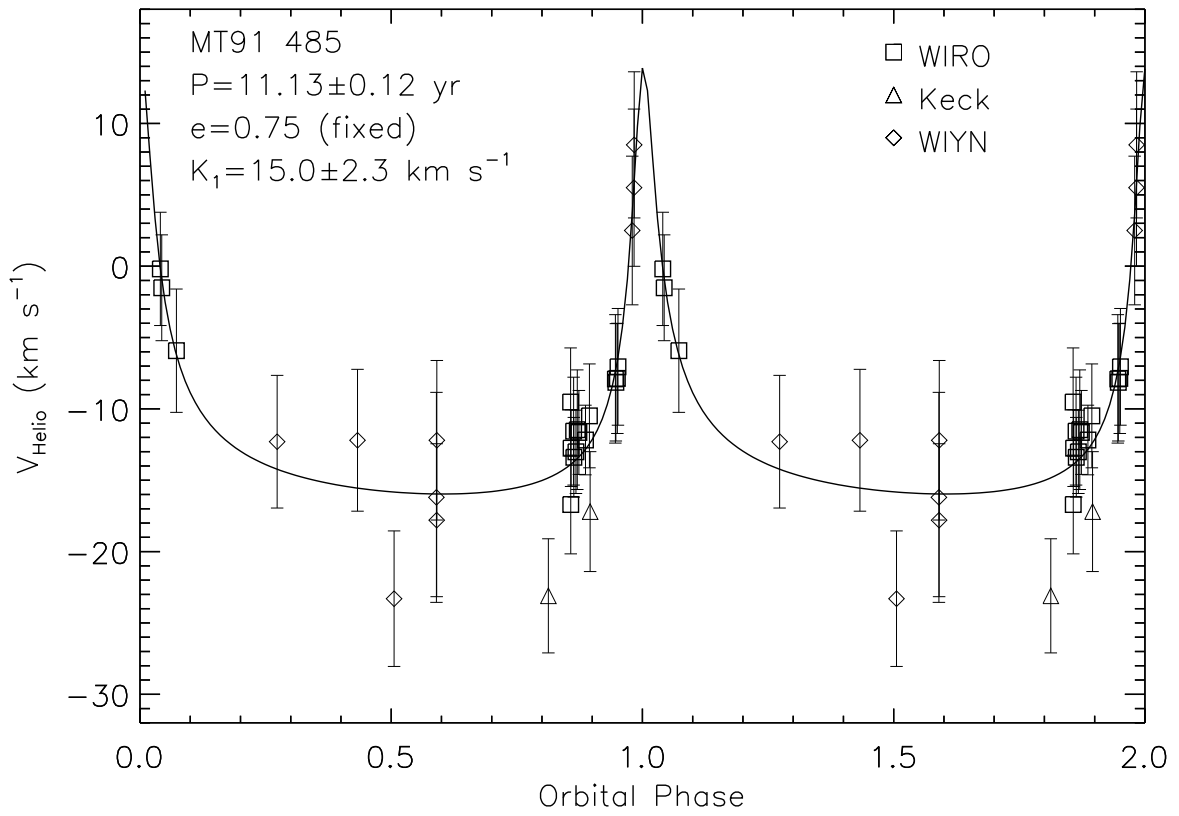


Fig. 19.— Folded radial velocity data and best-fitting solution for MT91 485.

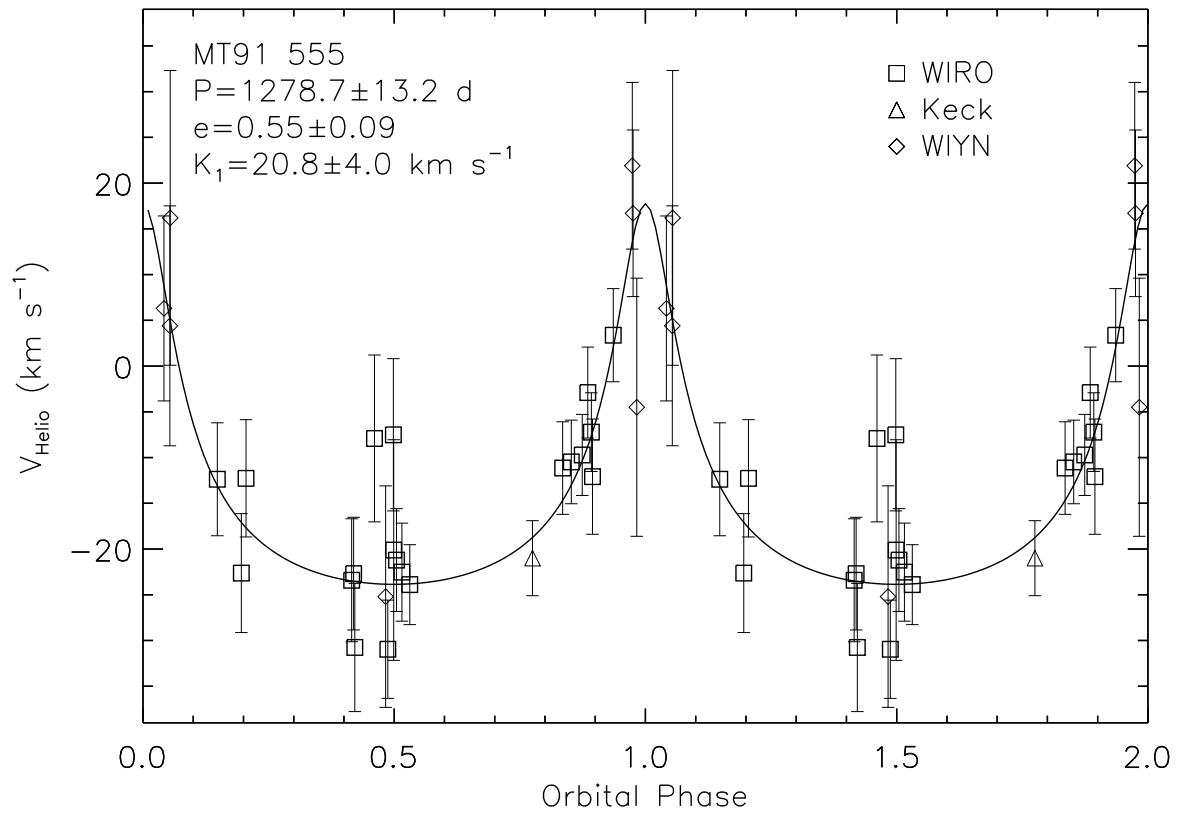


Fig. 20.— Folded radial velocity data and best-fitting solution for MT91 555.

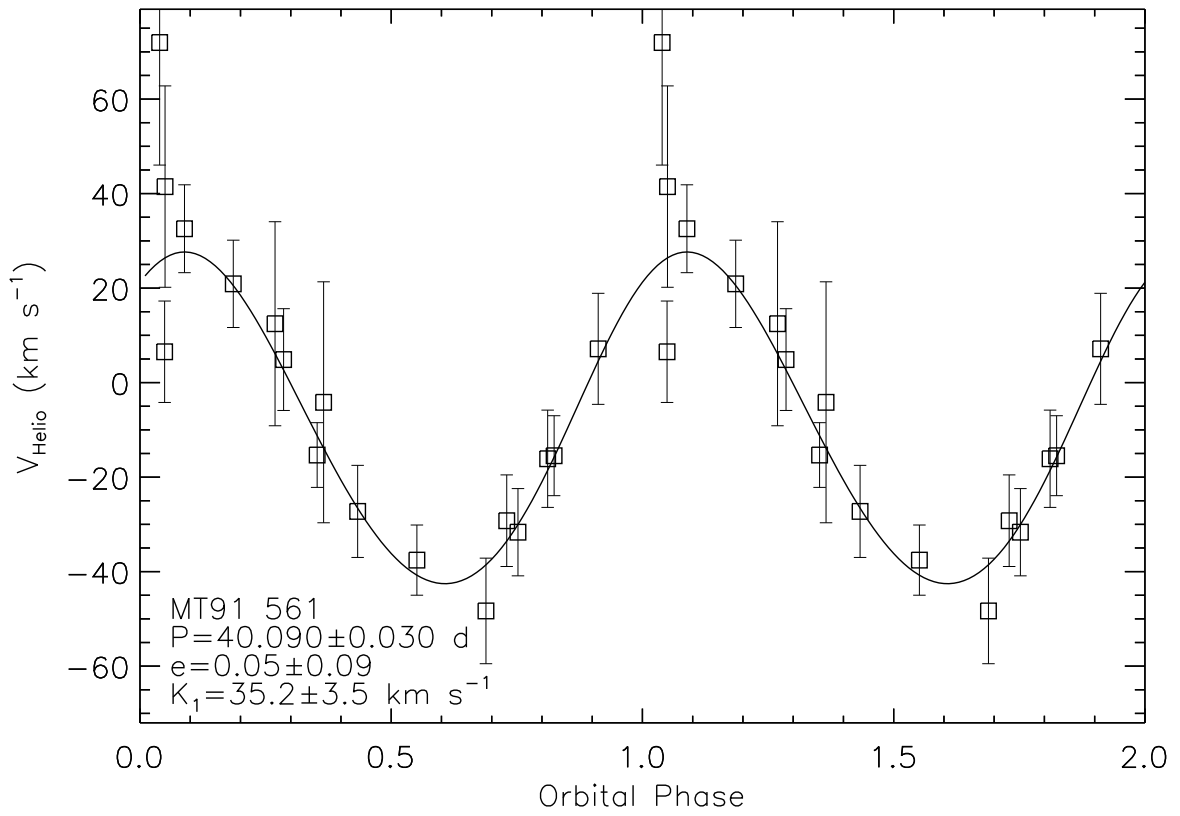


Fig. 21.— Folded radial velocity data and best-fitting solution for MT91 561.

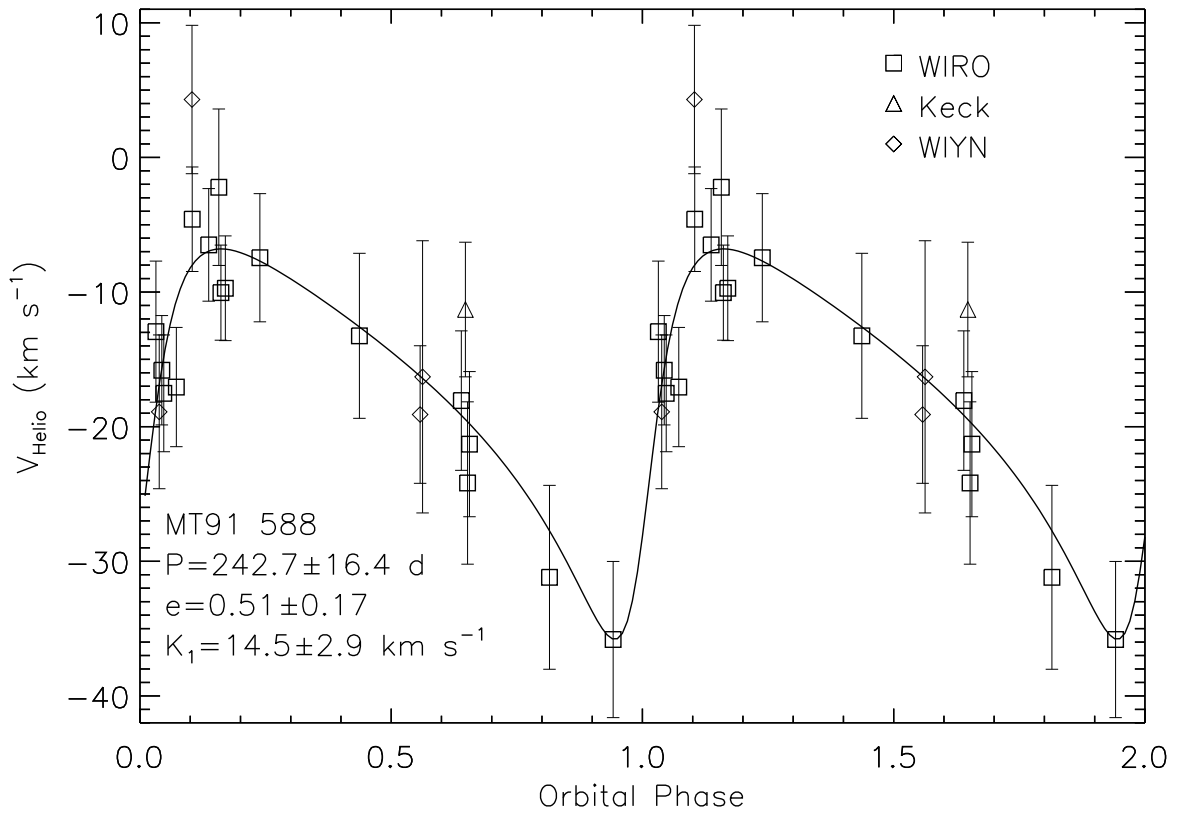


Fig. 22.— Folded radial velocity data and best-fitting solution for MT91 588.

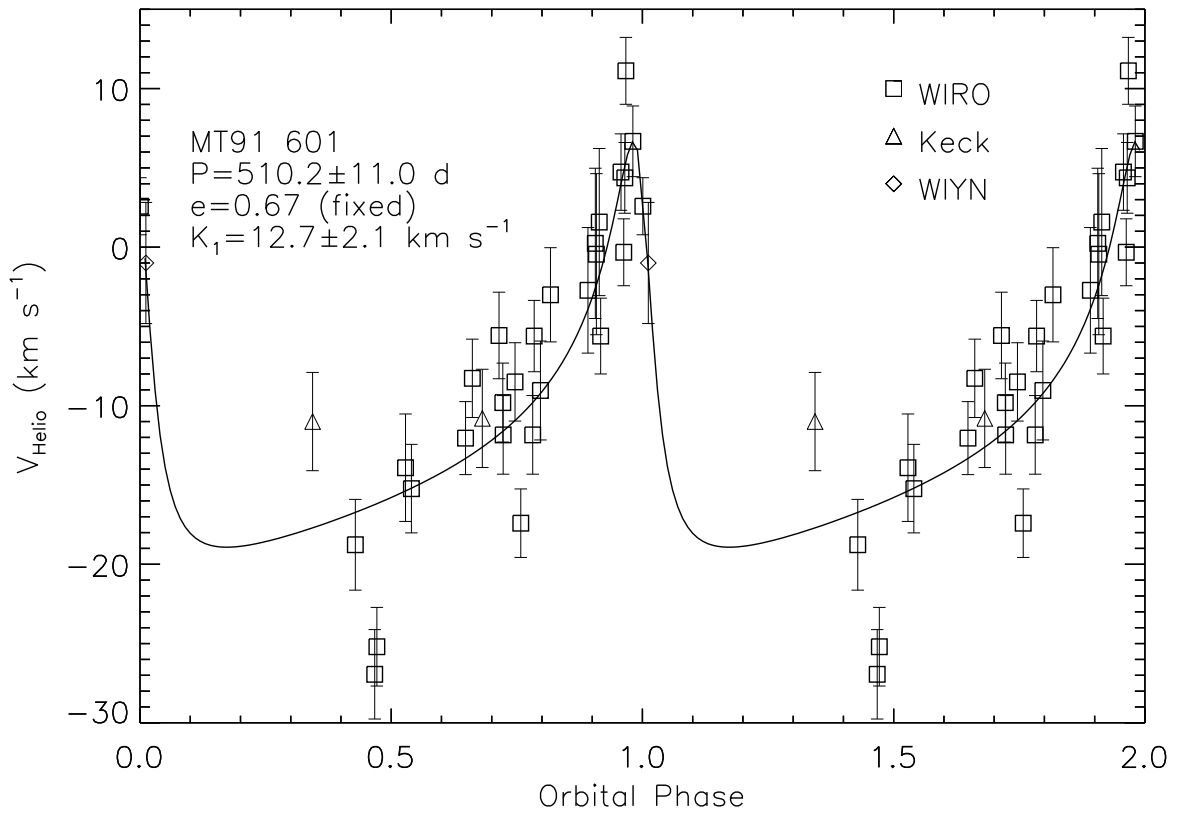


Fig. 23.— Folded radial velocity data and best-fitting solution for MT91 601.

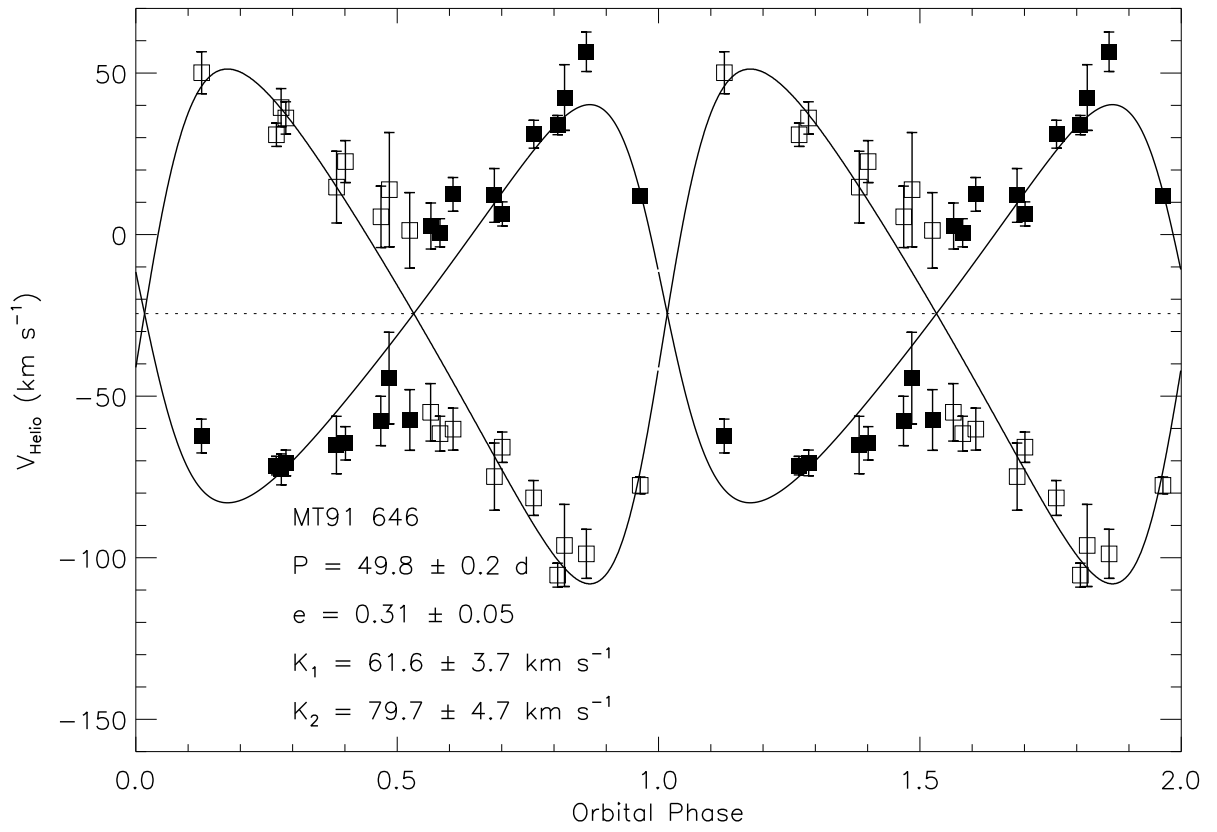


Fig. 24.— Folded radial velocity data and best-fitting solution for MT91 646.

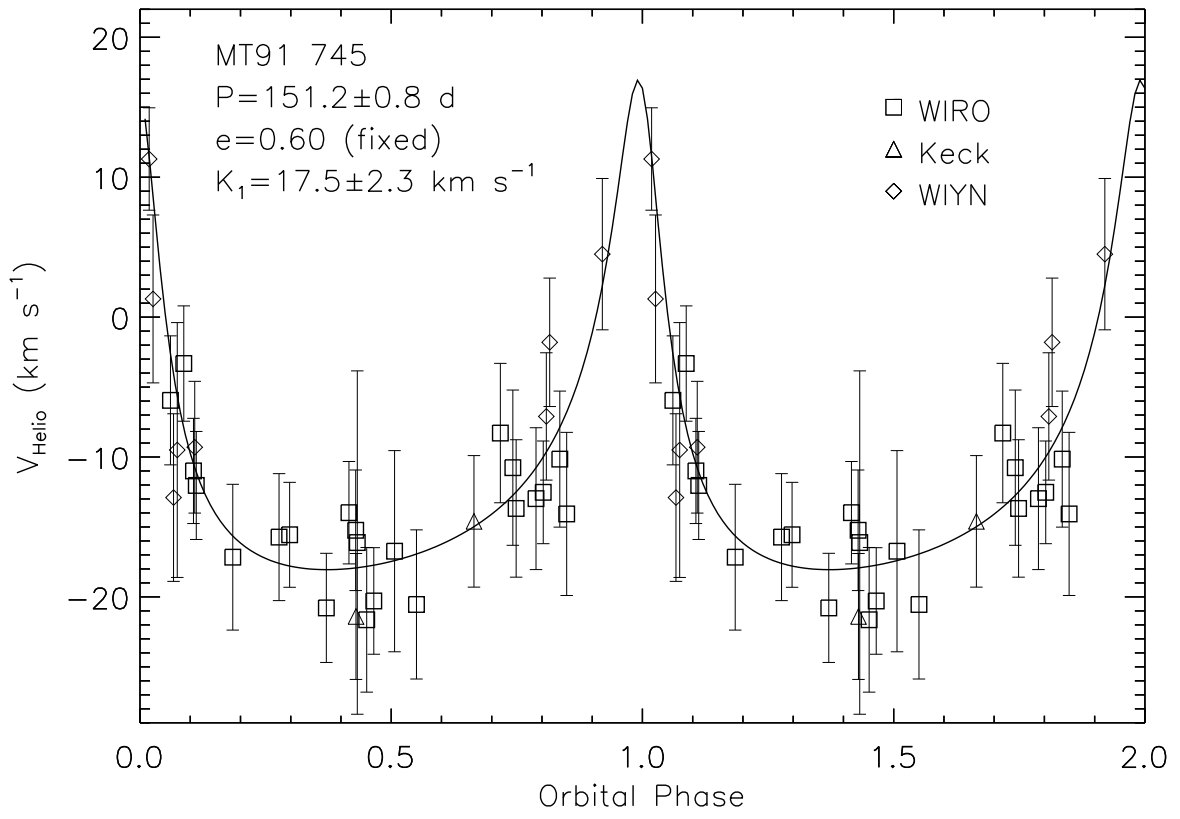


Fig. 25.— Folded radial velocity data and best-fitting solution for MT91 745.

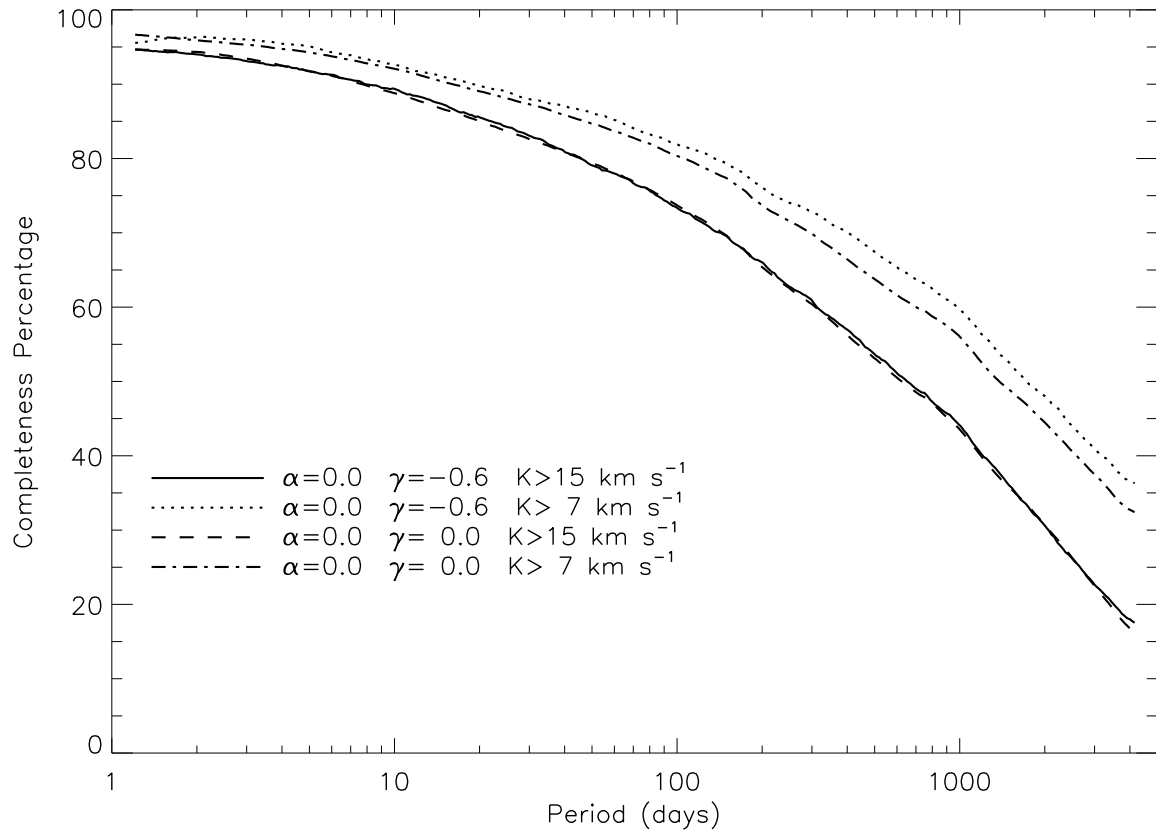


Fig. 26.— Survey completeness as a function of orbital period, based on the Monte Carlo simulations discussed in the text. Line styles denote different combinations of power law indices adopted to describe the distribution of mass ratios and eccentricities.

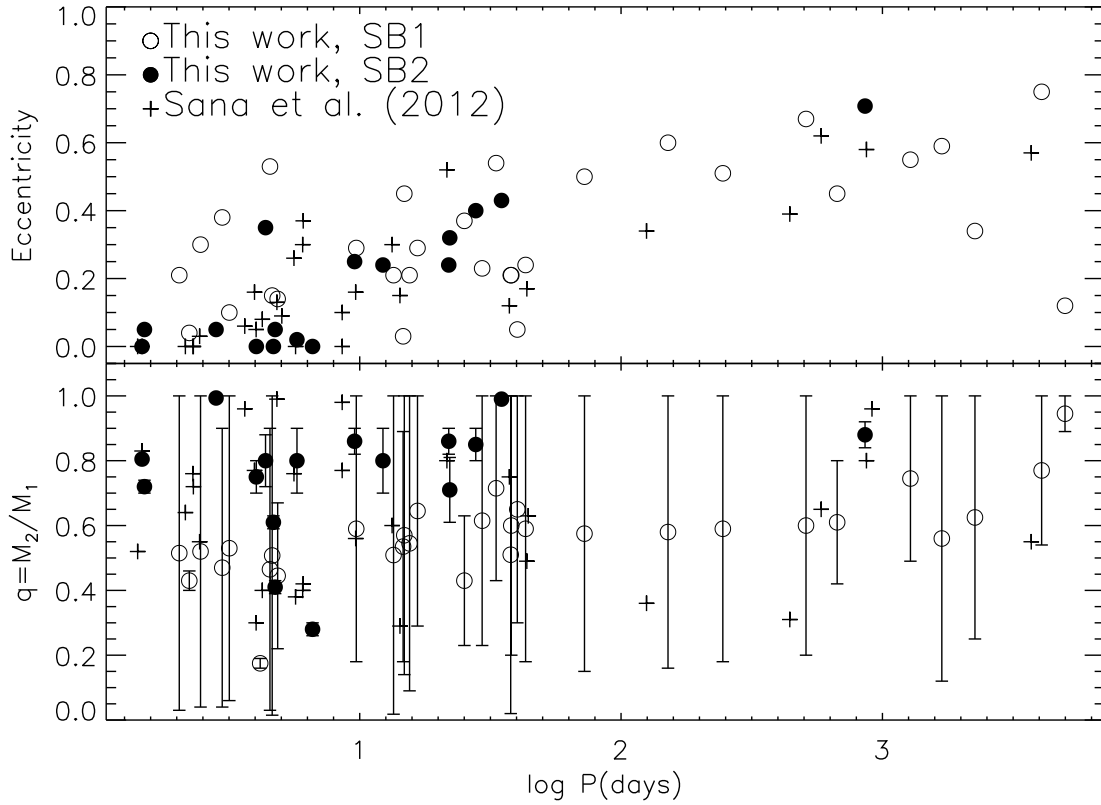


Fig. 27.— Eccentricity (top panel) and mass ratio (lower panel) versus orbital period in $\log(\text{days})$ for SB1 (open circles) and SB2 (filled circles) systems from Table 8. Pluses denote binary systems from Sana et al. (2012). Error bars in the lower panel designate the range of allowed mass ratios, given the extent of possible inclination angles.

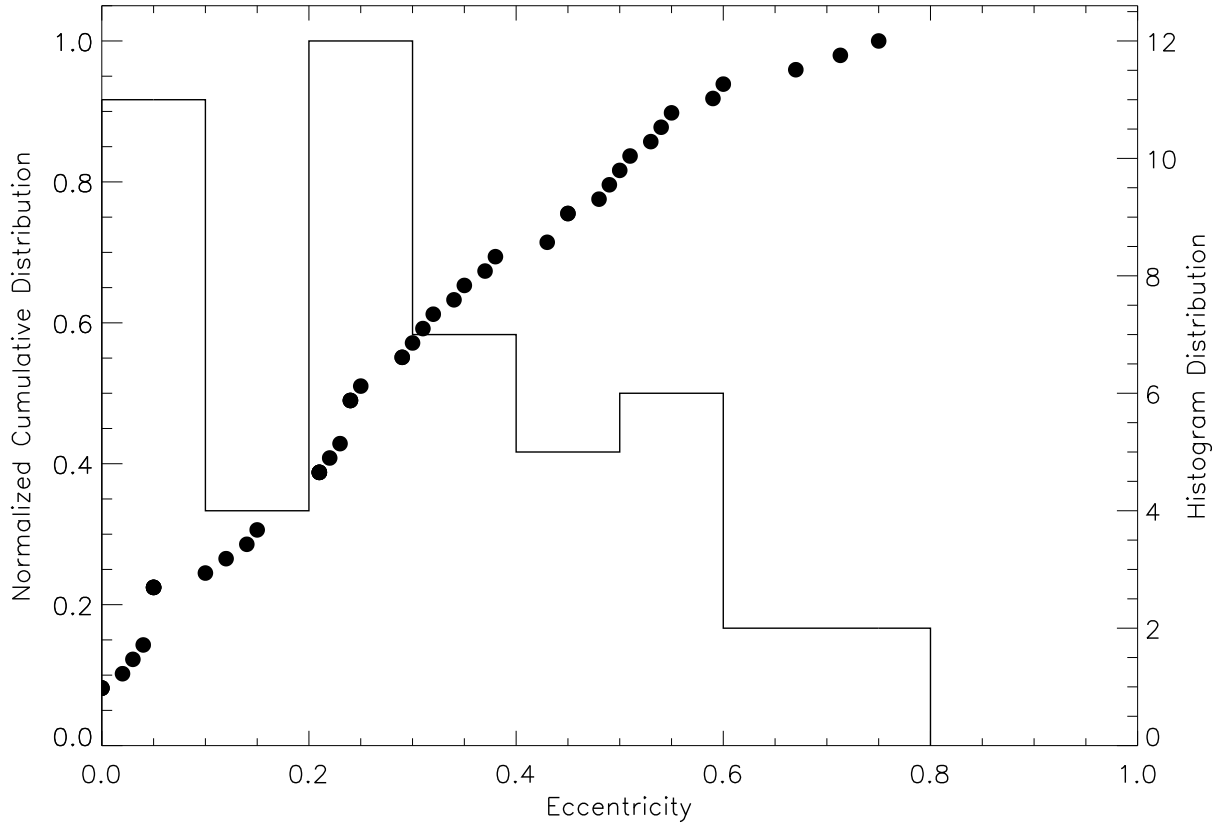


Fig. 28.— Observed distribution of eccentricity for the sample of Cyg OB2 binaries. The left-hand y-axis shows the cumulative probability, corresponding to the plotted points. The right-hand y-axis provides the number of objects in each histogram bin. The distribution is approximately uniform between $e = 0$ and $e \simeq 0.6$.

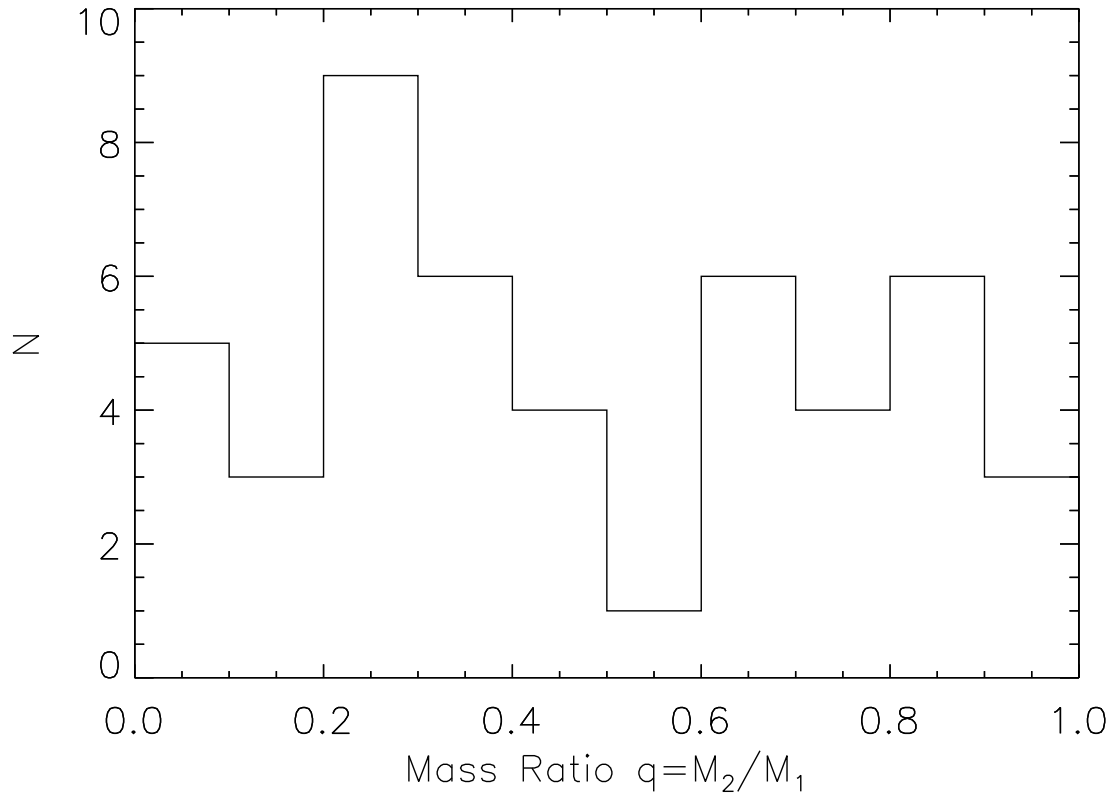


Fig. 29.— A statistical distribution of mass ratios for 48 known massive binaries in Cygnus OB2, based on Monte Carlo realizations over allowed inclination angles.

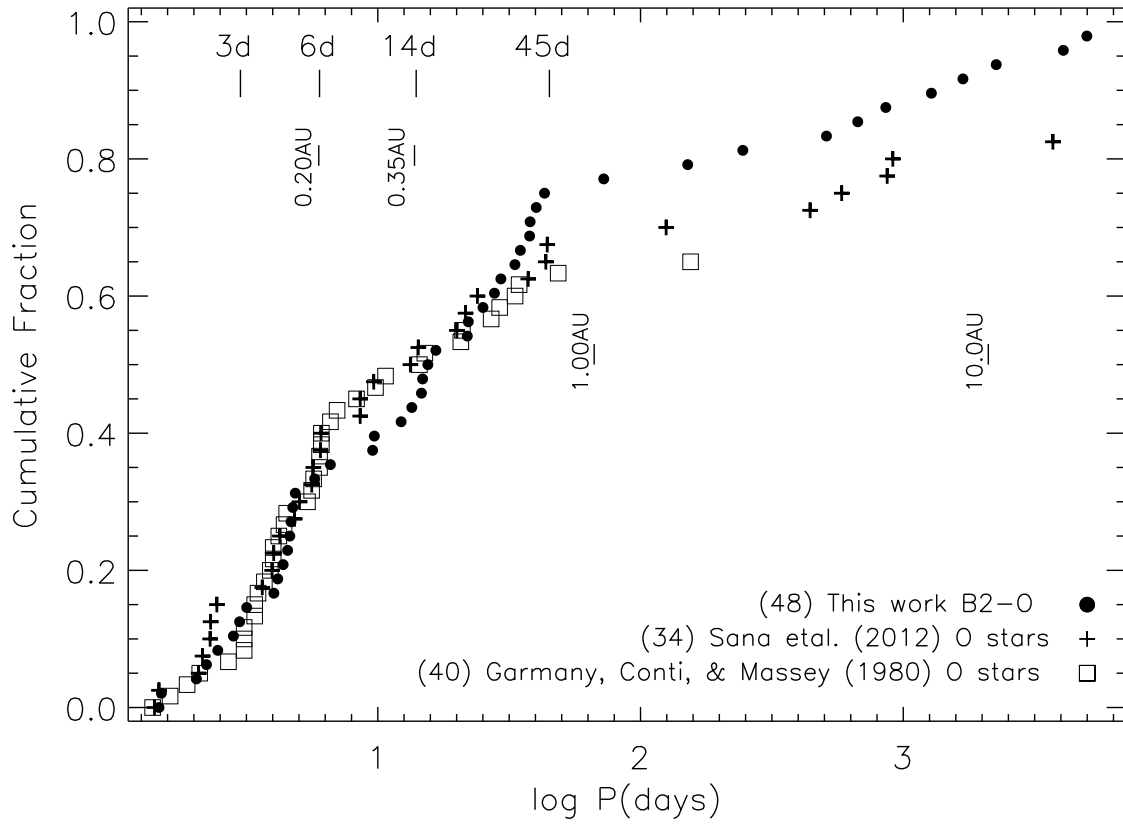


Fig. 30.— Observed cumulative distribution of orbital periods for the Cyg OB2 sample (*filled circles*), the Sana et al. (2012) sample of O stars in Galactic open clusters (*pluses*), and O stars from Garmany et al. (1980) (*open squares*).

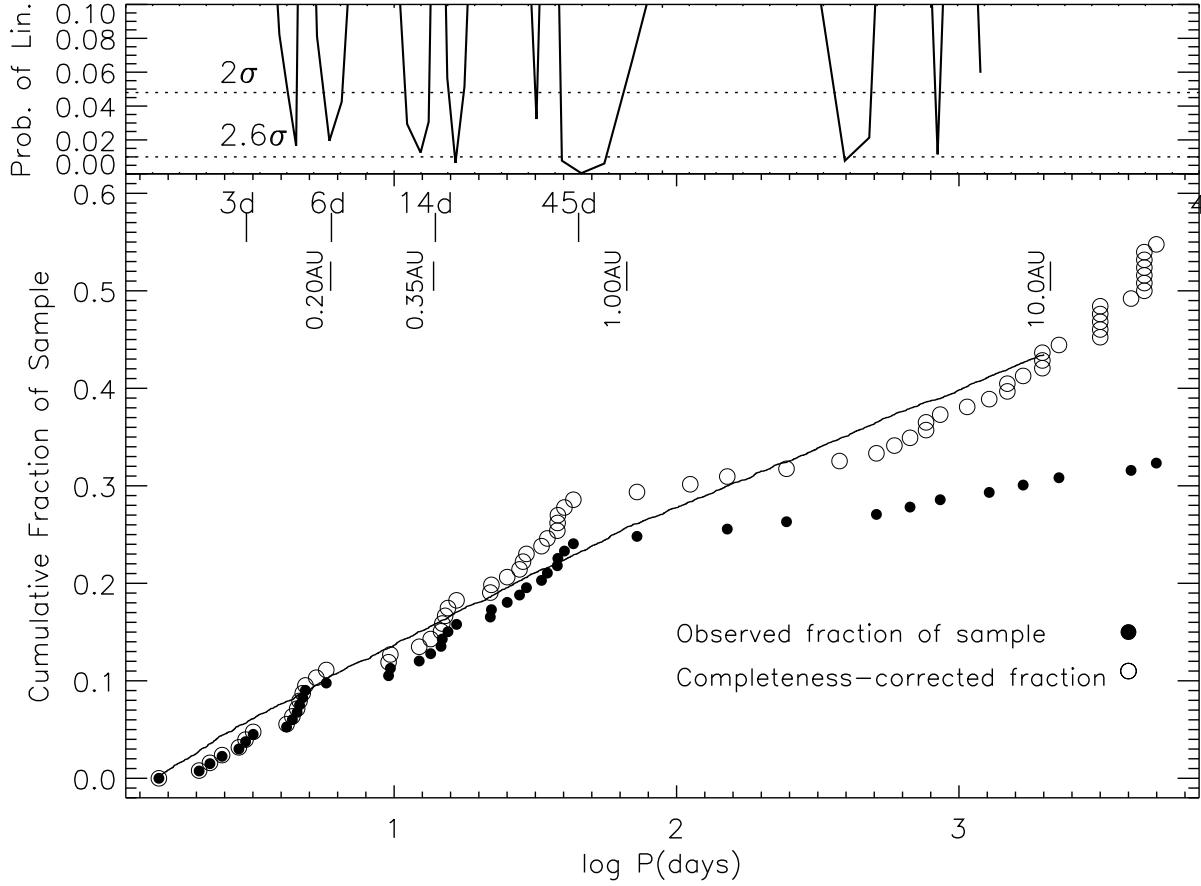


Fig. 31.— (Lower panel) Observed cumulative distribution of orbital periods in the unbiased Cyg OB2 sample as a fraction of the entire sample (*filled circles*) and the the inferred true distribution of orbital periods (*open circles*) using the completeness corrections shown in Figure 26 and assumptions for the underlying distribution of eccentricities and mass ratios, as described in the text. The solid curve is a power law with slope $\beta = -0.22$. (Upper panel) Probability that the observed distribution is consistent with uniform in a moving window of width seven observed systems. Probable changes in slope near 6 days, 14 days, and 45 days appear as dips in the probability curve.

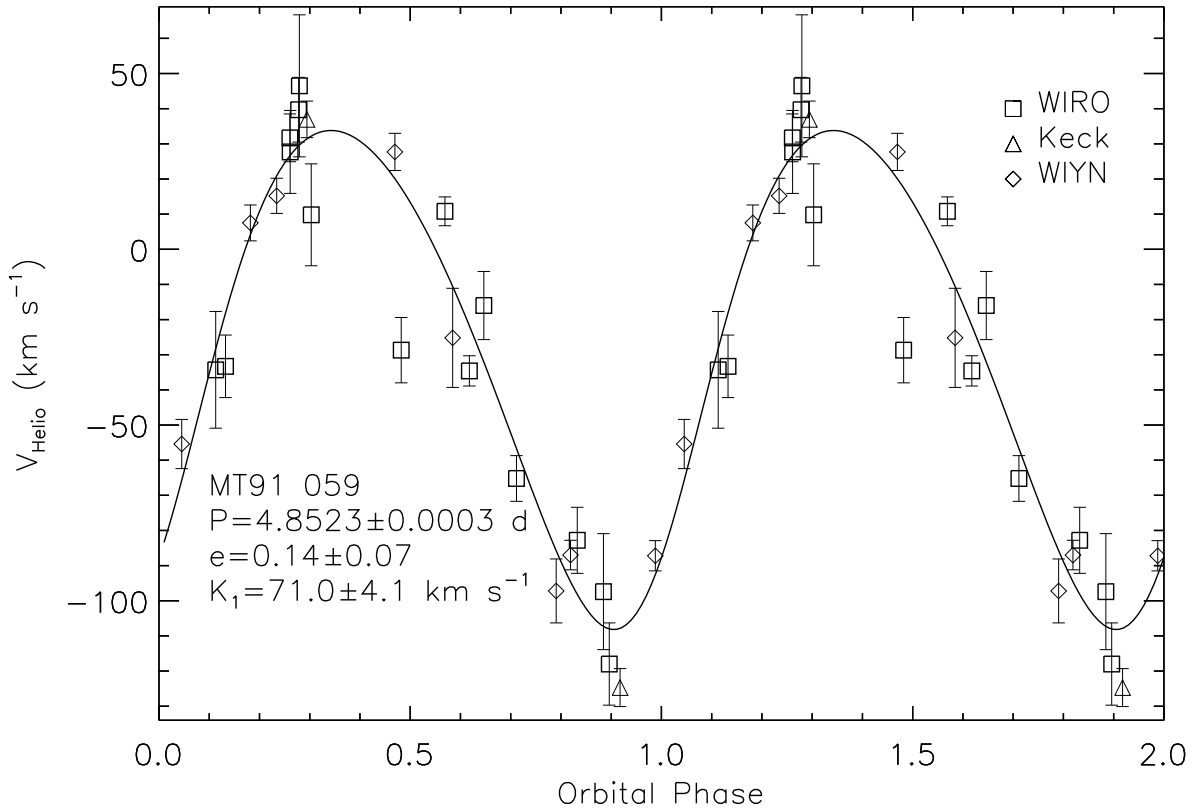


Fig. 32.— Folded radial velocity data and best-fitting solution for MT91 059, re-analyzed and updated slightly from Paper II. The large reduced χ^2 of 4.3 suggests either the presence of an additional velocity component or additional photospheric variability.

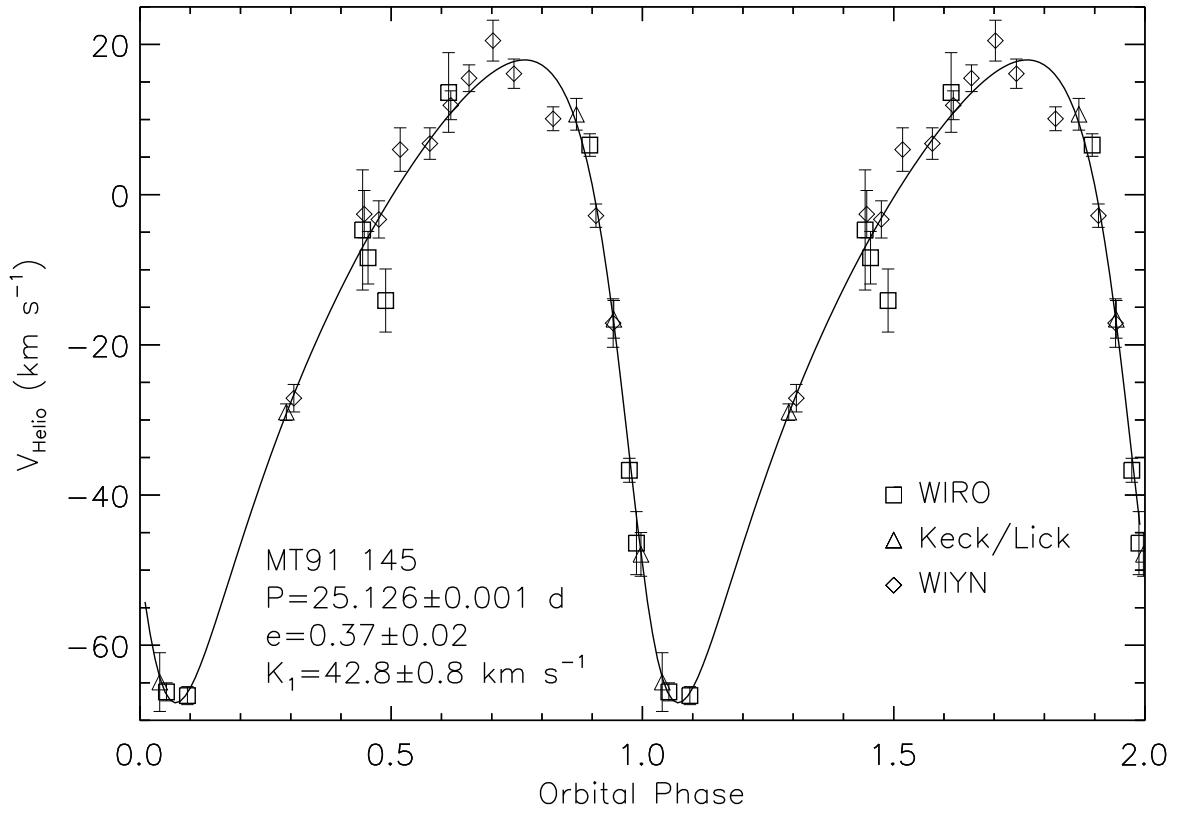


Fig. 33.— Folded radial velocity data and best-fitting solution for MT91 145, re-analyzed and updated slightly from Paper III.

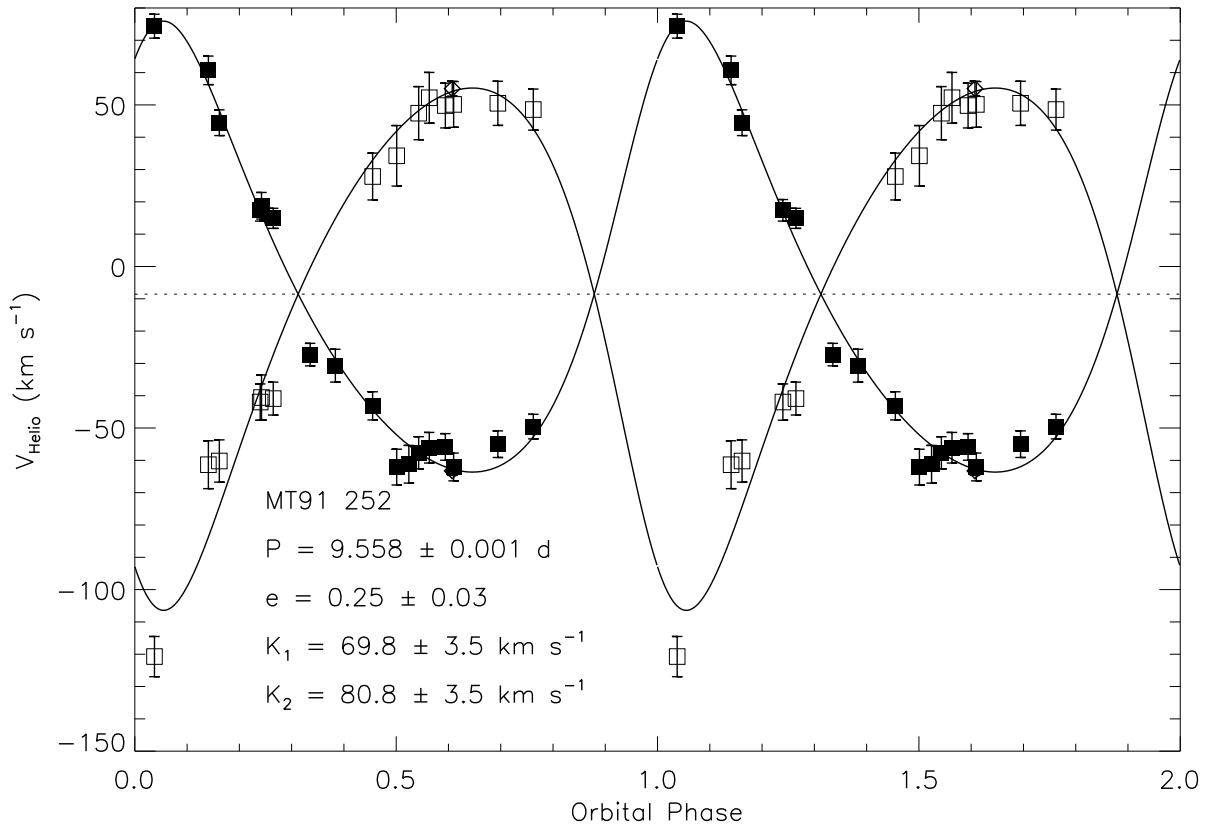


Fig. 34.— Folded radial velocity data and best-fitting solution for MT91 252, re-analyzed and updated from Paper II.

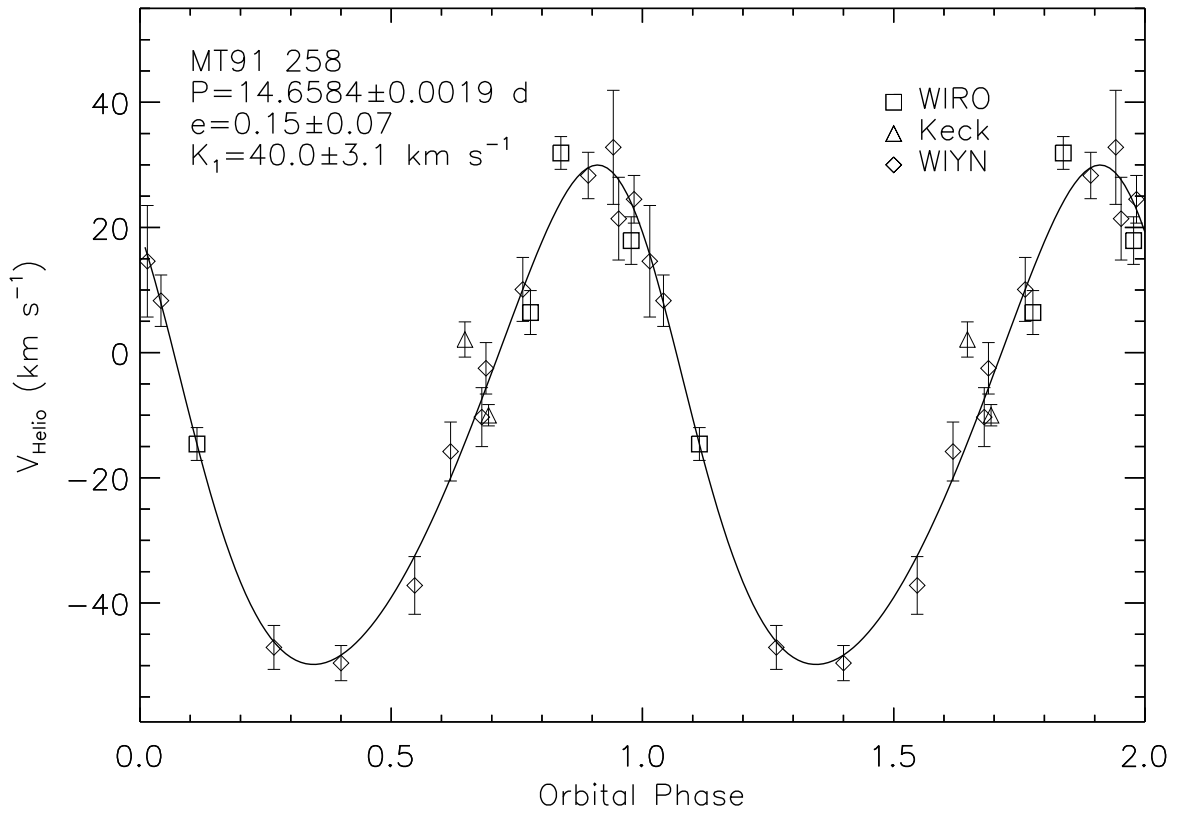


Fig. 35.— Folded radial velocity data and best-fitting solution for MT91 258, re-analyzed and updated slightly from Paper II.

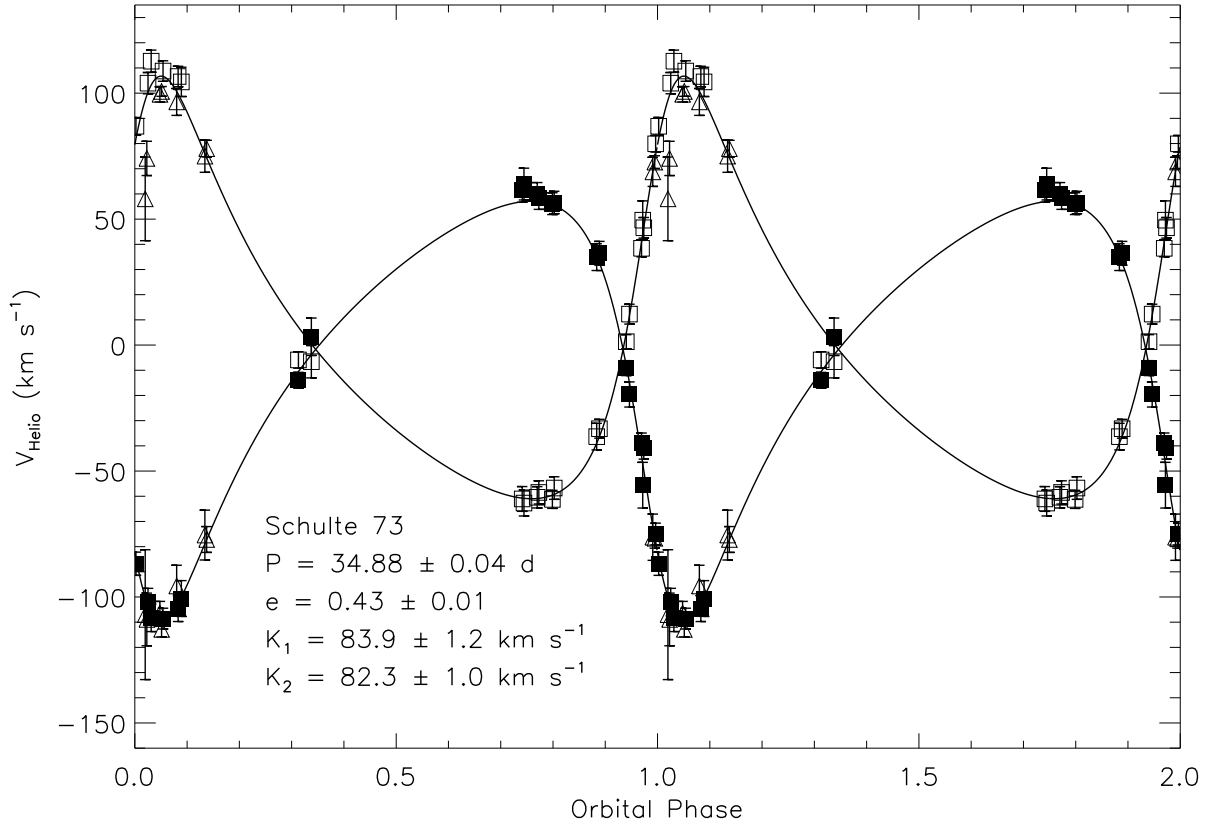


Fig. 36.— Folded radial velocity data and best-fitting solution for Schulte #73, re-analyzed and updated from Paper III.

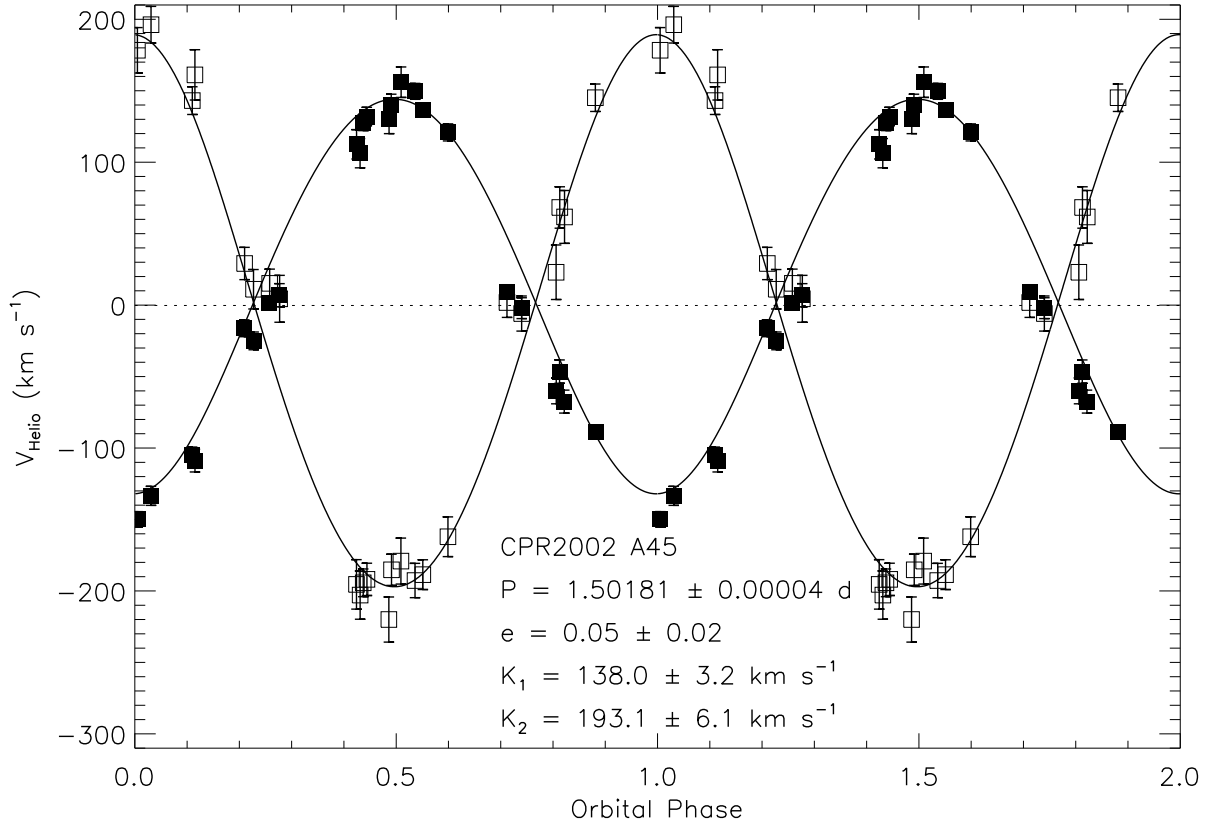


Fig. 37.— Folded radial velocity data and best-fitting solution for CPR2002 A45, re-analyzed and updated from Paper III.